Analytica Chimica Acta 1305 (2024) 342507

Contents lists available at ScienceDirect

Analytica Chimica Acta

journal homepage: www.elsevier.com/locate/aca

Liquid phase detection in the miniature scale. Microfluidic and capillary scale measurement and separation systems. A tutorial review

Cable G. Warren, Purnendu K. Dasgupta *

Department of Chemistry and Biochemistry, University of Texas at Arlington, Arlington, TX, 76019-0065, United States

HIGHLIGHTS

- Covers open and packed capillary HPLC, capillary and μchip electrophoretic platforms.
- Optical, Electrochemical and mass spectrometric detection.
- Recent coverage on applications but includes classic groundbreaking articles.
- Provides a detailed tabulation of topical reviews in last 12 years.
- Provides attainable and typical limits of detection for most approaches.

GRAPHICAL ABSTRACT

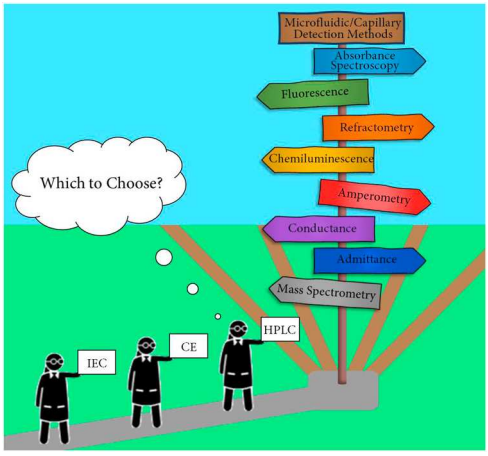

ARTICLE INFO

Keywords:
Microfluidic device
Liquid chromatography
Capillary electrophoresis
Ion exchange chromatography
Mass spectrometry

ABSTRACT

Microfluidic and capillary devices are increasingly being used in analytical applications while their overall size keeps decreasing. Detection sensitivity for these microdevices gains more importance as device sizes and consequently, sample volumes, decrease. This paper reviews optical, electrochemical, electrical, and mass spectrometric detection methods that are applicable to capillary scale and microfluidic devices, with brief introduction to the principles in each case. Much of this is considered in the context of separations. We do consider theoretical aspects of separations by open tubular liquid chromatography, arguably the most potentially fertile area of separations that has been left fallow largely because of lack of scale-appropriate detection methods. We also examine the theoretical basis of zone electrophoretic separations. Optical detection methods discussed include UV/Vis absorbance, fluorescence, chemiluminescence and refractometry. Amperometry is essentially the only electrochemical detection method used in microsystems. Suppressed conductance and especially contactless conductivity (admittance) detection are in wide use for the detection of ionic analytes. Microfluidic devices, integrated to various mass spectrometers, including ESI-MS, APCI-MS, and MALDI-MS are discussed. We consider the advantages and disadvantages of each detection method and compare the best reported limits of detection in as uniform a format as the available information allows. While this review pays more attention to recent

* Corresponding author.
E-mail address: dasgupta@uta.edu (P.K. Dasgupta).

https://doi.org/10.1016/j.aca.2024.342507
Received 8 January 2024; Received in revised form 18 March 2024; Accepted 19 March 2024
Available online 23 March 2024

developments, our primary focus has been on the novelty and ingenuity of the approach, regardless of when it was first proposed, as long as it can be potentially relevant to miniature platforms.

1. Introduction

Liquid phase separations encompass a variety of techniques including Capillary Electrophoresis (CE), High Performance Liquid Chromatography (HPLC), Ion Exchange Chromatography (IEC) and more. While regardless of scale, all three above largely utilize tubular conduits, in the last three decades there has been significant development of microfluidic devices (μFDs) and microfluidic separation devices (μFSDs) that do not necessarily use channels of circular cross section. There is a substantial recent interest in paper- and thread-based microfluidics. The latter is partly addressed in this review, only in the context of detectors used. We chose to not address paper-based platforms as the detection step with such devices are often carried out in a discrete discontinuous manner, unlike other platforms addressed here. Several reviews are available on μFD/μFSDs. Table 1 summarizes some of the major topics of interest that these reviews cover. Broadly, the term μFSD connotes a physically small separation system, often microfabricated on a single integrated platform, a subclass of lab-on-a-chip devices. For the purposes of this review, we consider μFSDs to have separation channels with all dimensions other than the channel length to be < 1000 μm.

If changes in operating conditions are considered significant in going from macro-to micro-HPLC, working with μFSDs represents an even greater change. Detector considerations are largely scale-specific: although considerations of dispersion may be more important in separation systems, the same considerations also apply to other miniature scale liquid phase analysis systems that do not involve separations. Dispersion affects both attainable LODs and sample throughput, even when no separations are involved.

Given the large number of disparate reviews already available, a rationale for this particular review is warranted. The classic overview of liquid chromatography detectors by Scott appeared in 1977 [1], well before any other liquid phase separation techniques had any importance. Of course, the contents were just as applicable to any other continuous flow liquid phase measurement technique. The importance of this work is evident in that within less than a decade another updated edition was warranted [2]. Today multiple platforms exist for fluidic processing, with or without separations. Some detection schemes may work seamlessly from one platform to another, others require platform-specific considerations. With electrophoresis platforms, the presence of an high electric field requires special considerations to apply electrochemical detection. On the other hand, a detection method like suppressed conductivity is uniquely applicable to ion exchange chromatography (IEC). Our objective is to provide an overview of the various detection methods that are presently in use where fluid manipulations are carried out in a miniature scale. Except for capillary liquid chromatography, where scale-specific considerations are numerous, we do not discuss the platforms themselves.

As this review is intended as a primer for the generally interested, we cite and discuss the original work that brought about the paradigm shift, even if that specific implementation is not in use anymore. As such, while most of the studies cited here are very recent, some original classics are included. As Christian has repeatedly advocated, there is merit in reading the very new *and* reading the very old (Christian, G.D. Personal communication).

1.1. Nomenclature. Where does microcolumns/microfluidics begin? Optimum flow velocities/flow rates

There is no universal agreement on dimensional demarcation lines between where macroscale LC systems end and micro, nano, capillary LC separation systems or μFSDs begin. Most regard packed column diameters $\geq$1 mm to belong to the conventional or "standard" scale, which are still the most widely used in both routine and research laboratories, except for those engaged in proteomics research where available sample amounts are very small. There is also a similar general agreement that the term nano LC should be limited to packed columns of $\leq$100 μm diameter [43]. Beyond this, however, opinions differ. *Capillary LC*, in particular, is rather vaguely defined; one early review suggests all inner diameters $<$500 μm qualifies [44]. Such a definition is not in conflict with commercial offerings of "capillary" ion chromatography, which use 400 μm i.d. columns [45], and hand-portable gradient capillary liquid chromatographs [46] that use cartridges containing 150 μm packed columns and one or two integrated UV LED-based absorbance detectors. Although some authors have referred to the latter as nano LC systems [47], capillary LC will be the more appropriate designation. A performance comparison of these commercial gradient capillary LC systems with standard scale systems has been reported [48].

1.2. The attraction of miniaturized separation systems and challenges

Some advantages of miniaturized systems are obvious - the instruments *can* have smaller footprints and power requirements and hence be portable. Their sample requirement, solvent consumption, and waste generation are also proportional to the separation channel cross section. Alternatively, a larger than scaled sample amount can be used for on-board enrichment prior to separation and detection [93].

There are, however, two barriers to achieving the goal of a self-complete portable sensitive instrument. The first hurdle is only present in particle-packed chromatography systems. As is well-known, in CE, electroosmotic and/or electrophoretic movement provide for analyte migration [19]. The same is true for open tubular capillary electrochromatography (OT-CEC) [21]. For CEC in particle packed columns, especially in so-called pressure-assisted or gradient CEC, external pumps are needed, however [49]. Similarly, while OT liquid chromatography (OTLC) [50] or ion chromatography [51] systems may be conducted with easily miniaturized pneumatic pumps, particle-packed columns typically require pressures beyond the reach of simple pneumatic pumps. Even in OTLC systems, gradient elution is difficult to perform without individual pumps; using conventional pumps and injectors and using a small portion of the flow after splitting have often been utilized [52], but this of course defeats much of the advantages claimed for miniaturization in terms of the instrument footprint. High pressure pumps capable of reliably delivering low nL/min flow rates are commercially available but are hardly miniature in size, power consumption and cost. Intermediate size integrated portable HPLC systems have been presented [53]. The pumping issue has been discussed in other reviews [18] and will not be further discussed here. An assessment of the status of mechanical micropumps [22] does not make one optimistic that such pumps will meet the needs of true high pressure pumping soon. However, one may be more hopeful about electroosmotic pumps [23,54]. A fully portable on-chip liquid chromatograph which utilizes electroosmotic pumping and is equipped with replaceable UV/Vis and contactless conductivity detector units has been described [55].

The second and perhaps the overarching limitation of all these devices is the focus of this review - providing sufficiently sensitive detection, especially in a small enough footprint. While small flow rates and very small individual band volumes are virtuous, they make it difficult to connect external detectors as is typical in standard HPLC. The dispersion in the connecting channel alone, much less the detection volume, can destroy any separation achieved prior to the detector.

Table 1
Summary of significant recent reviews covering μfluidic analysis systems.

Year	Brief Summary	Major Topics	Ref. No.
2012	A summary of the development of μfluidic chip-based liquid chromatography (LC) and its integration with mass spectrometry (MS) and their bioanalytical applications. Provides concise descriptions of various commercial LC μchips and their strategies for high throughput analysis. Explains a myriad of bioanalytical applications of μchip LC-MS with a focus on small molecules including drug metabolites, various biomarkers, and active pharmaceutical ingredients.	μchip LC-MS Commercial Instrumentation Bioanalytical Application Small Molecule Detection	[3]
2013	A summary of contemporary developments in μfluidic materials, functions, integration, and applications with a focus on Lab-on-a-Chip devices. Both inorganic and polymeric materials are discussed, including silicon, ceramics, glass, elastomers, and thermoplastics. Use of μfluidic chips for sample preparation, separations, sensing/detection, and fluid manipulation are all discussed. Integration of μfluidic chips with off-chip instrumentation and techniques such as μdialysis, digital PCR, and droplet μfluidics are described. Additionally, applications to point-of-care, cell analysis, nucleic acid assays, drug metabolism, omics, environmental analysis, and space exploration are provided, as well as brief discussion of opportunities for future development at the end of each major section.	Fabrication of μfluidic Devices μfluidic Materials Sample Preparation (Extraction, Purification, Preconcentration, Labeling) Separations (Chromatography, Electrophoresis, Fractionation) Detection (Optical, Electrochemical, MS, Biosensors) Fluid Manipulation (Pumps, Valves, Mixing)	[4]
2013	A summary of analytical detection methods for droplet μfluidics. The detection techniques discussed are bright-field and fluorescence microscopy, laser induced fluorescence, electrochemistry, MS, Raman and nuclear magnetic resonance spectroscopies, absorption detection, and chemiluminescence. Advantages and disadvantages are discussed for each technique. Also included is a brief discussion of sample pretreatment techniques.	Capillary Electrophoresis Spectroscopy Microscopy Electrochemical Detection Mass Spectrometry Optical Detection	[5]
2013	A summary of advances in μfluidic-MS systems. The review focuses on the integration of ESI-MS and MALDI-MS with μfluidic chips from 2008 to 2012. For ESI interfaces, various emitters including single, dual, and multi electrospray emitters are covered as well as nanospray interfaces. For MALDI interfaces direct analysis from μfluidic chips as well as automated spotters are discussed. Sample pretreatment is discussed at length and various biomedical applications including protein analysis, protein-protein interaction analysis, glycan analysis, and drug development are introduced.	Integration of μfluidics and Mass Spectrometry Electrospray Ionization Matrix Assisted Laser Desorption Ionization Biomedical Applications	[6]
2013	A summary of μfabricated on-chip HPLC columns with a focus on μpillar array columns. This thesis contains a vast amount of information including several unique application of on-chip μpillar array columns in single and multidimensional formats. Perhaps more relevant to this review are the sections pertaining to design and fabrication techniques for chip-based columns.	μchip HPLC Design and Fabrication of μfluidic Devices HPLC Column Design μpillar array	[7]
2014	An update to reference 3 and a summary of further advancements in μchip LC-MS and their bioanalytical applications. Beyond the previous review, descriptions of several commercial LC μchips and nanospray emitters for MS integration are provided. Applications for detection of small molecules are discussed and include glycans, active pharmaceutical ingredients, drugs of abuse, drug metabolites, and various biomarkers.	μchip LC-MS Commercial Instrumentation Bioanalytical Application Small Molecule Detection	[8]
2014	A summary of electrochemical detection methods for μ/nanofluidic devices. The review details the theory behind each of the detection methods described which include Amperometric Detection, Conductivity-based Detection, Voltammetric Detection, and Electrochemical Impedance Spectroscopy and also provides a brief overview of more niche techniques such as Chronocoulometry and Scanning Electrochemical Microscopy. It focuses on electrode selection and configuration for both working and reference electrodes. Electrode surface modification is also discussed.	Lab-on-chip Devices Electrochemical Detection Electrode Fabrication Materials Selection	[9]
2015	A summary of the use of μfluidic chips for electrophoresis. Provides a description of capillary electrophoresis and its use in a μchip format including explanations of the most common modes in which μchip electrophoresis is used. Describes the process of μchip fabrication including materials and machining techniques. Discussion of optical, electrochemical, NMR, and MS detection methods, as well as sample preparation techniques are included.	Capillary Electrophoresis Fabrication of μfluidic Devices Optical Detection Electrochemical Detection Mass Spectrometry Nuclear Magnetic Resonance	[10]
2015	A summary of μfluidic LC instrumentation with a focus on commercialized devices. The various components that make up a μfluidic liquid chromatograph are discussed individually and include solvent delivery system, sample introduction system, connecting capillaries, column, column heater, and detector. Advantages and disadvantages are provided for individual components of various commercial μ-LCs. A discussion of various μ-LC applications and future developments are also provided.	μfluidic Liquid Chromatography Solvent Delivery Systems in μfluidics Analytical μfluidic Columns Mass Spectrometry	[11]
2015	A summary of advances in nanoflow LC with a focus on the instrument components and construction. While special attention is paid to nanoflow solvent delivery and sample introduction systems, considerations of nanocolumns, fittings and unions, and detection methods are also included. Additionally, chip-based nano LC, nanoscale 2D-LC, commercial nano LCs, and nano LC at ultrahigh pressures are all discussed.	Nanoflow Liquid Chromatography Nanoflow Solvent Delivery Systems Nanoflow Sample Introduction Systems	[12]
2015	A summary of advances in the coupling of μfluidic devices with MS. Fabrication techniques for μfluidic devices are discussed before the topic of coupling to an MS. Coupling of μfluidic devices with ESI-MS and MALDI-MS are covered in depth, with individual sections dedicated to coupling μchip-LC and μ-chip CE to an MS as well as sample pretreatment and multi-functional integration methods.	Integration of μfluidics and Mass Spectrometry Electrospray Ionization Matrix Assisted Laser Desorption Ionization	[13]
2015	A summary of SERS-enabled Lab-on-a-Chip systems. The fundamentals of SERS are covered in depth before a discussion on SERS μchip fabrication. Fabrication topics covered include generation of μchips via reproducible metal colloid aggregation, controllable colloid aggregation, and solid-state SERS substrates. Various biochemical application of SERS μchips are also discussed including analysis of nucleic acids, biomolecular surface binding investigation, sorting and identification of bacteria, and in-situ monitoring of chemical reactions. Portable systems are briefly discussed as well.	Lab-on-a-Chip Devices Surface Enhanced Raman Spectroscopy Fabrication of μfluidic Devices Biochemical Applications	[14]
2015	A summary of coupling methods for μfluidic-MS. Coupling methods and applications for both ESI-MS and MALDI-MS are discussed. ESI coupling methods covered include integrated and external emitters, droplet μfluidics, and digital μfluidics. MALDI coupling methods covered include external MALDI plate interfaces, direct MALDI on μfluidic devices, droplet μfluidics, and digital μfluidics.	Integration of μfluidics and Mass Spectrometry Electrospray Ionization Matrix Assisted Laser Desorption Ionization	[15]
2016	A summary of advances in miniature and fieldable MS from 2009 to 2015. Ambient ionization and sampling, vacuum systems, analyzers, and electronics and data systems are all discussed in the context of instrument design. Various fabrication methods are discussed for both mass analyzers and μfluidic	Miniature Mass Spectrometry Design and Fabrication of Mass Spectrometers	[16]

(*continued on next page*)

Table 1 (*continued*)

Year	Brief Summary	Major Topics	Ref. No.
	interfaces which include lithographic methods, etching methods, film-based techniques, evaporation, and sputtering. Individual sections highlighting portable, mesoscale, and planetary and space science systems are included.	Design and Fabrication of μfluidic Devices Portable Analytical Devices	
2018	A summary of the design and performance of μfluidic LCs that utilize particle-based stationary phases. Stationary phase particle retention is discussed in detail and includes both frit-based and fritless methods. Design of particle-based μchip LCs including materials, sample injection, fluid control, separation modes, and detection are described. Applications of particle-based μchip LCs as well as commercial systems and separation performances are also included.	Particle-Based μfluidic LC Particle Retention Methods μfluidic Chip Design and Fabrication	[17]
2017	A summary of advances in μchip LC with a focus on individual instrument components. Fabrication of μchips is discussed with attention to material selection and device geometries. Pumps, injection and connection systems, columns, and detectors are all described. Special attention is paid to stationary phase supports such as packed beds, monolithic supports, and μfabricated support structures.	μchip LC Fabrication of μfluidic Devices Solvent Delivery Systems in μfluidics Stationary Phase Support Structures	[18]
2018	A summary of recent trends in CE analysis. The review covers three main topics: modification of capillaries via covalent, dynamic, or semipermanent coating, μfluidic CE, and online μextraction CE. Advantages and disadvantages for each topic/trend are discussed and specific applications are discussed for each method.	Capillary Electrophoresis Design and Fabrication of μfluidic Devices Biochemical Applications	[19]
2019	A summary of μfluidics for biological applications. Provides a discussion of the physical principles of μfluidics and various fabrication techniques. The main focus is on application of μfluidics in biological systems including bacteria, trypanosomes, yeast, slime molds, worms, flies, plants, and mouse immune cells. Additional biomedical methods such as biomimetics, organ-on-a-chip, biotic games, and diagnostics are described.	Fabrication of μfluidic Devices Biological Applications Biomedical Applications	[20]
2019	A summary of developments in OTLC and CEC from 2014 to 2018. The review provides and exhaustive analysis of OTLC and CEC literature, highlighting uniquely sensitive or selective applications in text whilst otherwise summarizing the bulk of the literature in tabular form. The review is split into sections based on the ratio between the capillary internal diameter and coating thickness (CID/CT). Techniques for characterization of capillary coatings are also briefly covered.	Open-Tubular Liquid Chromatography Capillary Electrochromatography	[21]
2019	A summary of recent advancements in the design and applications of μpumps. The review opens by covering the classification of various types of μpumps and their differences. Mechanical μpump drivers and actuators, μpump valves, chamber configuration, diaphragms (materials and design), materials, and fabrication processes are all covered. Relevant literature from 2008 to 2018 is tabulated and summarized in prose.	μpumps: Actuators Drivers Valves Chamber Configuration Diaphrams Materials Fabrication	[22]
2019	A summary of advancements in electroosmotic pump technology from 2009 to 2018. The review opens by covering the advantages of electroosmotic pumps. The pumps are separated into five subclasses: open channel, packed-column, porous monolith, porous membrane, and other, each receiving in discussion with advantages and disadvantages. Applications are then discussed, focusing on μflow analysis and μ/nano-LC. A brief note on the commercialization of these technologies is also provided.	Electroosmotic Pumps μflow Analysis μ/nano-LC	[23]
2020	A summary of major technological developments in μfluidic LC-MS. This comprehensive review discusses state-of-the-art commercial LC-MS devices, materials and device fabrication, stationary phase support and separation channel design, solvent delivery and injection systems, and various methods of MS coupling. Additionally, a broad range of applications including biochemical, biological, pharmaceutical, clinical, forensic, foodstuff, and quality control are briefly described.	μchip LC-MS Fabrication of μfluidic Devices Solvent Delivery Systems Sample Injection Systems Stationary Phase Support Structures LC-MS Coupling Mass Spectrometry	[24]
2020	A summary of advancements in μfluidics using chemiluminescence for food analysis. While the scope is restricted to food analysis, a wide variety of chemiluminescence reactions and systems are reviewed as well as multiple methods of coupling to μfluidic devices. Discussion of demonstrated methods are separated based on pre-separation technique: off-line on-chip, on-line off-chip, and on-line on-chip, as well as methods without a separation step. μfluidic chemiluminescence formats discussed include lab-on-a-chip, μfluidic thread-based analytical devices, lab-on-a-paper, and lab-on-a-cloth.	Chemiluminescence Detection Lab-on-a-Chip Lab-on-a-Paper Lab-on-a-Cloth μfluidic Thread-Based Analytical Devices	[25]
2015 2017 2019 2020	A series of four reviews summarizing advancements in capacitively coupled contactless conductivity detection (C^4D) for analytical techniques in two year increments from 2012 to 2020. Each review discusses the state of the art at the time for C^4D instrumentation. Applications are comprehensively reviewed and tabulated based on type of analysis which include: pharmaceutical, clinical, environmental, biological, forensic, and food analysis. Each review also discusses the coupling of C^4D with capillary electrophoresis and μfluidic separation devices.	Capacitively Coupled Contactless Conductivity Detection Capillary Electrophoresis μfluidic Separation Device Biomedical Applications Environmental Applications	[26] [27] [28] [29]
2021	A summary of μfluidic devices for use in the life sciences. The review is broken into three main sections: materials and fabrication, μfluidic components, and integration into complex μfluidic systems. Materials discussed include silicon, glass, and polymer materials such as polymethylmethacrylate, polystyrene, and polydimethylsiloxane. μpumps, flowmeters, heaters, coolers, temperature sensors, and μneedle arrays are all discussed in detail. The complex systems described include micro fuel reformers, micro dosing systems, and Lab-on-Chip and Point-of-Care systems.	Fabrication of μfluidic Devices μflow Pumps and Monitors Micro Temperature Controllers/Monitors Micro Fuel Reformer Micro Dosing System Lab-on-Chip Point-of-Care System	[30]
2021	A summary of advances in μfluidic chromatography focusing on methods of separation which include affinity, adsorption, ion exchange, and size exclusion/hydrodynamic chromatography and their applications. Affinity-based separations are further subdivided into metal oxide and metal complex -, antibody-, and aptamer-based separation. An extensive table is provided detailing the chip substrate, fabrication technique, stationary and mobile phases, and analytes for the mechanisms discussed.	Fabrication of μfluidic Devices Affinity Chromatography Adsorption Chromatography Ion Exchange Chromatography Size Exclusion Chromatography	[31]
2021	A summary of advances in coupling μfluidic devices with MS for high throughput, high sensitivity, and high specificity analyses. It focusses on ionization techniques which include Electrospray Ionization, Desorption Electrospray Ionization, Matrix-Assisted Laser Desorption Ionization, Surface-Assisted Laser Desorption Ionization, Inductively Coupled Plasma, and Acoustic Wave Nebulization. The methods are discussed in the context of popular μfluidic analytical approaches in biotechnology, covering continuous-flow systems, μchip electrophoresis, droplet μfluidics, digital μfluidics, centrifugal μfluidics, and paper	μfluidic Techniques Biotechnology Applications Mass Spectrometry Ionization Methods High Throughput Analyses	[32]

(*continued on next page*)

Table 1 (*continued*)

Year	Brief Summary	Major Topics	Ref. No.
	μfluidics. Additionally, the review covers a number of recent applications of μfluidic-MS integration in biotechnology and provides an outlook for future growth in the sector.		
2021	A summary of recent advances in the design and construction of μfluidic electrochemical devices. Broken into three main sections, this review covers the design and fabrication of μfluidic devices utilizing electrochemical detection and common challenges and solutions therein. Design aspects discussed include working, reference, and counter electrode design, electrode arrays, flow patterns and channels, and numerical modelling. Fabrication techniques covered include photolithography, CNC machining or other physical machining, 3D printing, and briefly discusses printed circuit boards.	Fabrication of μfluidic Devices Design of μfluidic Devices Electrochemical Detection Common Challenges & Solutions	[33]
2022	A summary of recent advancements in nanoflow LC with a focus on bioanalytical applications and targeted quantitation. Individual instrument components such as pumps, injectors, connectors, and detectors are described, with a special focus on nanocolumns. An in-depth discussion of multidimensional μfluidic separation is provided, including schematic diagrams and step-by-step methodology. Proteomics, metabolomics, and enantiomeric separation applications are discussed along with a detailed future perspective of the field.	Nanoflow Liquid Chromatography Nanocolumns Multidimensional μfluidic Separations Proteomics Metabolomics Enantiomeric Separation	[34]
2022	A summary of applications of cyclic olefin copolymer to μfluidic devices. Specific features and composition, production processes and fabrication techniques, potential advantages and uses of cyclic olefin copolymers are covered. Integrations with μfluidics cover a vast range of applications in biological, organic semiconductor, thermal, optical, and membrane processes.	Cyclic Olefin Copolymer Fabrication of μfluidic Devices Biochemical Applications	[35]
2022	A summary of advancements in nanoelectrospray ionization (nano-ESI) and relevant devices. Emitters, sample injection, and electrical contracts are the main focus and are reviewed in the context of instrument performance and functionality. Single, μchip-based, and multinozzle emitter design and fabrication are discussed in depth. Online and offline sample injection methods are considered. Coupling to CE and LC are discussed.	Nanoelectrospray Ionization Design and Fabrication of μfluidic Devices Capillary Electrophoresis Liquid Chromatography	[36]
2023	A summary of advances in integration of optical detection methods with μfluidic chips for biochemical analysis. Optical detection methods reviewed include UV–Vis absorption, fluorescence, infrared, surface plasmon resonance, chemiluminescence, and optical tweezers (photon resonance-based optical traps). Optical detection methods are first briefly introduced before highlighting prominent biochemical applications involving integration with μfluidic chips.	μfluidic Chips Optical Detection Biochemical Applications	[37]
2023	A summary of recent developments in chemiluminescence for bioanalysis. This review focusses heavily on chemiluminescence bioassay, mostly achieved through the use of μchips. Various chemiluminescence reagents, amplification systems, and coupling with μfluidic devices are discussed.	Chemiluminescence Detection μchip Design Biomedical Application	[38]
2023	A summary of novel developments in CE from 2013 to 2023. Liquid handling, sample injection, μsampling, flow control, power supplies, detectors, data acquisition, and 3D printing are all discussed in the context of instrument design. The detectors covered in depth include contactless conductivity, absorbance, and laser induced fluorescence detectors. Applications through modular CE, Portable CE, miniaturized palmtop CE, CE for spaceflight missions, and CE coupling to sample pretreatment are discussed in detail.	Capillary Electrophoresis Contactless Conductivity Detection Absorbance Detection Laser Induced Fluorescence Detection Portable Analytical Devices	[39]
2023	A summary of advances in portable LC with a focus on detection methods and fully integrated, portable LC systems. The detection methods discussed include optical, electrochemical, and MS. Portable, small footprint UV/Visible absorbance detection and their integration with μfluidic LC is discussed in considerable detail with special attention afforded to multi-LED and multi-wavelength -based detection methods. Several state-of-the-art fully integrated and portable LC systems are described in detail including size and weight considerations. In addition, recent instrumentation for on-site environmental analyses is described including a portable LC-MS for quantitation of 12 target poly/perfluoroalkyl substances (PFAS).	Fully Portable LC System UV/Visible Detection Electrochemical Detection Mass Spectrometry Commercial Instrumentation Environmental Applications	[40]
2023	A summary of application and detection options for μfluidic thread-based analytical devices. The review covers driving forces in fluid transport such as wicking action, gravitational forces, and electrophoretic forces in thread-based μfludics. Detection methods covered include colourimetric detection, electrochemical detection, electrochemiluminescence detection, fluorescence detection, and spectrometry-based detection. Applications discussed range in discipline and include biological diagnostics, immunoassays, wearable devices, health monitoring, and food and environmental safety.	μfluidic Thread-Based Analytical Devices Fluid Mechanics Optical Detection Electrochemical Detection Biochemical Applications Environmental Applications	[41]
2023	A summary of the state of the art in CE instrumentation as of March 2023. Commercial, as well as home-built and μchip instruments are reviewed under a number of criteria. Classical figures of merit such as precision, resolution, linearity, sensitivity, and speed are considered along with several metrics for application and user experience including flexibility, ease of use, reliability, sustainability, dedication, and cost. Multiple detection methods are explored including UV, laser- and LED-induced fluorescence, C^4D/admittance, and MS. Instruments are compared under equivalent conditions whenever possible and user experience metrics are evaluated based upon the designer-specified intended use of each instrument rather than speculative applications.	Capillary Electrophoresis Commercial Instrumentation μchip CE UV Detection Fluorescence Detection Admittance Detection Mass Spectrometry	[42]

Smaller separation channels require proportionally small detection volumes, preferably located on/in the separation channel, if possible. When such a location is not possible, e.g., for a mass spectrometer, the integration/interfacing scheme between the separation scheme and the detector must produce a small enough dispersion to maintain the separation achieved. Consider the separation of a tryptic digest in a $d_c = 2$ μm OT column; the median base peak width was as small as 8.4 s, or ~273 pL. Assuming the base width spans ±3 σ, the peak variance is 2.1 nL. To keep the peak variance from increasing by 10%, additional dispersion must be < 15 pL. Fast efficient separations also require adequately high data sampling rates to achieve sufficient data points across a peak [56]. The resolution of the above separation was said to be already data sampling rate limited by the highest scan rate mass spectrometer available at the time. Obviously reduced sample volumes require detectors with exquisite mass sensitivity. In the above example, 114 separate proteins were detectable in a 0.75 pg sample. Even making the rather implausible assumption that the entire injected mass is present in the observed peaks, the detection ability had to be ≤ 1 fg/s. For an average MW of 0.7–2 kDa in a tryptic digest [57] this translates to 300,000–850,000 molecules/s. Few detection techniques can offer such sensitivities and commercial μHPLC applications on the polyimide or the iKey platforms have thus remained limited to large pumps and large mass spectrometers. While this does not lead to portability, the extraordinarily rich information only a mass spectrometer can provide, including the ability to detect and identify analytes that have not been physically separated, certainly makes up for it.

1.3. Capillaries, μchips and threads: similarities and differences

Geometries and differences in construction material and morphology

(in the case of threads) do significantly affect both performance and what type of detection is possible.

Fig. 1 provides a generic classification of detection techniques as consumptive, partially consumptive (laser induced fluorescence or amperometry for example destroys some of the analyte, the extent may be variable) or non-consumptive. All of the consumptive methods operate end-column or off-column (hereinbelow we just use the term end-column). While the non-consumptive methods permit the use of serial detectors (provided dispersion can be managed), these are therefore necessarily on-column, or on-chip (denoted in Fig. 1 in red font). It is easier to arrange for such serial detection in a μchip format. Of course, all end-column (or off-column) detection techniques apply equally well to μchips and capillaries, except for open tubular chromatography, where the added dispersion from connecting to an external detector may become prohibitive. Regardless of classifications based on consumption, detection methods can also be divided into two classes, where the sensors/transducers must contact the solution as in all electrochemical techniques except for admittance measurement (also commonly called capacitively coupled contactless conductivity measurement, C^4D). When measurement must involve sensor/transducer contact, μchips have the advantage that electrodes and such can be built-in; however, this may require a somewhat more sophisticated μfabrication facility.

Beyond the above classifications there is the more common principle-based classifications, e.g., optical, electrochemical, etc. and each of these have further subclassifications. None of the optical detection techniques require solution contact. If on-column detection is not possible, the next best possibility to avoid excessive dispersion is to position the sensing probe at (perhaps protruding into) the fluid exit point; this is typically done in amperometric or potentiometric sensing. In general, detection that can be done on-column/chip can also be carried out end-column/chip; a purple font in Fig. 1 indicates that either can be (and often are) used. Optical absorbance detection for example is used in both locations – while radial/*trans*-channel path on-column detection may provide the least dispersion, a longer path end-column cell may provide much greater sensitivity, at the expense of greater dispersion.

Some of the most sensitive detection schemes such as mass spectrometry must operate off-column/chip, post-column/chip liquid phase dispersion is often arrested by larger flow of nebulization gas or drop isolation. However, these processes themselves or the interface can create additional dispersion. Additional dispersion is inevitable for processes involving post-column/chip reagent addition to elicit chemiluminescence or other detectable phenomena.

The most used optical methods rely on the absorption of light. While absorbance detection (primarily in the UV), has been the mainstay of standard scale HPLC as well as CE, achieving sensitive absorbance detection becomes increasingly challenging as the dimensions of the separation channel decrease. Still, there are commercial offerings of stand-alone optical absorbance cells that range from a radially illuminated capillary cell with a volume of 10 nL to a 10 mm path cell with a volume of 100 nL [58,59]. Contrasting optical detection on capillary vs μchip platforms, rectangular/square cross section channels in the latter permit optical interrogation with less scattering issues and typically requires less demanding optical arrangements. In a chip it is also possible to build the detection zone with a geometry different from the main channel to provide a relatively long optical path of small volume. However, material typically used for μFD fabrication can pose limitations. μFD's are typically composed of polymers that are not UV-transparent. Only a few, notably cyclic olefin copolymers (COCs), permit interrogation to ~280 nm [35]. In contrast, fused silica, the most common material used in the capillary format, permits use over the entire UV–Visible range. Fabrication of microchips in silica is possible but requires sophisticated equipment.

With the availability of relatively inexpensive lasers that can be focused to very small spots and notch filters that exclude scattered laser light selectively (up to 6 orders of magnitude in a narrow band centered on the laser emission) makes laser induced fluorescence (LIF) a particularly attractive detection mode. Square or rectangular channels are also typically constructed in a rectilinear profile; in separation systems this limits the separation channel length. A curved, e.g., a circular or spiral channel is not possible in silicon or glass microfabrication. Although it is hardly impossible in other microfabrication techniques, it is still less common. If channel length is increased by having an overall footprint in the form of any geometry that involves sharp angular turns, separation efficiency decreases because of the "racetrack effect", travel along the inner side of the perimeter provides a shorter path than the outer parameter. For chromatography, channels of non-circular cross section pose another issue: Unequal distances of all points on the perimeter from the center. Although the technology for making channels of circular cross section on glass has been known for more than two decades [60] and has been occasionally used [61], it is rarely practiced; also, a circular cross section does not mean an overall circular shape of the entire channel is feasible.

Refractive index (RI) detection has not enjoyed widespread use in HPLC (except in the early days of HPLC or in niche applications, e.g., size exclusion chromatography), because of its incompatibility with gradient elution but otherwise it has the considerable merit of being a universally applicable detector that, in its laser-based interferometer form can be deployed on-column and probe extremely small volumes [62–64].

Among optical techniques, Raman spectroscopy has the unique potential to provide meaningful structural information. Raman or infrared spectrometry has generally been regarded as too insensitive to be used for on-line detection in liquid phase separations; these were the conclusions of a 2005 review [65]. However, the increasing facility of making nanostructured surfaces which foster surface enhanced Raman spectroscopy (SERS), a much more sensitive technique, has generated a renewed interest in SERS detection coupled both to chromatographic systems and μFSDs; a review on the later topic is available [14]. There is considerable current interest in thread-based microfluidics. Based on a recent near-comprehensive review of thread microfluidics by Chen et al. [41], except for electrochemical/electroluminescence detection, most other detection approaches are off-line. Threads permit a unique opportunity to incorporate wire electrodes in desired zones in the thread network and thus performing electrochemical detection, in a disposable manner if one so wishes. There is also a unique and relatively easily executed opportunity of preparing gold nanoparticles in-situ on the thread in the desired detection zone [66]. SERS-based detection has already made an impact on this platform. However, we do not discuss this topic further.

While RI (or SERS) detection is universal, laser-induced fluorescence (LIF) is highly selective. It is relatively easy to practice and is typically a highly sensitive technique with very low detection limits. If the target of interest can be excited by a relatively inexpensive diode laser, fabricating the detector is inexpensive. However, few molecules fluoresce. Most commonly, light absorption results in nonradiative relaxation, ultimately leading to heating. This forms the basis of detection by photothermal spectroscopy, reviewed comprehensively in a dedicated monograph [67]; a more succinct review is also available [68]. The temperature rise can be followed by the lensing effect caused by the local change in RI, which is most commonly carried out in the photothermal deflection spectroscopy (PDS) mode. An excitation laser utilizes a wavelength where the analyte absorbs and the path of a second probe laser passing through the same spot is altered due to the refractive index gradient caused by the local heating, often referred to as the thermal lensing effect, and this deflection is measured [69]. The rise in temperature may also be followed by the decrease in solvent viscosity, which in turn increases electrical conductivity [70]. The temperature change can also be followed by directly measuring the change in temperature with some micro transducer in contact [71], or in a noncontact fashion by measuring infrared emission. The latter technique is generally perceived as insensitive and has not yet been exploited analytically. Finally, the photoacoustic effect, as elicited by a pulsed light source is

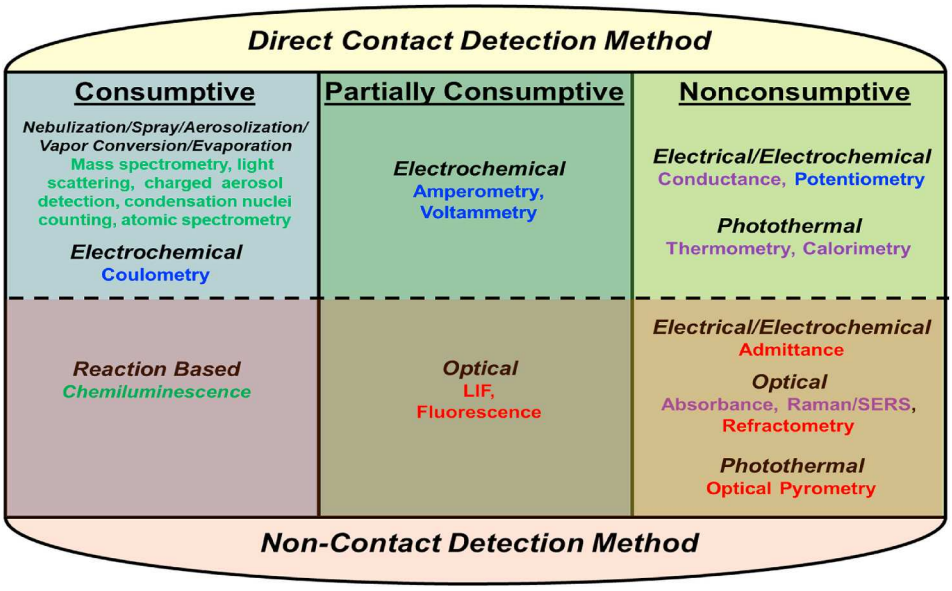

Fig. 1. Diagram of detection processes organized based on solution contact, analyte consumption, and detector location. A red font indicates that on-column/on-chip sensing is possible, a blue font indicates a typical end-column location, a purple font suggests both locations are used. A green font indicates an off-column location. (For interpretation of the references to color in this figure legend, the reader is referred to the Web version of this article.)

one of the earliest characterized photothermal effects (used originally by Bell in his *Photophone* [72]); there are many excellent reviews on photoacoustic spectroscopy [73,74]. It relies on acoustic waves generated from pulsed heating in a locally confined environment, the frequency of pulsation can be chosen to be in a domain where a microphone or similar transducer can measure the intensity of the acoustic pulsations. Although photoacoustic measurement of a trace gas concentration is commonplace, liquid phase measurement is problematic. It is particularly susceptible to pump pulsations [75] and reported liquid phase limits of detection (LODs) are not especially alluring [76] – it will not be further discussed in this review.

Another optical technique is chemiluminescence (CL) detection, in its present embodiment it must take place off-line; here, light is emitted as a result of a reaction. Interestingly, liquid core waveguide (LCW) based chemiluminescence detectors are known for decades now [77,78]. Teflon AF, often used in making such LCW conduits is also highly gas permeable, any reagent with significant vapor pressure can be readily introduced through the walls. The ability for a device to simultaneously behave as a LCW and a chemical reactor where gaseous reagent permeates through the wall has also been demonstrated [79]. As μFSDs are often made of optically transparent polymer material [35], and efficient coupling of the more traditional fused silica capillaries or injector fabrication through capillary channels in such polymer material has been demonstrated, and further that intrinsically nanoporous (gas--permeable) membranes can even be 3D-printed [80], gaseous reagent introduction to induce CL and in-situ detection holds significant promise. Finally, electrogenerated CL offers yet another way to perform CL detection whether on-device/column or at the device exit [81].

In contrast to optical techniques, electrochemical techniques, as well as direct measurement of electrical conductivity, requires direct solution-electrode contact. High frequency admittance measurements are possible without solution contact and have been widely used, especially in CE. While admittance measurement is generally referred to as (Capacitively Coupled) Contactless Conductivity Detection (with the acronym C^4D), it really measures admittance and not conductance [82].

The rest of the detection techniques take place off-line, mass spectrometry being the most powerful and most common. While the necessary intervening step of nebulization/aerosolization adds to some dispersion, it also prevents further dispersion. Although unlike their optical or electrical/electrochemical counterparts, mass spectrometry is not easily miniaturized (albeit significant advances have been and continue to be made [83]), the sensitivity and dimensionality of information MS can provide makes it very attractive. Electrospray sources are the most common and while aerosolization/ionization is not very efficient, it has been recognized for some time that this efficiency improves markedly as the scale is reduced; OTLC is particularly simple to couple to a (nano)electrospray source [84]. Although several other methods have been listed in Fig. 1 for off-line detection, in practice only MS and ICP-MS have sufficient sensitivity for practical use.

As to miniature analysis systems coupled to MS detection, droplet microfluidics [85] has often been used: an immiscible liquid phase is used to create nL-fL volume isolated microreactors, generating up to tens of thousands of droplets, these reactors permit excellent mixing, allowing one to carry out further reactions or other manipulations. A review specifically addressing the coupling of droplet microfluidics to MS is available [15]. It is important to note that much like aerosolization which always utilizes far greater gas flow than liquid flow, isolation by an immiscible droplet phase also greatly reduces further dispersion.

In this review we first therefore briefly discuss the two major separation modes, chromatography and electrophoresis in a scale-specific format. Then we explore the more commonly used detection methods used in miniature scale separation systems, with a summary of each technique and how they are implemented in this landscape, as well as literature applications and achievable sensitivities which are given as mass LODs where possible.

2. Chromatography on a miniature platform

2.1. Packed column HPLC in the miniature scale

In its number of applications and hence commercial use, HPLC is by far the most widely used liquid phase separation technique. It is worthwhile to consider how implementation of HPLC changes from macro to the miniature domain. The first and most obvious change is the physical dimensions of the separation device and the consequent associated changes in operating conditions. The length of the separation column in conventional and micro-HPLC typically range between 0.5 and 30 cm; column lengths rarely exceed 15 cm for sub 2-μm packing due to the large pressure drops. It has long been known that as particle size decreases, the plate height minimum decreases, the optimum flow

rate range of the van Deemter plot (H plate height, vs. u_{av}, mean fluid velocity) becomes flatter. For example, Nguyen et al. [86] observed H_{min} for 5, 3.5 and 1.7 μm particle packed columns to be 12.3, 8.8, and 3.9 μm, respectively and the corresponding u_{opt} values to shift from 0.72 to 0.89–2.11 mm/s. For practical operations, where separation time is considered, the respective optimum velocity ranges were 0.8–1.4, 1–1.9 and 2–3.5 mm/s. In contrast, Knox plots (h, reduced plate height, defined as H/d_p where d_p is the particle diameter vs. ν, reduced velocity, defined as $u_{av}d_p/D_m$, where D_m is the diffusion coefficient of the analyte in the mobile phase) were essentially identical for the various d_p columns with butylparaben as a model analyte. Compared to fully porous particles used above, comparably sized superficially porous core-shell particles perform even better – providing lower H_{min}, higher u_{opt} and substantially flatter van Deemter plots [87].

At least down to column diameters of 1 mm, other than solvent savings, there are no documented performance advantages in using smaller bore columns with the same packing. In the capillary domain, however, while the exact results depend on the particle size and particle size distribution, Kennedy and Jorgenson noted early on [88] that packed capillary columns with column internal diameter (d_c) in the range of 100–350 μm tend to fare worse in terms of plate heights compared to their counterparts of larger, more conventional diameters, especially at higher mobile phase velocities. This behavior was believed to be due to the "wall effect", which results from particles in the wall region, a zone extending several particle diameters from the wall, not being as densely packed as the center of the column. This radial dispersion of column permeability thus results in flow dispersion, especially at higher velocities. They also observed that once one goes down to a d_c range of 20–50 μm, however, plate height improves with decreasing d_c; the entire column now behaves as the "wall region". In this domain, with decreasing d_c, flow dispersion, flow resistance and the resistance to mass transfer in the mobile phase all decrease. Generally, a d_c/d_p ratio of <10 provides better performance than those with a higher value [89].

Later, 3-D microscopic examination has shown that the "wall effect" is not a conjecture; with fully porous particles with $d_p = 1.7$ and 1.9 μm, the particle packing density is indeed less at the wall [90]. However, these observations may be acutely dependent on mean d_p and the particle size distribution. Packing density is a complex function of size distribution and the nature of the particles, as well as the slurry density used for packing. Regardless of d_c (30–75 μm) and d_p (0.9, 1.7, 1.9 μm, fully porous, size RSD 12–16%; as well as 1.9 μm core-shell particles, size RSD 5.8–6.2%) packing density increased and efficiency increased at higher slurry concentrations used for packing [90], paradoxically especially for the more polydisperse porous particles. It was observed that columns with d_c/d_p ratios >25 may benefit more from increased packing slurry concentrations. Beds packed with higher slurry concentrations suppress particle size segregation. However, more packing voids can form in this case, at least with the porous particles used herein with a wider size distribution. In the cited study [90], the size distribution of the core-shell particles was significantly narrower and rather few packing voids were found; with these particles, a higher slurry concentration allowed for an additional densification of the bed's wall region, as revealed by an analysis of the mean particle distances as a function of radial position. However, these columns were already well-packed and increase in efficiency was not significant. Again, this behavior is very dependent on the nature and size distribution of the packing as well as the extremely small bore (<75 μm φ) columns.

With nonporous 1.0 μm particles, column efficiency continuously improved with decreasing d_c in the range $d_c = 10$–150 μm; h_{min} monotonically decreased from 2.5 to 1.3 while u_{opt} monotonically increased from 1.2 to 1.8 mm/s as d_c was reduced from 150 to 10 μm. However, extrusion of the packing (possible only for the larger-diameter column range) and microscopic examination suggested increasingly ordered packing at the wall region with decreasing d_c [91]. These authors demonstrated column efficiencies as high as 730,000 plates/m and run pressures over 6800 bar (100,000 psi) using custom UHPLC systems for $d_c = 10$ μm capillaries.

2.2. μchip HPLC. Past and present commercially available chips for μHPLC-ESIMS

In contrast to demonstrated ultrahigh pressure capabilities of capillary HPLC, an important limitation of μchip HPLC microfabricated by standard approaches, whether made from glass/quartz or polymeric substrates, is that they cannot withstand HPLC level pressures and delaminate easily. Therefore, neither of the two main platforms for μchip HPLC commercialized thus far have relied on conventional microfabrication techniques, and both were expressly designed for use with a mass spectrometer, with the electrospray tip built on the chip.

In 2003, Agilent scientists introduced a polyimide film-based platform. Thin polyimide sheets were cut with a 355 nm laser to form 50 × 75 μm trapezoidal cross-section channels. The channels were then packed with particles and thermally sealed on either side with further polyimide sheets [92,93]. Layers were selectively metallized with evaporated gold that extended to the fluid flow channel near the tip to provide electrical contact for electrospray. Tips with outer and inner dimensions of 50 and 15 μm, respectively, were formed by ablating the polymer material concentrically around afinished channel. A micromachined outlet frit retained the stationary phase that was slurry packed at pressures up to 4000 psi [94]. The maximum pressure recommended for the commercialized chips, introduced by 2005, was a more modest 2175 psi [95]. Ehlert et al. [94] investigated bed densities as a function of the packing conditions; higher bed densities were consistently correlated with higher pressure drops and better separation efficiencies. High bed densities are critical to separation performance in noncylindrical packed beds; only at high bed densities can hydrodynamic dispersion in noncylindrical packings be reduced to a level close to those attained with cylindrical beds. Ehlert et al. demonstrated that the separation channels of these HPLC μchips can be packed as densely as the cylindrical fused-silica capillaries used in packed capillary LC and comparable separation efficiencies can therefore be achieved. A monolithic column avoids the need to fabricate a bed support or optimize packing pressures – such approaches have also been developed for the polyimide chips [96]. A particularly novel feature of the polyimide chip was integrating an interface to a standard macroscale 6-port rotary injector, permitting leak free, high-pressure fluid switching by locating six apertures in the chip, aligned to valve port configurations, between the stator and rotor of the valve. Figs. 2 and 3 show the arrangement. Sample or eluent enters the chip by standard capillaries connected to the valve. While the polyimide chip with its spray tip was specifically developed for ESI-MS, successful UV detection has been performed by using a UV cell of 50 μm i.d. and 300 μm path length (nominally 0.6 nL in volume) at the chip-exit and a photodiode array detector [94]. Much larger cells (0.12 × 0.12 mm cross section, 6 mm long, ~80 nL volume) have also been used [96]; while maximum efficiency could not obviously be obtained, attractive performance was still possible, especially as the monolithic packing permitted high flow rates, reducing the effects of extra column dispersion. An early review is available on the polyimide μchip HPLC platform [97].

The ionKey(iKey)/MS™ platform,[1] based on particle-packed 150 μm × 150 μm rectangular channels on a ceramic substrate, was first described by scientists from Waters Corp. in a white paper in 2013 [98], and robustness of such devices for the analysis of pharmaceutical compounds over 1000 injections was addressed shortly thereafter [99]. Similar devices with other channel diameters have since become available. Devices with 300 × 300 μm cross section allow for higher throughput and devices with open channels as small as 85 × 85 μm in

[1] The initial version of this device was introduced under the name Trizaic and also generally referred to as the "Nanotile" chips.

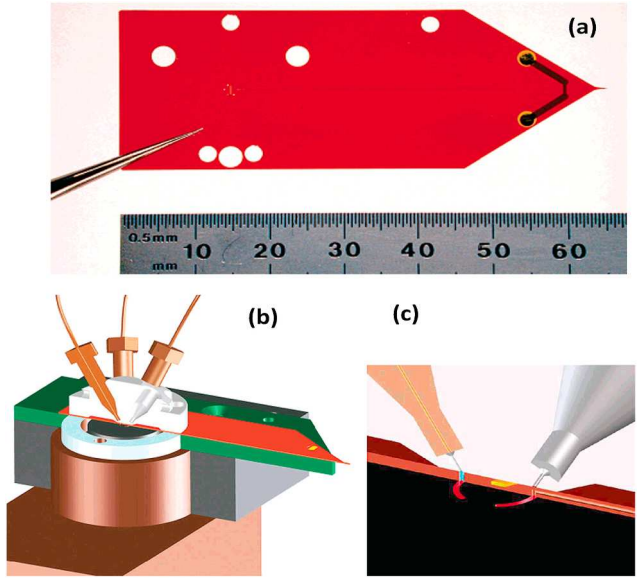

Fig. 2. Agilent polyimide chip (a). The separation channel (packed with stationary phase) on the polyimide sheet runs from left to right. The holes along the periphery were used for alignment. The dark pattern towards the right end of the chip shows the electrodeposited metal for contact to the fluid flow channel near the electrospray tip. The much smaller inlet ports that align with the conventional macro injector (more details in Fig. 2) are visible 15 mm from the left end of the chip. (b) Mounting of the chip on the valve assembly. The support block (grey), support plate (green), and the stator and fittings have been sectioned above for clarity. (c) Fluid enters from a connected inlet capillary through the aligned hole in the chip to the red groove in the rotor (black). From Ref. [93], reprinted by permission from the American Chemical Society. (For interpretation of the references to color in this figure legend, the reader is referred to the Web version of this article.)

cross section allow for direct operation/infusion into a MS in a flow-injection mode. Most of these devices allow for post column addition of pH modifiers/solvents to promote ionization [100]; similar applications were also demonstrated for the Agilent platform [101]. iKey chips are presently available packed with a variety of 1.7 and 1.8 μm particles in both 150 × 150 and 300 × 300 μm channels. The column lengths range from 50 to 100 mm. The exterior dimensions are 16 × 5 cm. As with the Agilent chip, the column exit terminates in a sharp tip that is used for electrospray. Fig. 4 shows a workflow diagram on how such a chip is made.

Operating linear velocities in packed columns are typically in the range of 1–2 mm/s, with core-shell particles allowing larger flow velocities, regardless of diameter. The typical range of flow rates for various column diameters is thus easily computed from the flow velocities and also appear in many places [44].

2.3. Open tubular liquid chromatography (OTLC)

An OTLC system may be the simplest of all miniature separation platforms; the open tubular mode is almost exclusively used in gas phase separations but the practice of OTLC is far more limited compared to packed column chromatography in the liquid phase due to far smaller diffusion coefficients that dictate very small column diameters. This in turn limits options for sensitive detection. From the simplest form of the van Deemter equation applicable to an OTLC system, the optimum velocity u_{opt} is derived to be:

$$u_{opt} = \sqrt{\frac{2D_m}{C}} \ldots \quad (1)$$

where C is the resistance to mass transfer in units of time. However, the value of C is typically not widely available and is usually derived from measurements of u_{opt} itself. The kinetic approach of Knox and Gilbert [102] can be used more readily where the optimum velocity is computed to be:

$$u_{opt} = \frac{D_m}{d_c}(1+k)\sqrt{\frac{192}{1+6k+11k^2}} \ldots \quad (2)$$

where d_c is the inner diameter of the capillary and k the retention factor of the analyte.

For k < 5, the simpler expression

$$u_{opt} = 13.2\,\frac{D_m}{d_c}\,\frac{1+k}{1+3k} \ldots \quad (3)$$

produces the same values as eq (2) within ±4.5% error.

For 10 > k > 5

$$u_{opt} = 4.0\,\frac{D_m}{d_c}\,\frac{1+k}{k} \ldots \quad (4)$$

can be used with <1.5% error, or

$$u_{opt} = 4.61\,\frac{D_m}{d_c} \ldots \quad (5)$$

can be used with ~<3% error. Thus for a D_m of 10^{-5} cm^2/s (e.g., hydroquinone in 50% ACN-water [103]) the optimum velocity will range approximately from 0.25 to 1 mm/s for d_c ranging from 20 to 5 μm. However, in practice to save time, regardless of the format, chromatography is nearly always conducted at higher than optimum velocities. The flow velocity used for the separation of a tryptic digest sample on a $d_c = 2$ μm OT column derivatized internally with C18 functionality was ~4 mm/s [104].

Microfluidic devices are rarely fabricated with perfect cylindrical channels. If at least one channel dimension is sub-mm, it is typically assumed to have met the definition of a μfluidic device. In μFSDs using a packed channel format, linear velocities used are comparable to those used for packed capillary columns of similar cross-sectional area. However, based on the number of reports in the literature, separations in μFSDs are conducted as often by electrophoresis or electrochromatography as chromatography. In these modes, separation efficiency is typically governed by the applied field strength, which also govern analyte migration velocities. However, the maximum field strength that can be applied is often limited by Joule heating, which in turn is controlled by the device geometry [19].

2.4. Scaling up OTLC? Micropillar array columns

In the chromatographic separation mode, open tubular columns provide for the highest separation efficiency per unit pressure drop but detection is hampered by the extremely low amounts of analyte available. Is it possible then to have a thousand identical capillaries, where the inlet flow is thus divided into a thousand parallel streams all flowing at the same rate and then recombined at the exit end before entering the detector? Nearly a half century ago Golay referred to this as “too fantastic” [105], whether wistfully or declaring it as impossible. Periodically, others have taken on this challenge, often enamored by the improving precision of contemporary optical fiber manufacturing. In 1983, Meyer et al. [106]. attempted fusing together 3900 35 μm diameter optical fibers creating ~7800 interstitial channels. Because such fibers could be produced with a diametric standard deviation of 0.3%, they computed that the 95% span of the linear velocity through individual channels would fall within 1.2%. Based on this, they computed a potential efficiency of 500,000 plates/m. Even after blocking the peripheral pathway (which led to 2 peaks from a single analyte), the results were very disappointing. Photonic crystal fibers (PCFs) were invented by Russell two decades ago [107]. This has the form of a finite, two-dimensional photonic crystal with a “defect” in the center which

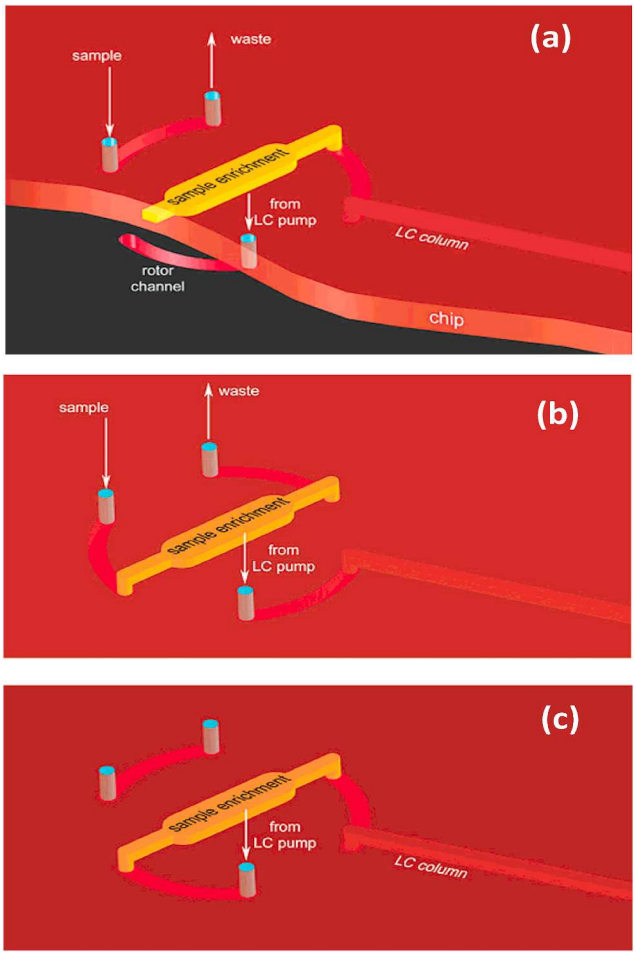

Fig. 3. Flow arrangement with a sample enrichment column built on the chip (this column is also visible in Fig. 2(a). Panel (a) shows the grooves in the valve rotor and the grooves in the chip in vertically separate and differently colored panes, the subsequent panels do not make this distinction for simplicity. Panel (b) shows the loading/enrichment step where a known volume of sample is concentrated on the on-chip preconcentration column and panel (c) shows this column being eluted. From Ref. [93], reprinted by permission from the American Chemical Society.

may consist of either a solid or a hollow core, the cross section being like that of a multicapillary bundle. The analytical applications of PCFs and multicapillary bundles have been reviewed [108]. PCFs have been appropriately functionalized and used for extractive preconcentration and then coupled to a miniature separation system downstream [109,110]. Kazarian et al. [110] used a fused PCF containing 126 4-μm i.d. parallel channels silanized and coated with a 100–300 nm thick layer of polystyrene-divinyl benzene. A plate count of 5000 plates/m was attained for cytochrome C ($k = 0.6$) eluted in the reverse phase mode. In systems like this, the departure from theoretical expectations is brought about more by disparities in the wall coating thickness (which leads to difference in the retention factor) than the lack of bore uniformity (which leads to differences in individual velocities). With uniform active thickness of the stationary phase (SP), two extreme cases can be considered (a) when the SP thickness is negligible compared to the channel i.d., and (b) when it is not. Even in the most favorable case, the retention is directly related to the stationary phase volume. Consider just two columns with the following base case parameters: $L = 1.00$ m; $\eta = 0.809$ mPa s (~90% MeOH), $\Delta P = 4.31$ Mpa (145 psi), and $D_m = 10^{-5}$ cm^2/s, with the standard column having $d_c = 5.000$ μm. In case (a) SP active volume is directly proportional to d_c. In this case, if the other column respectively has $d_c = 5.005$, 5.010, and 5.015 μm and one of these is operated in parallel with the benchmark 5.000 μm column, there will be 20%, 49% and 68% plate loss respectively compared to the benchmark column. Indeed, in the last case, the peak will appear not as a single peak but be bimodal in shape. In case (b) the SP is of appreciable thickness, this case is often common to situations where the inner surface of a narrow bore OT column is derivatized primarily with a view to increase capacity [111]. The difficulty in maintaining constant average SP thickness across multiple columns now becomes even greater. In this case increasing the SP volume has an even greater effect than case (a), as the static mobile phase volume is also affected. For the same parameters as above, with a constant SP thickness of 0.2 μm, with a $d_c = 5.005$, 5.010, 5.015 μm column operated in parallel with a 5.000 μm column, there will be 23%, 54%, and 72% plate loss, respectively compared to the 5.000 μm column alone. Finally, the entry and exit from a multicapillary column also need to be considered. If a multicapillary column connects for example to a single cylindrical header that has an i.d. fitting the o.d. of the multicapillary assembly, the fluid that comes through that header tube does not have a velocity distribution that is radially uniform. To start with, the fluid will enter the peripheral tubes in the multicapillary assembly with a lower velocity than those at the center. Similar considerations will apply for the conduit connecting the exit of the multicapillary separation conduit and the detector.

Micropillar array columns (μPACs) are microfabricated HPLC columns that can be considered both packed or OT columns, perhaps more of the latter than the former. Microfabricated pillar columns were first introduced by Regnier's group [112]; the topic has since been extensively reviewed [7,113,114]. However, the present generation of μPACs must be credited to Desmet and de Malsche [115,116], who were also the first to demonstrate the attainment of a million theoretical plates in a liquid chromatography column [117]. Fig. 5(a) shows a μPAC column conceptually. To get enough capacity, the silicon pillars must be oxidized (by anodic oxidation in HF, a 300–500 μm porous layer can be created as shown in Fig. 5(b). Then to get functionality, the oxide layer can be reacted with a suitable organosilane. Inlet and outlet flow distribution must be critical to get equal flow into the parallel channels, a flow distributor is shown in Fig. 5(c). An actual silicon micropillar array is shown in 5(d), the pillar radius and interpillar spacing (wall to wall) are both 2.5 μm; these have already been oxidized and functionalized with C18. A practical consideration on microfabricating such columns is the longest length of a lane that can be made; this depends on the wafer size - the capital cost of equipment to handle the wafers increases exponentially with the wafer diameter. As such, at the present state of affairs, it is common to concatenate multiple shorter columns on the wafer (Fig. 5(e)). A complete finished column assembly from Pharmafluidics (now Thermo Fisher) is shown in Fig. 5(f).

In essence, the μPACs can be considered multicapillary OT columns where flow differences between the individual paths are self-correcting [118]. In a recent analysis, Desmet et al. show that at low flow rates (sub-10 μL/min) μPACs will provide greater efficiencies than packed columns and can prove to be superior even at higher flow rates if interpillar distance can be reduced [119]. Although μPACs have been commercially available for the last few years, they are not as yet widely used. The cost of microfabricating such columns (which are hardly used as widely as semiconductor components) is still substantial. Some limitations of the microfabrication technologies were discussed early on [120], but this will continue to improve and evolve, only the future will define whether they will become competitive on a price/performance basis.

3. Zone electrophoresis

By far the majority of analytical electrophoretic separations today are carried out in the zone electrophoresis mode where a small plug of the sample is injected at the head of a capillary/microchannel electrokinetically or by pressure/gravity. Typically, the channel is filled with a solution of a background electrolyte (BGE, free solution electrophoresis)

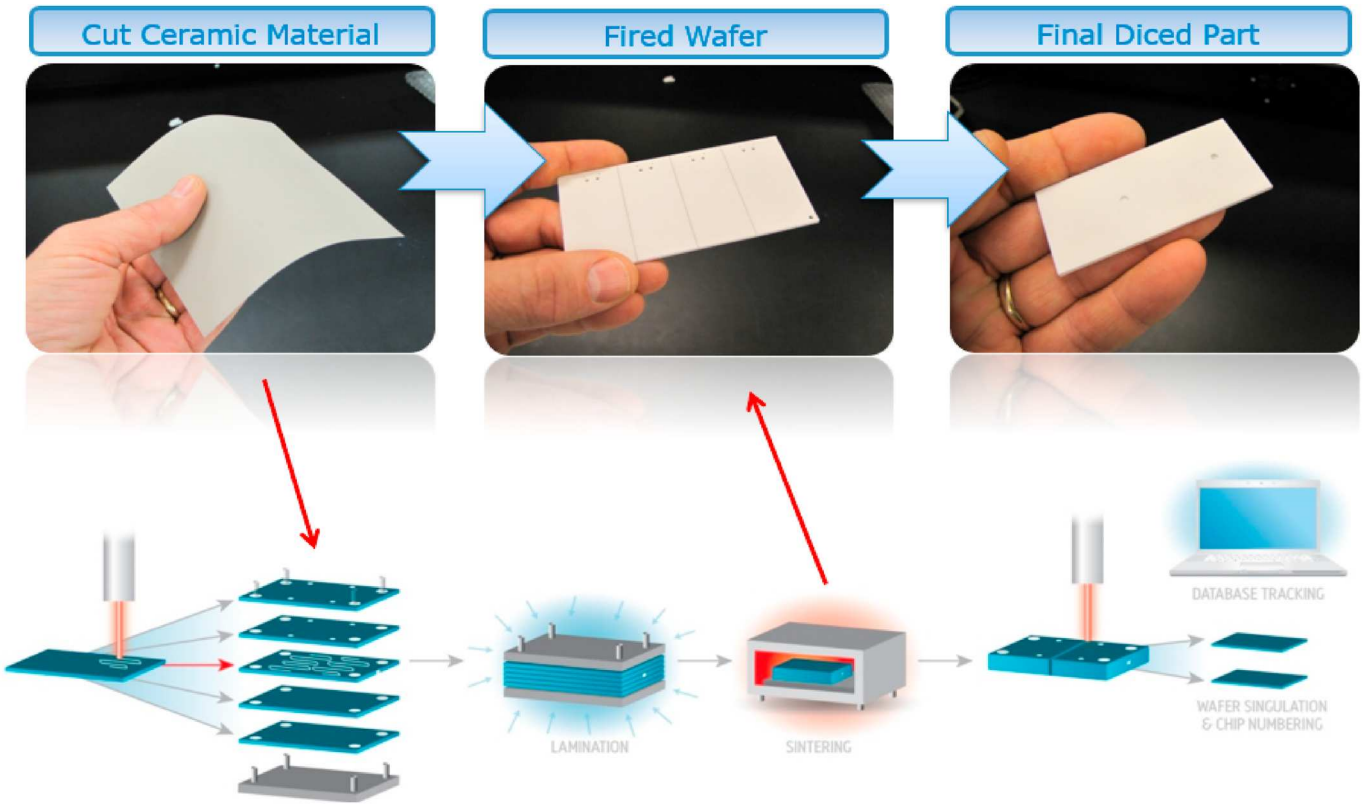

Fig. 4. Workflow diagram for the fabrication of the ceramic mHPLC chip (iKey/MS) from Waters Corp. The separation channel is laser engraved on a central ceramic sheet that is sandwiched between other similar sheets that provide both sealing and inlet access. These are then sintered together to form a sealed device capable of withstanding 10000 psi. Courtesy Jim Murphy, Waters Corp.

but may in addition be filled with a lightly crosslinked gel (capillary gel electrophoresis, CGE). The modern era of capillary zone electrophoresis (CZE; this original term has now become CE; presently CE is hardly ever conducted in any other mode) was ushered in by Jorgenson and Lukacs [121] in 1981, using 75 μm φ, 550 μm od, lab-drawn glass capillaries. Although in this classic work (cited now more than 3000 times) the authors credit Mikkers et al. [122] as the pioneers for their work on zone electrophoresis in 0.2 mm μm φ, 0.35 mm OD PTFE capillaries (these authors had termed their efforts high performance zone electrophoresis (HPZE) and credited earlier work of their own group and the thesis work of Virtanen for originating these efforts, while stating the equipment available to the latter was poor). To the present-day reader there is a gulf of difference between the execution, exposition and the quality of the electropherograms between the works of Jorgenson/Lukacs and Mikkers et al. By far the majority attributes the origin of the current practice of CE to Jorgenson/Lukacs.

Mikkers et al. have long worked on isotachophoresis (described later in this review) and their work made use of equipment originally developed for that purpose. Beyond what has already been stated, some of the other key differences between the two efforts involve injection and detection conditions. Conductivity detection is typically carried out using an alternating voltage, this is difficult to apply in the presence of a high DC electric field. If a constant current i is applied through the system, however, the potential difference ΔV between any two adjacent locations (the volume therebetween being the effective detection volume) is a direct measure of the resistance R ($=\Delta V/i$) and hence, the reciprocal of it to conductance. This was generally referred to as potential gradient detection. Mikkers et al. used constant current mode of operation (20–100 μA) and utilized potential gradient or 254 nm UV detection throughout. They used a modified 4-way injector valve; earlier they had also used a microliter syringe through a tap and other similar approaches to inject. Jorgenson/Lukacs used constant voltage operation throughout; indeed, all illustrative examples in their original paper used 30 kV as the operating voltage (the limit of their HV supply), and electrokinetic migration of the analytes into the capillary for injection. The analytes were tagged with various fluorophores in their work and detection was accomplished with a custom-built fluorescence detector.

Electrophoretic separations on a microchip were introduced by Harrison, Manz et al. [123]. The principles are fundamentally the same as that in CE but this pioneering article not only integrated electrokinetic injection into the chip, it also clearly outlined the possibilities of more complex on-chip sample manipulations.

3.1. Principle of electrophoretic separations

In an electrophoretic system, an analyte moves from the injection to the detection point as governed by its electroosmotic mobility (μ_{eo}) as well as its electrophoretic mobility (μ_{ep}). The first of these is dependent on the zeta potential (ζ, the potential at the interface of the solution and the separation conduit surface). For most cases of native polymers or glass/silica, this is negative at neutral pH but can be rendered positive in some cases at low pH, or more effectively by surface modification through coatings or covalently bonded cationic functionalities. It can also be made zero or near zero if desired. When ζ is negative and the separation conduit is of small diameter, the BGE cation, say Na^+, moves in the field direction (+ electrode to – electrode). The water of hydration associated with the sodium ions are hydrogen bonded to each other, this, as well as the viscous coupling result in both the ions and the associated solvent in a particular field-plane moving in the field direction as a single united front. This can only happen in conduits that have a small characteristic dimension (viz., radius for a circle, the smaller of the two sides for a rectangle), as the perimeter/cross section or surface/volume ratio increases with the reciprocal of the characteristic dimension. Otherwise, the electroosmotic force generated at the wall is insufficient

to move the entire fluid in a cross-sectional front, only surface flow or local (re)circulation results. In channels of small cross section, however, the fluid moves with a flat velocity profile, unlike pressure-driven flow, where under laminar flow conditions, the velocity profile is parabolic, the root cause of band dispersion for flow in an open tube.

The electrophoretic mobility μ_{ep} of any ion is related to the infinite dilution equivalent conductance λ_0 by the Faraday Constant, F

$$\mu_{ep} = \lambda_0/F \ \ldots \tag{6}$$

For most small ions, λ_0 values can be easily found tabulated in textbooks (see, e.g. Ref. [124]) and μ_{ep} thus calculated. The overall velocity of an analyte, ν_{tot}, is the vector sum of the electroosmotic and electrophoretic velocities (ν_{eo} and ν_{ep}), each of which being the products of the electric field strength E and the corresponding mobilities:

$$\nu_{tot} = \nu_{eo} + \nu_{ep} = E\,(\mu_{eo} + \mu_{ep}) \ \ldots \tag{7}$$

The field strength E is taken as positive when the injector is +ve with respect to the detector. In eq (7) all terms can have either sign. Here we consider the migration velocity to be positive when the movement is towards the detector. When ζ is -ve, μ_{eo} is +ve. Similarly, μ_{ep} is +ve for anions and -ve for cations. As a result, many scenarios are possible, the net velocity can be negative to zero to positive. Of course, in the manner we define velocity, if the velocity is zero or negative, the analyte will never reach the detector. Most commonly, the analyte is anionic, ζ is -ve, E, and μ_{eo}, are all + ve. If the analyte is a cation, μ_{ep} is +ve, both electroosmotic and electrophoretic movements occur in the same direction, ν_{tot} will obligatorily be positive and the analyte is certain to reach the detector. If it is negatively charged, μ_{ep} is -ve, electroosmotic and electrophoretic movements oppose each other and μ_{eo} must exceed μ_{ep} for the analyte to reach the detector. For cases where ν_{tot} is negative, reversing E will also reverse the situation. A change in the pH can be a very powerful fine adjustment tool, however. Decreasing the pH makes ζ more positive, thereby causing μ_{eo} to be less positive and for protolyzable analytes, this can also lead to their becoming more positively charged, hence effecting an increase in μ_{ep}. In this context, note that if the analyte charge and ζ are opposite in sign, some degree of chromatographic interaction with the wall is unavoidable but is generally ignored.

Consider that the electric field E is created by applying a voltage V over length L. For simplicity, we assume that this is the same length in which the separation occurs; this is not strictly true either on a capillary or a μchip platform, as either grounding point - detector location or the injection point - HV origin are not the same. Thence

$$E = V/L \ \ldots \tag{8}$$

and the time for the analyte to reach the detector, the migration time t is given by:

$$t = L/\nu_{tot} = L^2/((\mu_{eo} + \mu_{ep})V) \ \ldots \tag{9}$$

The minimum locational variance σ_L^2 as the analyte enters the

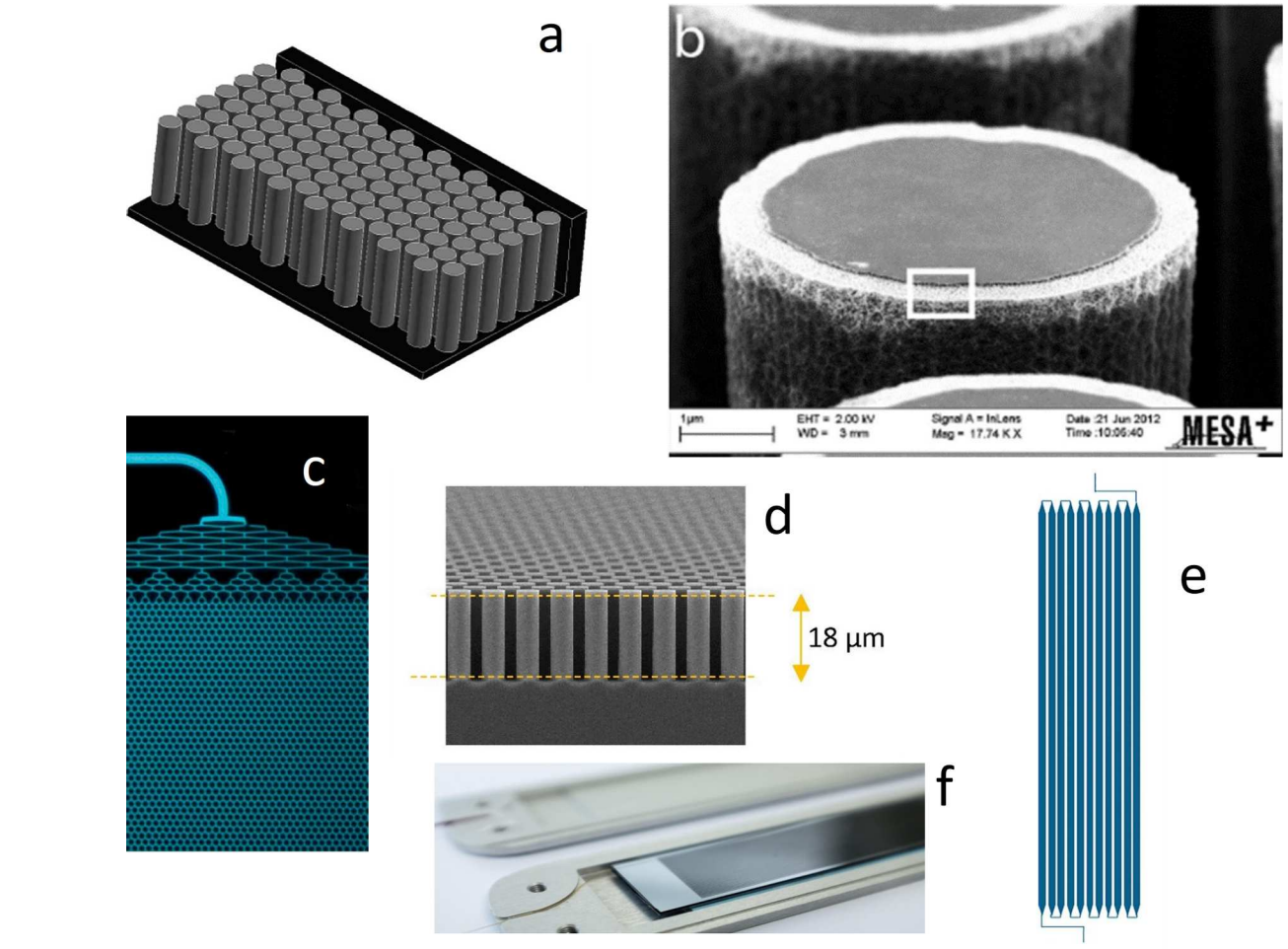

Fig. 5. (a) A conceptual view of a μPAC column. (b) To have meaningful capacity a 0.3–0.5 μm-thick porous layer is created by anodic oxidation in HF (c) An inlet flow distributor (d) An actual micropillar array, the pillar radius and interpillar spacing (wall to wall) are both 2.5 μm; these have already been oxidized and functionalized; (e) Separation channels. 10 lanes, each 5 cm long and 315 μm wide. The pillar-filled lanes are concatenated into a 50-cm long separation column. (f) a complete commercial column from Pharmafluidics, now Thermo Fisher). Courtesy of Prof. Gert Desmet, Vrije Universiteit Brussel (VUB).

detector after time t will be given by (this assumes the variance at the injection point is zero and thereafter the only contribution to the variance is diffusion, the diffusion coefficient being D):

$$\sigma_L^2 = 2\,Dt = 2\,D\,L^2/((\mu_{eo} + \mu_{ep})V)\ \ldots \quad (10)$$

If the chromatographic concept of theoretical plates is applied, the number of theoretical plates, N, will be given by:

$$N = L^2/\sigma_L^2 = L^2/(2\,Dt)\ \ldots \quad (11)$$

Substituting the denominator in eq 11 with the expression in eq 10 gives:

$$N = L^2/\sigma_L^2 = (\mu_{eo} + \mu_{ep})V/2D = \nu_{tot}/2D\ \ldots \quad (12)$$

The expression in eq 12 is simple and elegant, but also potentially misleading as will be seen below.

3.2. Implications of the model

In our model, the sole contributor to band broadening is diffusion and thence only factor that governs the efficiency is the time the analyte spends undergoing diffusive broadening. Except for effects of temperature, viscosity of the solvent, etc., the diffusion coefficient of an analyte is an intrinsic property that cannot be altered. In eq 11 therefore, the sole way that N can be increased is to reduce the migration time t, which is accomplished by getting the net velocity to be as high as possible, thence V alone can control N; the two are linearly related to each other. This view overlooks two unrelated issues. The first is encountered in chromatography as well, a direct parallel exists for example in OTLC, where diffusive transport in the mobile phase is also the sole/primary contributor to band broadening. As a result, analytes with the lowest retention factors are often observed to have the highest N. Having a high N does little towards resolving two peaks which both elute early, however. Indeed, when other efforts fail to increase the differences in their retention, in a seeming paradox, we resort to a longer column or a more retentive stationary phase, both of which actually increase the retention time and hence diffusive broadening. Electrophoresis often offers more facile control of analyte velocity over chromatography in that both μ_{eo} and μ_{ep} may both be manipulated, e.g., by pH. The electroosmotic mobility is changed by changing ζ, whereas the effective μ_{ep} is changed by changing the fraction, f, of the analyte that exists in the ionized or protonated form, the effective μ_{ep} being the product of f and the mobility of the fully ionized/protonated form. The second overlooked issue is discussed in sec. 3.4.

3.3. An illustrative challenge

The basic separation challenge is to separate two analytes with very close μ_{ep}. The electroosmotic mobility μ_{eo} will add to μ_{ep} in both cases to determine the overall mobility. If we have a μ_{eo} of the same sign as μ_{ep}, the higher the μ_{eo}, the greater will be ν_{tot} and the N. Yet, the relative difference in overall mobility of the two species will decrease as μ_{eo} increases, the separation will be poorer, regardless of an increase in efficiency. A particularly powerful prospect arises when μ_{eo} and μ_{ep} have opposite signs. If we make μ_{eo} exactly equal in magnitude and opposite in sign to that of the analyte with the lower μ_{eo}, its net mobility will be zero, it will sit stationary while the analyte with even slightly higher μ_{ep} will reach the detector. The situation is analogous to a swimming meet: two swimmers with very close abilities cannot be differentiated if the competition is over a relatively short length, but there will be eventually a differentiation if the course is long. In electrophoresis, we cannot make the separation length increasingly longer: if we apply the same voltage the field strength will decrease; if we try to keep the same field strength, the voltage needed will become unmanageably high. In a swimming competition we can make a swimmer swim a longer distance over the same duration, if (s)he is swimming upriver (against the current) or in a so-called "infinity pool" where a very substantial counterflow is created.

A remarkably powerful illustration of this approach is the work of Yeung and Lucy [125] who separated ^{14}N and ^{15}N as their corresponding NH_4^+ ions. Two factors were utilized: The first of these is that $^{14}NH_4^+$ with the lighter isotope has a slightly higher K_a than $^{15}NH_4^+$, as a result there is a maximum relative difference of the effective μ_{ep} of the two at a certain pH. A positive E was used, normally the μ_{eo} would also have been positive but an opposite μ_{eo} almost exactly equal in magnitude to that of the effective μ_{ep} of $^{15}NH_4^+$ was created by coating the capillary with a judiciously chosen mixture of a neutral and a cationic surfactant. With only 20 kV applied, the authors were able to baseline resolve the two isotopomers in 11 min.

Another major challenge is separating DNA mixtures where the analytes vary in the number of base pairs. As more base pairs are added, the charge of the molecule increases proportionally but so does its size. The electrophoretic mobility, which depends on the charge to size ratio, does not change markedly with the number of base pairs and free solution electrophoresis is not effective to achieve a separation. If a crosslinked gel-filled capillary is used however (CGE), the longer molecules experience significant retardation because of the necessity to navigate through the gel and excellent separations can be achieved [126].

3.4. Increasing voltage is not a panacea

As previously stated, eq 12 indicates that increasing voltage increases efficiency. However, this overlooks another factor implied as the second issue in section 3.2. As current passes through the BGE, Joule heating. equaling V^2/R, occurs where R is the resistance of the solution. Heat is generated throughout the solution but can be dissipated only through the outer wall, leading to a radial temperature gradient, from the center to the outer wall. An increased temperature increases electrophoretic mobility, so an analyte at the center travels faster than one located closer to the wall. As the solution is progressively heated as it travels down the conduit, an axial temperature gradient can also develop. This only exacerbates the axial dispersion.

A circular cross section provides the lowest surface/volume ratio compared to a rectangular/square cross section and is not the best for heat dissipation. The surface/volume ratio is inversely proportional to φ and heat dissipation becomes worse as φ increases. For the same BGE, R decreases inversely with φ^2, heating increases proportionally, further compounding thermally induced band dispersion. As μchip channels typically have rectangular cross section, it may seem they would be better in aspects of heat dissipation, but they are typically made with thicker walls and the materials are substantially less thermally conductive compared to fused silica, the capillary material used in the vast majority of CE studies.

3.4.1. BGE resistivity and upper limit of analyte concentration

At the same applied voltage, Joule heating can be minimized by increasing R, which is possible by decreasing the concentration of the BGE. With simple electrolytes, the practical limits to which this strategy can be deployed is modest. Because of electroneutrality requirements, the peak analyte concentration (in eq/L) cannot exceed the BGE concentration without causing severe peak distortion. Low conductivity zwitterionic BGEs (amino acids, Good's buffers [127]) that also behave as pH buffers have proven effective from this standpoint; these can maintain electroneutrality even in the presence of relatively higher analyte concentrations via a change in pH.

4. Optical detection

Most optical detection methods rely on the absorption of light by the analyte, typically in the ultraviolet–visible range. The detector itself consists of a photosensitive semiconductor or a photo-emissive plate which generates a measurable electrical signal proportional to the

number of photons it receives. Ultraviolet/Visible (UV/Vis) Absorbance Spectroscopy, Fluorescence, and Chemiluminescence detection, all have been used widely in miniature separation systems. Optical detection systems in μfluidic chips have been specifically reviewed [128,129] and a recent review demonstrates the state of the art for optical detection integrated μfluidic chips for biochemical analysis [37]. In CE, absorbance detection has been the mainstay; it can be particularly useful for large biomolecules [130,131].

4.1. UV/Vis absorbance spectroscopy

4.1.1. Introduction and theory

Traditional optical absorptiometry measures the decrease in the transmitted light intensity (I) compared to the original light intensity (I_0) by passage through a path of length l and an extinction coefficient α following Bouguer-Lambert's law [132].

$$I = I_0 10^{-\alpha l} \ldots \quad (13)$$

Absorbance (A) is then computed from

$$A = \alpha l = \log\left(\frac{I_0}{I}\right) \ldots \quad (14)$$

To chemists, the important addendum of Beer that the extinction coefficient α can be given as the product of the molar extinction coefficient ε and the molar concentration of the absorbing species c is paramount for quantitation:

$$\alpha = \varepsilon\, c \ldots \quad (15)$$

The overall principle should ideally be called Bouguer-Lambert-Beer's law if proper chronological sequence is followed, but all possible variations have been used; for an excellent article on this venerable principle see Ref. [133].

UV/Vis absorptiometry is easily the most common optical detection method for conventional macroscale separations. Many compounds absorb light in the UV/Vis range of the electromagnetic spectrum, so this detection method can be applied to many types of analytes. In some cases, especially in ionic analysis, whether by IEC or CE, electroneutrality holds. To detect an optically non-absorbing ion, the eluent/background electrolyte is deliberately chosen to contain an optically absorbing ion of similar charge polarity: the emergence of the non-absorbing analyte is indicated by a concomitant and equivalent decrease in the absorbing ion concentration [134]. Application of this principle in CE has been specifically reviewed [135]. However, such a detection method is attractive only when the analyte has no useful optical absorption, or the absorptivity is very low. The presence of an absorbing ion in the background raises the baseline, which increases noise and thence a poorer LOD than what is typical in direct absorbance detection.

Direct absorbance measurement is much more common. In conventional scale HPLC absorbance detectors, the best performance is considered to be that when the detector is shot-noise limited [136], i.e. the detector performance is limited by the amount of light reaching the detector. As Kraiczek et al. have appropriately noted [137]: … *a shot-noise limited detector is not necessarily a good detector,* but the irony is that is the best we can do. Shot-noise limitation simply implies that all other sources of noise, e.g., flow and thermally induced noise, Johnson noise etc., have been minimized by technical advancements to the point that the statistical noise from the number of photons reaching the detector (i.e., the intensity of the available light) has become the limiting factor. In going to a miniature system, whether a capillary column or a μFSD, the simplest and the most obvious way to implement absorbance detection would be to measure the absorbance across the channel, immediately at the fluid exit, ideally past any bed support, weir or equivalent, preferably in a continuation of the same channel. This effectively equates the transverse dimension of the separation channel to the path length l. Equation 14 indicates that the decrease in l will be directly reflected in the measured absorbance and the attainable concentration LOD will deteriorate proportionally. In fact, it may be worse than simply comparing with a macrosystem on the basis of pathlength only, because the reduced aperture necessary for a small channel will cause a substantially smaller amount of light to reach the detector, thus increasing noise. A laser source may solve the light throughput problem, but such sources are inherently noisier than most other light sources, and only a limited number of wavelengths are easily accessible. On the other hand, there are clear limits to how tightly light from a broadband source typically used in UV–Vis absorbance measurement can be focused to accommodate a small aperture. It is also important to note first that if a detector is shot-noise limited, the absorbance noise will increase with the reciprocal of the square root of the photon flux reaching the detector; to avoid excessive stray light, there is an obvious upper limit of the aperture that can be used in a miniature detector. Absorbance increases with path length; however, detection limits do not continue to improve with path length without bounds; past a certain point, light throughput becomes poor enough that more is lost in increased noise than what is gained in increased absorbance. For a shot noise limited detector, the maximum path length L_{max}, beyond which there is no advantage in increasing the pathlength, is given by eq. 16 [138] where α_b is the extinction coefficient of the background medium:

$$L_{max} = \frac{2}{\alpha_b} \ldots \quad (16)$$

Beyond the transparency of the fluid serving as the background, α_b is markedly lower and thus L_{max} is proportionally higher when the conduit behaves as a liquid core waveguide (LCW).

4.1.2. Exploring cell geometry

Several alternatives have been explored towards how a suitable UV–Vis detection arrangement can be implemented in a miniature analysis system that provides for a path length greater than the transverse/radial path. A general review is available [131]. Greater pathlengths at the end of the separation conduit have been attempted with a bubble cell (or simply increasing the channel diameter) and z-cell [139] designs. Even within a radial/transverse geometry, for example in an OTLC setup, limits of detection can be improved by increasing the length of the illuminated zone – although this does not increase the pathlength, the light throughput increases and thus reduces noise. However, increasing the illuminated length, no matter whether the light travels axially or radially, does introduce extra band broadening, which leads to less efficient registration of the actual separation, especially when the conduit bore is deliberately changed to increase path length as in a bubble cell [140]. Often it is a compromise: How much increase in peak variance is acceptable as penalty for gaining a certain amount of sensitivity? Kadjo et al. [138]. has provided detailed values for OTLC columns of d_c = 1–50 μm and column lengths of 10 and 100 cm, the maximum allowable illuminated detection zone length for a 1%, 2%, 5%, 10%, 25%, and 50% plate loss for a reduced plate height value of 0.1. For d_c = 5 and 20 μm, for 10(100) cm column length this illuminated length ranges for example, respectively from 77(240) and 160 (490) μm for 1% plate loss to 390(1200) and 780(2400) for 25% plate loss. They also similarly provide maximum allowable illuminated cell volumes for packed columns of specified efficiency.

Increasing the axial path length for a capillary column whether packed or OT is nontrivial. Chervet et al. [141]. created a U-shaped cell that was used with a nanoflow liquid chromatograph for protein separations and achieved an LOD of 0.5–3 fmol. Sestak et al. [142] created a L-shaped cell; they inserted the exit end of a packed column into the shorter arm of the 0.15 mm i.d. fused silica L-cell. Light was introduced through the L-bend and the uncoated silica capillary, behaving as an LCW, provided for efficient light transmission. The exit light was transmitted thorough a 100 μm optical fiber (Fig. 6). The authors

demonstrated attractive operation over 500–2700 μm path lengths with corresponding volumes of 9–50 nL; an excellent upper limit of photometric linearity (2.2 absorbance units (AU)) was demonstrated.

Subsequently these authors incorporated a second, transversely illuminating light source to excite axially read fluorescence, exploiting the LCW properties of the system [143]. The axially transmitted light was read by a multiwavelength charge coupled device (CCD) array spectrometer, permitting simultaneous absorbance and fluorescence detection (Fig. 7) [144]. More recently, these authors introduced a capillary flow cell in which a tapered optical fiber is inserted and fused to one end of a 150 μm i.d. capillary and serves as the light input fiber (Fig. 8) [145]. At the other end of the cell (3–10 mm long, volumes 55–175 nL), the tapered end of a 50 μm i.d. capillary, functioning as the inlet tube, is inserted until it reaches the other terminus. The transmitted light is conducted to the detector by a 100 μm core high-OH silica fiber. The gap between the exit fiber and the cell wall served as the liquid outlet. A filtered high output 265 nm UV LED is used as the light source. The optical arrangement used no focusing optics and/or slits. They reported noise levels below 50 μAU, and effective optical path lengths 83–97% of the cell's physical length and linearity (<1% deviation) to 1.7 AU. It is expected that as in this paper, light emitting diodes (LEDs) will play an increasingly important role in miniature optical detectors. An early review specifically addressed the use of LED-based light sources for use in absorbance detection in CE [146].

In keeping with such expectations, Hemida et al. [147] demonstrated that a multiwavelength UV absorbance detector is not only possible with multiple UV LED sources using a multifurcated fiber (Fig. 9), it provides excellent performance (>3 AU upper limit of linearity, ~0.3 mAU noise, thus a range spanning 4 orders of magnitude); they used a commercially available Z-path flow cell of 500 nL volume and 10 mm path. The same group has since demonstrated pulsed, rather than continuous, operation of three different UV LEDs as light sources with a fast response photodiode detector [148].

Early on, Yeung and his students explored a unique "on-column" absorbance detection approach which utilized the entire length of the column as the detection path [149]. An OTLC column terminated at each end in a tee; liquid entered and exited through the perpendicular arms and optical fibers provided light I/O via the through ports. The arrangement was adapted for CE, both with a laser [150] and a broadband light source [151]. In principle, if the column behaves as an LCW [152] then the arrangement can provide good light throughput [150]. The astute reader will perceive that when the sample is injected into the separation conduit, the observed absorbance is the sum of all the absorbances of the individual analytes. This absorbance will decrease as the analyte(s) begin to elute off the column and thus are removed from the light path. The absorbance (A) vs. time plot will thus represent a descending staircase; the conventional chromatogram will be the negative first derivative vs time ($-dA/dt$ vs. t). This can be advantageous in that the volumetric resolution is not controlled by the entire column volume but is equal to $F\Delta t$ where F is the flow rate and Δt is the time interval for each acquired signal datum. The downside is that differentiation increases noise and deteriorates the LOD. Another, and perhaps intrinsically more troublesome problem of this arrangement is that such a scheme can work meaningfully only if the total absorbance due to the sample is modest. Otherwise, light throughput will be poor, and noise will be high. The presence of a single highly absorbing component can be problematic and even more so if it elutes from the column late in the separation.

4.1.3. Multireflection cells

Perhaps the most straightforward means of performing on-column detection with a pathlength greater than the radial path, without bending the conduit or any other geometric manipulation, is to design the detection zone as a multireflection cell. This was originally introduced with a focused laser source almost three decades ago [153] and patented [154] but never commercialized. Relative to a cylindrical capillary, it would seem more straightforward to adapt the approach to a planar μchip. Accordingly, Harrison and his students demonstrated the utility of the multireflection principle for 10–30 μm deep channels for glass μchip-based electrophoresis [155]. Aluminum mirrors were evaporated on the outer surfaces of the channels. With laser light I/O through 30 μm apertures placed 200 μm apart, they were able to get effective path lengths 5–10x greater than the channel depth. It is simple to compute, depending on the angle of incidence, the number of reflections and hence the anticipated path length. However, the observed path length was substantially lower than that computed and upper linear dynamic range was also relatively limited at 0.5 AU. Interference of the coherent light used in this study is possible, as the expanding beam of one reflection begins to overlap with the preceding reflection. The device then can act as an etalon, creating output intensities that depend on the incidence angle, and the possibility of fringe patterns within the device that lead to dark zones within the fluid channel and reducing the effective pathlength. Ellis et al. [156]. examined the utility of a multireflection cell with an LED source for use in a Flow Injection Analysis (FIA) system; the cell was decidedly of much larger bore (0.8 mm φ) than would be used in a miniature system. The path length and sensitivity gain were significant but again not as great as may be estimated from the calculated number of reflections. An additional virtue these authors observed was the marked immunity of the absorbance signal to refractive index changes. An LED source based multireflection cell was also examined by Mishra and Dasgupta [157] in the capillary scale. They investigated externally silvered 180 μm φ circular capillaries and 100 × 100 μm square bore (circular 375 μm o.d.) capillaries at incidence angles of 15, 30, 45, 60, and 75° and linear distances between the I/O apertures of 10, 20, 30, and 50 mm. These experiments also showed greater immunity of the absorbance signal to RI changes. While the S/N was better in all cases than a corresponding radial path cell, the striking finding was that the effective path length was actually lower than the physical distance separating the apertures, suggesting that a significant part of the light may be travelling through the wall than the solution. Nevertheless, an LOD of 4 fmol (1 μL of 22.0 nM injected dye) was attainable for injected bromothymol blue. A recent application of the multireflection technique demonstrated a 52-fold increase in pathlength for a μfluidic device using a microplate reader platform [158]; in comparison, the bubble cell and z-cell designs rarely provide for more than a 7–10× path length gain [139,140]. However, an optimized radial path detector can also provide respectable sensitivities.

4.1.4. UV/Vis sensitivity and considerations

The detector developed for the previously mentioned hand-portable gradient capillary LC utilizes high output UV LEDs; with appropriate ball lenses the reported short-term noise levels were 4.4 μAU for a 150 μm pathlength (the packed columns used are of the same diameter) and LODs of 25–300 nM depending on the analyte [159]. This level of absorbance noise is comparable to or better than macroscale HPLC detectors on an absolute basis. More recent publications (see e.g., Ref. [160]) do not show markedly better performance; the typically achievable LODs for microfluidic UV/Vis detection for a strongly absorbing analyte is closer to 100 fmol. The advantages of using UV/Vis detection are that the approach is robust, easy to operate, requires little or no maintenance, and can be used for a wide range of samples. The main disadvantage to UV/Vis detection in the miniature scale is the decrease in path length and the accompanying increase in concentration LODs. To counteract this, specially designed cells or optical arrangements may be needed but that still causes additional dispersion. Some have argued such dispersion is best mathematically corrected for by post processing the data [138].

4.2. Fluorescence detection

Fluorescence detection operates by first exciting sample molecules to higher electronic energy states with the incident light, and then

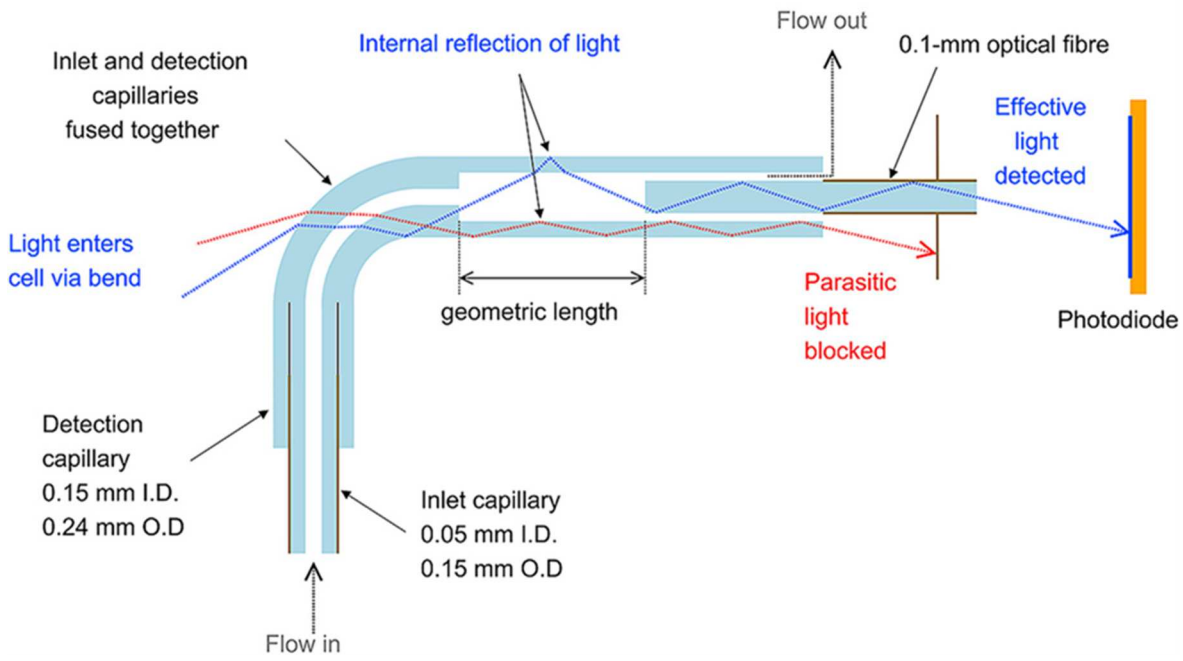

Fig. 6. An L-shaped absorbance detection cell for use with packed capillary columns. Reprinted from Ref. [142].

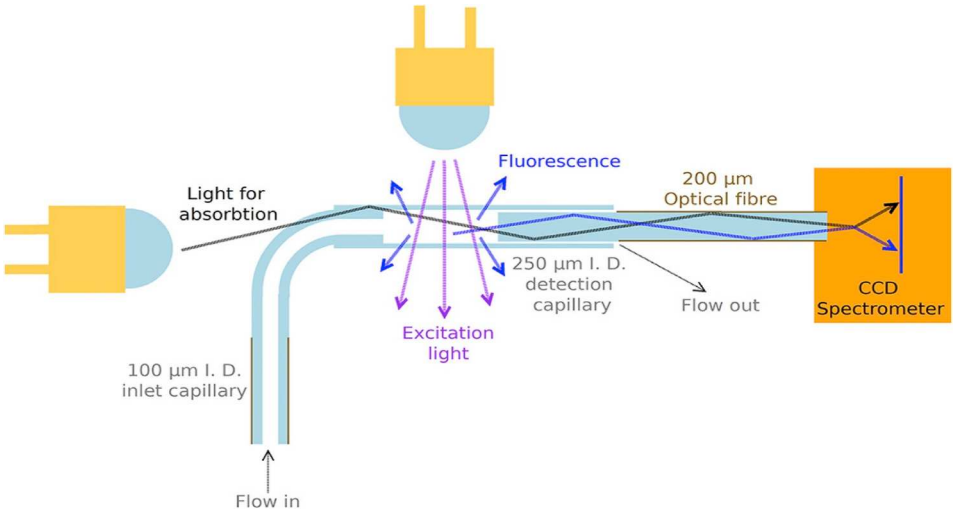

Fig. 7. Simultaneous absorbance and fluorescence detection arrangement with the L-cell. Reprinted from Ref. [144].

detecting the photons emitted by the sample as it relaxes back to the ground state. Emitted photons are detected at a 90-degree angle from the excitation light beam allowing for measurement with near zero background signal; however, total removal of background signal is never possible. The most significant sources of background in fluorescence detection are attributed to stray light from the excitation source and light scattering, be this specular reflection or diffuse scattering from the capillary cell or the microfluidic channel, Raman scattering from the solvent, or Rayleigh scattering from any background electrolytes (most common in CZE). Each source is subject to shot noise, and any flicker noise in the excitation source intensity will add to the noise in the background signal [161]. Rejection of stray/scattered light greatly improves detector performance and optimization is necessary to achieve the best S/N. Fortunately, emitted photons are almost exclusively lower in energy than the exciting photons due to vibrational relaxation of the sample in the excited state prior to fluorescence. This Stokes shift provides the opportunity to reject a majority of the scattered light through the use of simple optical filters. For applications with particularly small Stokes shifts, notch filters may be used to selectively reject the excitation wavelengths and are particularly useful when utilizing laser excitation sources [161]. The process of excitation, vibrational relaxation, and fluorescence occurs on a nanosecond timescale. Thus, there is no measurable band broadening added by the detection method itself, as the entire process of detection occurs in less than a microsecond [131, 162]. The fluorescence signal is proportional to the intensity of the excitation source, the quantum yield of the sample, the probability that an emitted photon will reach the detector, and the signal multiplication rate. The signal multiplication rate is controlled by the detector, typically, a photomultiplier tube (PMT) or an avalanche photodiode (APD), both of which greatly amplify the number of electrons ultimately produced for each incident photon, an essential step for high sensitivity detection. However, the magnitude of noise from this process of multiplication also increases with the amplification factor that cannot therefore be increased indefinitely; the exponential increase in noise

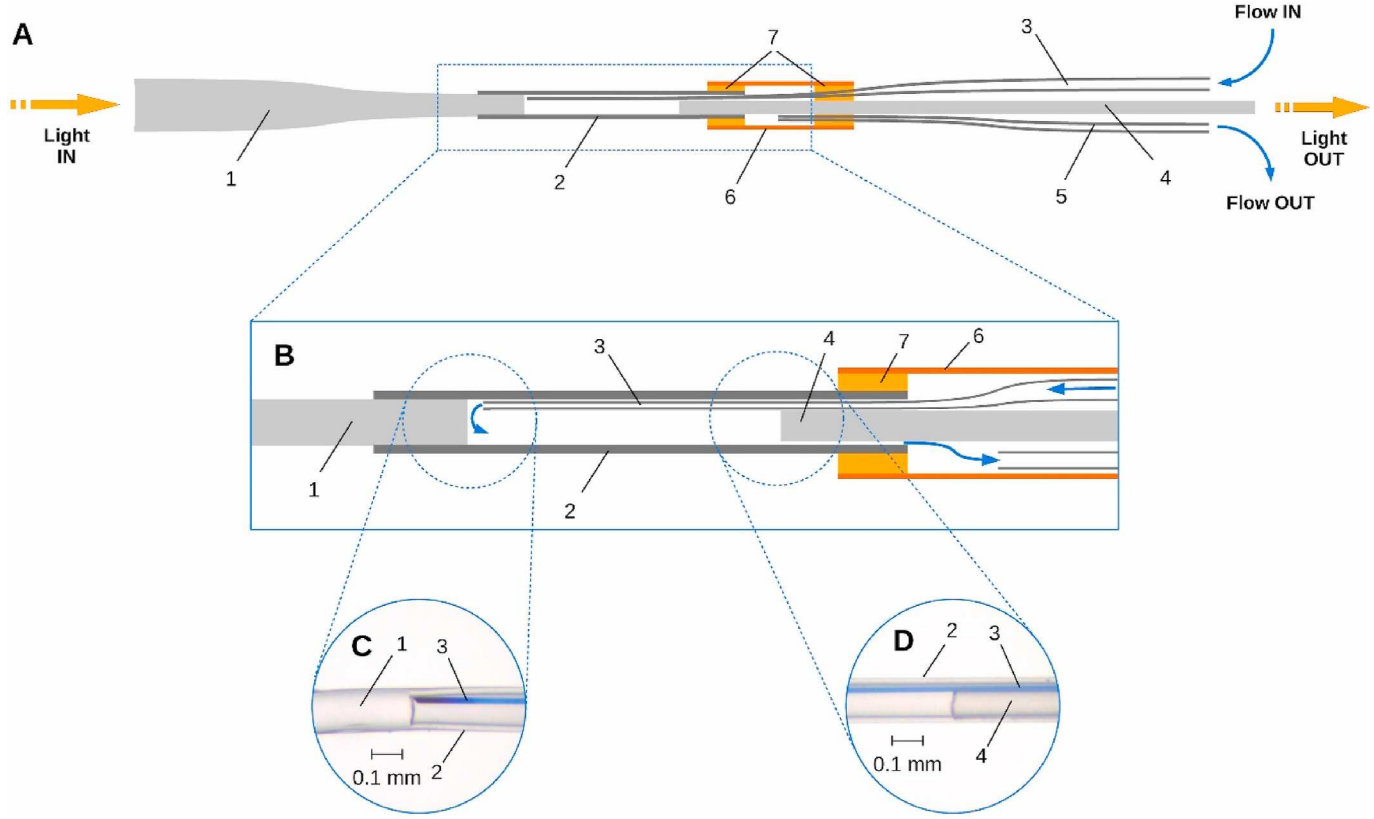

Fig. 8. A,B: Schematic representation of the detection cell design; **C, D:** Photographs. 1 – Light input, a 300 μm optical fiber tapered and fused into the detection capillary; 2 – Detection capillary; 3 – Inlet capillary; 4 – Light output, 100 μm core optical fiber; 5 – Outlet capillary; 6 – Exit envelope capillary; 7 – Epoxy adhesive. Arrows indicate the flow direction. Inlet capillary in C and D is filled with a blue dye solution for better visualization. Drawings not to scale. Reprinted from Ref. [145]. (For interpretation of the references to color in this figure legend, the reader is referred to the Web version of this article.)

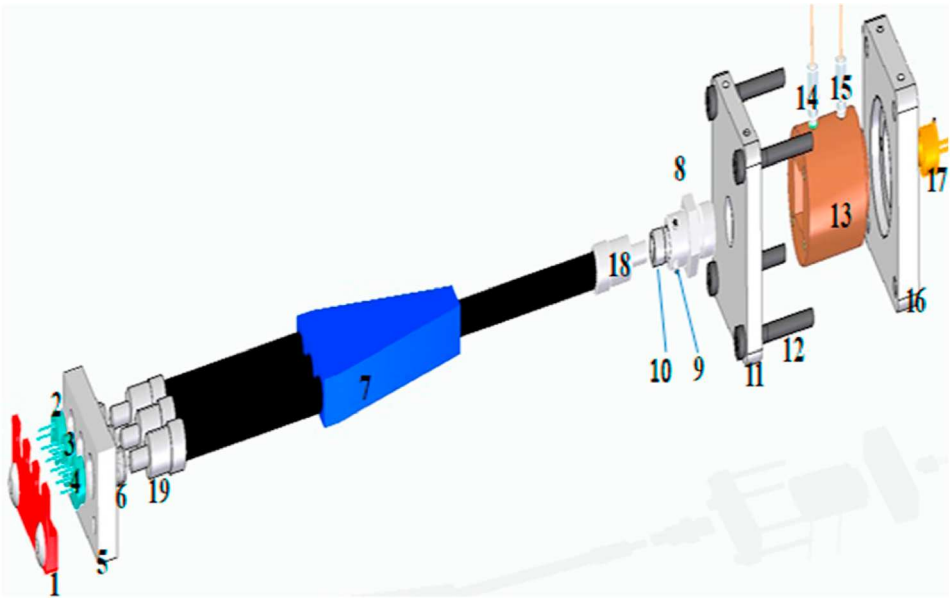

Fig. 9. Tri-LED detector using 245, 255, and 275 nm LEDs. Schematic illustration of the multiple LED-based detector: (1) 3D printed retainer with screws, (2) 240 nm LED, (3) 255 nm LED, (4) 275 nm LED, (5) aluminum mounting block, (6) in-line optical adapter, (7) trifurcated fiber optics assembly, (8) UV collimating lens assembly, (9) grub screw, (10) adjustable barrel, (11) aluminum housing part 1, (12) screw, (13) capillary Z-flow cell, (14) Peeksil inlet connector, (15) Peeksil outlet connector, (16) aluminum housing part 2, (17) Si–UV photodiode detector, (18) SMA connector for common leg, and (19) SMA connector for individual legs. Reprinted from Ref. [147] with permission from the American Chemical Society.

amplification will overtake the signal enhancement. A very detailed recent review on fluorescence-based measurement of polynucleic acids by μchip electrophoresis is available [163].

Laser induced fluorescence (LIF) is the preferred method of fluorescence detection for μFSDs. Fluorescence detection schemes are quite similar between macro and micro devices. However, precision laser light sources are more compatible with the smaller excitation areas utilized in μFSDs [131,164] as well as narrow open tubular columns [165]. A variety of lasers are used depending on the desired excitation wavelength, cost, and commercial availability. In compact LIF detection arrangements, a confocal detection geometry using a microscope objective and a dichroic mirror is the most widely used. A complete arrangement of a liquid chromatography/flow-injection analysis system using 2 μm id tubes and a split-flow (70,000:1) setup that permits sub-pL injection volumes and correspondingly small flow rates is described in detail in Ref. [166]. There are three basic optical configurations of an LIF detector, as illustrated in Fig. 10.

Using a 5 mm window on a 50 μm φ fused silica capillary, an 80 mW 450 nm blue laser diode as the light source and a high-gain integrated photodiode-opamp detector, the authors of this work [167] reported fluorescein detection limits of 40, 50, 1000, and 7000 pM for configurations a, b, c1, and c2, respectively. The authors consider important practical aspects of capillary positioning, alignment of the laser spot, choice of filters, etc. Aided by ray tracing simulations to reduce scattered light, the final orthogonal configuration chosen was able to attain an LOD of 10 pM in a 50 × 20 × 46 mm package.

Fluorescence detection finds the most use in CE, with the bulk of high sensitivity microfluidic applications utilizing CE as a separation method [131,162,168]. LIF detection was applied to detect Alzheimer's indicators in brain tissue samples utilizing capillary migration on a μchip with low amol LODs [169]. LIF detection was also utilized to create a high sensitivity, high dynamic range fluorescence detector for CE on a μchip [170]. The schematic of the detector is shown in Fig. 11(a) with an illustrative electropherogram in Fig. 11(b) magnified at different scales to demonstrate the dynamic range of the detector. The detector utilizes three different APDs, each receiving a different percentage of the total fluorescence signal. APD 1 receives the most signal and is thus the most sensitive, yet it saturates at high fluorescence intensities and cannot measure high sample concentrations. APDs 2 and 3 are intended for measuring signals from more concentrated analytes. This design allows for the detection of a complex sample with a wide range of analyte concentrations, while still maintaining an achievable concentration and mass detection limits as low as 3 pM and 150 ymol (~90 molecules, y = yocto = 10^{-24}) respectively [170]. LIF detection has been utilized to achieve single molecule detection for large biomolecules functionalized with multiple fluorescent tags [171]. One notable publication describes a palmtop CE system complete with a LIF detector, weighing 350 g [172].

LIF is certainly not the only method to achieve high sensitivity fluorescence detection. Recently, much less expensive methods utilizing light emitting diodes (LEDs) have been developed for CE μchips which have seen fluorescein detection limits as low as 10 pM [173,174]. Widely achievable LODs for fluorescence detection of high quantum yield molecules is 1 zmol. The outstanding advantages of fluorescence detection include the extremely low LODs, ease of use, and specificity.

A highly integrated battery-powered, remotely operable instrument that contains a separate sample handling chip and a coupled separation/detection (confocal fiber coupled LIF) chip has been described [175]. The authors report application of the system for amino acid analysis coupled to an extraction unit in order to demonstrate automated sample-to-data operation, the system was remotely operated aboard a rover during a simulated Mars mission in the Atacama Desert in Chile to attain analysis of soil samples relevant to planetary exploration.

The main disadvantage of fluorescence detection is also specificity: an analyte must be able to absorb and fluoresce at a detectable wavelength. In some cases, it may be possible to tag the analyte with a fluorescent label; many biomolecules with reactive functional groups fall in this category. While this extends the suite of analytes amenable to fluorescence detection, it is an added time-consuming step. Often the derivatization agent is itself fluorescent and must be separated from the tagged analytes. Samples that are directly detectable are mostly limited to large (poly)aromatic species. Postcolumn derivatization has the limitations of reaction kinetics, inevitably added dispersion/dilution, and reagent fluorescence; it is rarely used in miniature systems. On the other hand, precolumn tagging is usually inapplicable to small molecules as the tag is typically much larger than the analyte and separation becomes difficult - separation is dominated by the nature of the tag, not the analytes [176]. Sample compatibility remains the main disqualifier for fluorescence detection in many microfluidic applications. Cost of a commercial LIF detector is typically greater than that of a UV/Vis detector. While diode-lasers are making LIF more affordable and accessible, powerful laser sources for UV excitation are still very expensive. Two-photon excitation (TPE) provides a unique solution to this problem. In TPE, analytes are excited by near simultaneous interaction with two photons, promoting the molecule to a higher excitation state than can be achieved by the individual photons. TPE allows for the excitation wavelengths from the UV into the visible and NIR region. It will be readily realized that the probability of a TPE process increases with the square of the excitation light intensity; hence it requires high intensity laser sources. TPE has the benefit of allowing a wider choice of materials in the construction of μFSDs, which would normally prohibit traditional LIF in the UV [177,178], but TPE allows UV absorbing material to be used.

4.3. Refractometry

Refractometry, or refractive index (RI) detection, is often referred to as a universal detection method; this sets it apart from all other optical detection methods, for microfluidic devices. RI detection finds widespread use for this universality, and it is commonly used in conjunction with other detection methods in a complementary or supporting fashion. RI detection, as the name implies, probes the differences in refractive index between the analytes and the matrix solvent. In macroscale RI detection, light incident on the flow cell changes its beam path upon refraction at the cell windows (which remains constant) as well as by the flowing liquid (mobile phase or background electrolyte solution). The light beam exiting the cell falls on a photodiode or preferably an array detector or otherwise position-sensitive detector (PSD). As the presence of an analyte changes the RI of the flowing liquid, the exit beam moves from its previous position where the photodiode was originally placed to collect the maximum amount of light, the decrease in the photocurrent is thus related to the extent of change in the refractive index. It would be apparent that with this arrangement, the optimal placement of the detector will have to change as the original liquid composition (and hence the RI) is changed. If a combination of two photodiodes (this is the simplest PSD/array detector) is used, the initial position may be set such that equal amounts of light fall on the two detectors and their difference is taken as the signal. In this case, a change in RI in either direction from the original RI is easily measured. It will be apparent that the overall applicable RI span is increased with the number of elements in the detector array; in fact, with an appropriate optical arrangement, the RI resolution is improved as well. In microscale LC, PSDs have been utilized for RI detection for 35 years now [179]. In translation from a macro to micro scale, laser-based interferometry has emerged as a simple and effective method of interrogating RI change within capillaries. Most notably interferometric backscatter detection was able to leverage high sensitivity from low nL volume detector cells, a feat for the time, made from short lengths of silica capillary without the need for removal of the polyimide coating [180]. The evolution of which can be seen through a series of publications by Bornhop et al., pioneers of the technique with their microinterferometric backscatter detector (MIBD) [180–184]. Backscatter of the He/Ne laser generates a fan-like interference pattern

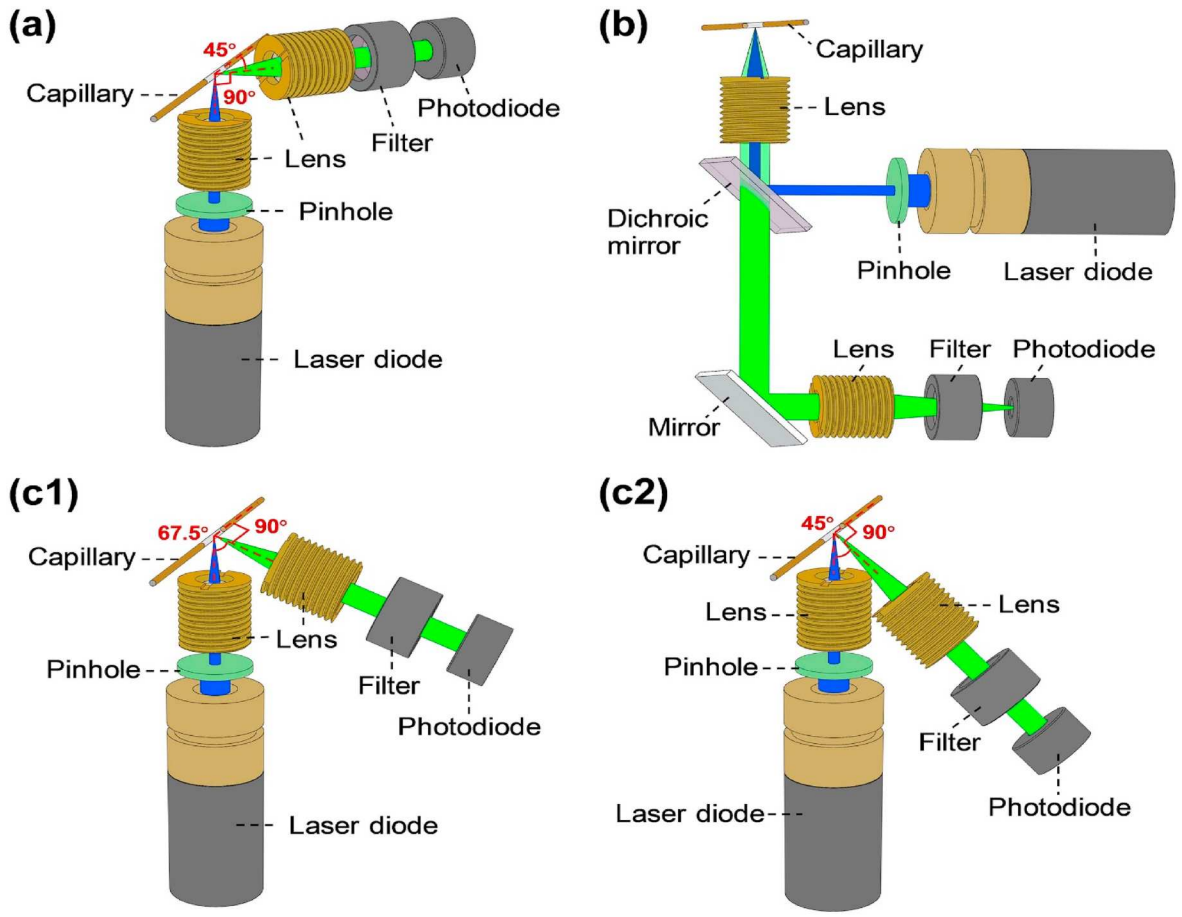

Fig. 10. The three basic configurations of a LIF detector (from Ref. [167]). (a) The orthogonal configuration where the fluorescence emission is detected at a right angle to the incident beam (much as in benchtop fluorescence spectrometers), (b) the collinear confocal configuration where a dichroic mirror separates the fluorescence emission from the incident/reflected laser light, and (c) an oblique detection arrangement where the fluorescence emission is measured at some angle <90° relative to the incident beam – the figure shows two examples at angles of 67.5 (c1) and 45° (c2), respectively. Emission filters are necessary in all the arrangements.

of light and dark fringes which shift based on the RI of the sample. In the original MIBD configuration, the exit light passes through a slit to illuminate a photodetector. Strategic placement of the slit leverages the gaussian intensity distribution of each interference fringe to generate a positive or negative change in photocurrent depending on the direction of RI change in the sample, much like a PSD. Fig. 12 illustrates the interference patterns generated by interference backscatter in the MIBD and the signal observed by the photodetector in each case [182]. More recently, Dunn introduced several refinements in backscatter interferometric detection in the capillary scale. Refractive index is wavelength dependent – if a tunable diode laser source is used and the wavelength is modulated, the interference fringe positions will be spatially modulated, and any overall movement can be very sensitively detected as small phase shifts via a lock-in amplifier [185]. Dunn's group demonstrated the ability to detect ppb levels of glucose in a detection volume of 90 pL. They also showed that the optical pickup head technology used in a typical CD or DVD player can also be used to monitor the interference fringe pattern, enabling a highly sophisticated

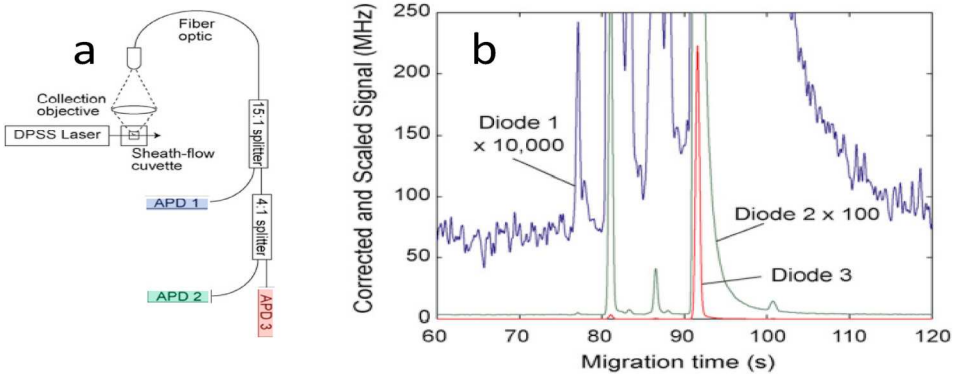

Fig. 11. (a) Schematic of a high sensitivity, high dynamic range fluorescence detector, (b) Electropherogram of complex sample mixture generated by the fluorescence detection. Figure reproduced from Ref. [170].

fL-volume detector that can be constructed very inexpensively [186]. With very thin-wall capillaries to permit efficient heat dissipation and active thermostating to maintain a high degree of temperature stability (±4 m° C), very high speed (under 30 s) separation and sensitive detection of inorganic ions and amino acids were demonstrated in the CE mode [187,188]. With lasers that can be used both as the source for exciting fluorescence and for backscatter interferometry (BSI), an ingenious arrangement has been proposed for simultaneously performing both modes of detection (see Fig. 13) [189,190].

Optical resonance-based detectors that have become popular in recent years also ultimately monitor RI changes. These detectors rely on internally reflected light beams to probe a region for RI change. Optical resonance is observed at specific wavelengths which shift based on the refractive index of the probed region [191]. The most prominent configurations of this exquisitely sensitive paradigm are surface plasmon resonance (SPR) detectors and optical ring resonators (ORRs). The former operates by placing a dielectric medium in contact with a thin metallic film, most commonly gold or silver, resulting in a charge density oscillation referred to as a surface plasmon wave (SPW). This interface is optically interrogated, and optical resonance is observed as surface plasmons absorb the incident light at the frequency of the SPW [192]. Changes in the RI of the region directly beyond the metallic film also changes the resonant wavelength of the interface. The shift in wavelength corresponding to maximum light attenuation is used to relate the refractive index of the sample [191]. The fact that the region probed by SPR necessarily has a very small depth makes it an ideal technique for microscale detection and hence has seen wide use in that format [193,194].

Optical ring resonators operate by coupling specific wavelengths of incident light into a ring-shaped waveguide. The wavelengths that are coupled into the ORR are determined by its effective refractive index and are referred to as whispering gallery modes (WGMs). The most commonly used ORRs are made from thin-walled silica capillaries through which sample is passed. The thinner the capillary, the greater the influence of the sample RI on the effective RI of the ORR. As analytes pass through the ORR, its effective RI changes, shifting the wavelengths of the WGMs. Much like in SPR, incident light is attenuated as it is coupled into the ORR and the shift in the maximum attenuated wavelength is used to relate the RI change of the solution in the cell [195]. Fig. 14 provides a conceptual illustration of a liquid core ORR array as well as a cross-sectional view of a single ORR.

Refractive index detection is universal, yet its sensitivity varies greatly between analytes. RI detection measures the difference between the RI of pure mobile phase and that of the sample, thus samples with RIs far from the RI of the mobile phase will be much more sensitively detected than samples with a RI similar to that of the mobile phase. To normalize the understanding of sensitivity for RI detection, most literature sources report detection limits in terms of refractive index units (RIU) instead of concentrations as concentration can be misleading depending on the mobile phase and sample choice. The sensitivities of resonant RI detectors are commonly reported in the form of nm/RIU, denoting a spectral shift per RIU. Detection limit can be calculated for these sensors by dividing the spectral resolution by the sensitivity, yielding a value in terms of RIU [191]. However, for the purposes of this review to provide comparative LODs among different detection techniques, it would be desirable to find an appropriate conversion of RIU to molarity. Glucose and other sugars are common analytes in many biological analyses and benefit from RI detection as they are not amenable to detection methods relying on light absorption. Thus, glucose will act as a benchmark for the concentration sensitivity of RI detectors. While this is not entirely wavelength-independent, the data in one recent paper for glucose [196] suggests that the expected change should be of the order of 0.026 RIU/M.

Unlike conventional absorbance measurements, RI detection is typically not pathlength dependent and is therefore well-suited for miniaturization. However, the Achilles' heel of RI detection is its extreme temperature sensitivity, an RI detection arrangement must be meticulously temperature-controlled. In macroscale detectors, for this reason, a reference cell is almost always used to compensate for thermal fluctuations and associated noise and drift. High sensitivity RI detectors have reported LODs between 10^{-6} and 10^{-8} RIU for a wide range of compounds which translates to between 400 and 4 μM [194,197]. Considering injection volumes between 0.1 and 1 μL and a reasonable dilution factor of 5–10 from injection to detection, the concentration LODs fall in the mid to low pmol range. It is possible to design more sensitive RI detectors based around specific experimental conditions, for example a micro-ring resonator was used to probe RI with theoretically infinite sensitivity near experimentally determined, "critical RI" values [197].

For general applications, limit of detection is on the order of 100 pmol, less than or approaching that of UV/Vis absorbance detection, although one must note that RI detection is often performed when the analyte does not have useful absorption (e.g., carbohydrates). It thus serves as a complementary detection method to UV/Vis absorption. However, at 190 nm, many state-of-the-art UV–Vis absorbance detectors approach the LODs that RI detectors can achieve for sugars [198]. Importantly, UV/Vis detection is far more compatible with gradient elution whereas gradient elution is largely impossible with RI detection. Refractometry does have some other unique attributes: the molecular weight of an analyte can be determined from the dependence of the refractive index on concentration [199].

4.4. Chemiluminescence detection

Chemiluminescence (CL) detection resembles fluorescence detection in that the analyte is electronically excited and then relaxes by emitting photons that are detected. Fluorescence is a subclass of photoluminescence, indicating the excitation energy comes from photons, in CL, the excitation energy comes from the chemical reaction itself. The analyte can be a direct participant in the reaction (often an oxidation reaction with a powerful oxidant); alternatively, the analyte is fluorescent, or is tagged with a fluorescent tag, or is a catalyst for a CL reaction. In fluorescence, the process of photon absorption and emission occurs within a ns time scale, and the detection process does not add to any band dispersion. Reactions leading to CL occur in a considerably slower time scale and thus can contribute to additional band broadening, noticeably so for fast separations. In some cases, a suitable micellar medium can be used to accelerate the reaction, with a concordant increase in the signal intensity [200].

Many CL reactions have been reported. Some of the more common ones involve luminol, peroxyoxalates, tris(2,2′-bipyridyl)ruthenium(III), or various Mn-based oxidants. Yamaguchi et al. [201], Francis et al. [202], Huertas-Pérez et al. [203], Adcock et al. [204,205], and Brown et al. [206] have reviewed the analytical applications of these reagents, the most common platform being flow injection analysis, however, there is an increasing number of publications on CL detection in CE and μFSD's. One review focuses exclusively on μfluidic CL detection systems [207]; another focuses on electrophoresis based CL detection systems [208]. A recent review exclusively addresses the application of CL detection for food analysis on μfluidic platforms [25]; this paper also points out that a lot of the growth can be attributed to the recent interest in growth of self-contained thread-, paper-, and cloth-based μfluidic devices as well as other disposable *lab-on-a-chip* platforms. Detection by CL may be uniquely useful in such systems, no light source is needed; the detector can be part of a non-disposable reader. Another very recent review on CL detection focuses exclusively on bioanalysis [38].

Luminol reacts with oxidants like H_2O_2 or ferricyanide in alkaline solutions to produce light; with some oxidants a catalyst may be required. Hydrogen peroxide itself is a common measurand of interest as it is produced during the oxidation of a substrate of interest by oxygen in the presence of an *oxidase* enzyme (e.g., oxidation of glucose mediated by *glucose oxidase*, that of histamine in the presence of *monoamine*

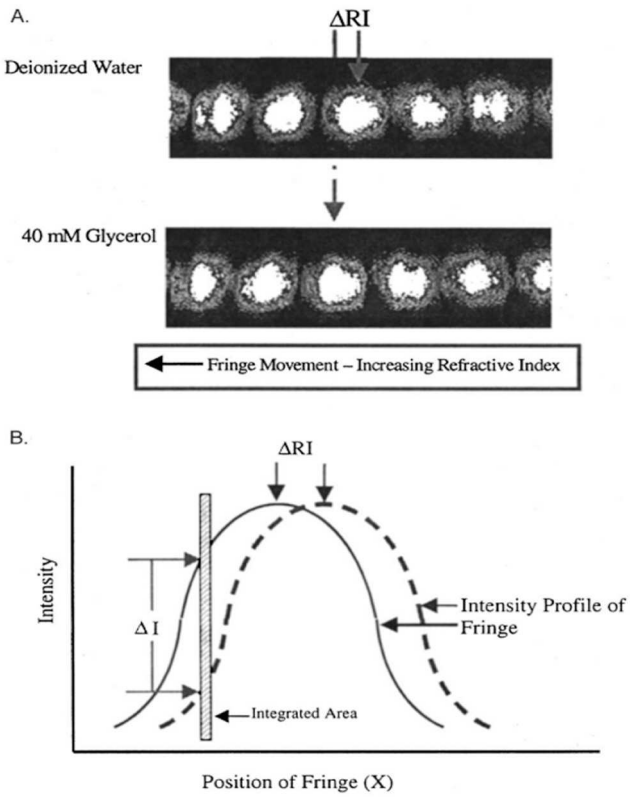

Fig. 12. (A) Reconstruction of the fringe pattern illustrating fringe movement in response to changes in the refractive index of the solution in the probe volume of the MIBD. (B) The pictorial graph illustrating the intensity change observed by the slit/photodetector assembly as a result of fringe movement or a change in RI. Figure reproduced from Ref. [182].

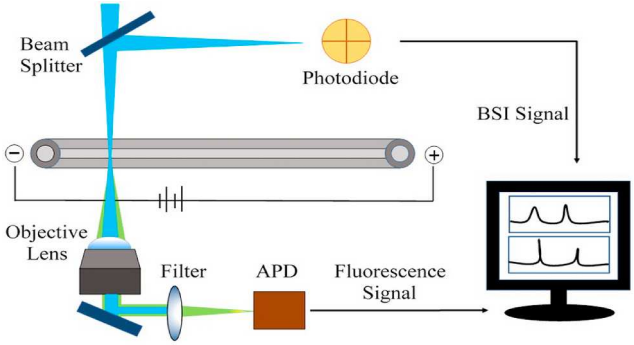

Fig. 13. Schematic of the dual detection high speed capillary electrophoresis platform using a single 455 nm laser excitation source to generate the BSI and fluorescence signals. Excitation light is focused into the detection zone of the capillary and reflected back to form the BSI fringe pattern. A beam splitter reflects the fringe pattern towards a split photodiode detector aligned on two of the fringes. The differential output is amplified and recorded as the BSI signal. Fluorescence excited by the same excitation source is collected from below the capillary with an objective, filtered, and detected with an APD (From Ref. [189] by permission of Nature.com).

oxidase, etc.), in each case producing an equimolar amount of H_2O_2, which is then measured as the surrogate analyte. As such, many analytes of clinical interest can be measured in this fashion: in serum, glucose is present at mM levels, and CL can be measured easily on a μfluidic platform [209]. An attractive example of another luminol CL-based glucose sensor in a cloth μfluidic platform appears in Ref. [210]. Very early on, in one of the pioneering papers on CL detection μfluidics, xanthine, a product of purine degradation was measured via the production of H_2O_2 mediated by *xanthine oxidase* using an on-chip immobilized enzyme reactor [211]. Hydrogen peroxide is also an analyte of considerable interest in atmospheric chemistry, a Co(II)-catalyzed luminol reaction can measure parts per trillion levels of atmospheric H_2O_2, following a continuous aqueous collection interface [78], this paper also demonstrates the utility of a LCW cell to confine the generated CL and collect it from one terminus of a flow cell. Other strong oxidants like ozone, chlorine/hypochlorite/chlorine dioxide, etc. also produce CL with luminol. A general review of luminol-based CL reactions is available [212]. An ingenious μfluidic chlorine gas sensor utilizes lenses already fabricated in the chip for focusing the generated CL [213]. While such oxidants generate CL with luminol, if a constant level of such oxidants can be maintained, their consumption by some other analyte can then be used to measure the said analyte(s). A highly constant level of hypochlorite can be easily generated by electrochemical oxidation of chloride solutions; consumption of the hypochlorite by ammonia has been used to measure ammonia using a LCW CL cell [77]. There are other unusual oxidants that oxidize luminol and generate CL. Arsenic (V) can be precipitated as an ion pair of the heteropoly anion arsenovanadomolybdate and a surfactant cation, e.g., hexadecyltrimethylammonium, and preconcentrated on inert hydrophobic substrates like polystyrene microbeads, contained in a microwell in a μfluidic device. Luminol contacting the immobilized oxidant generates CL; the reported detection limit for As(V) was ~100 nM [214].

The luminol-oxidant reaction and consequent light production is quite slow in the absence of a catalyst, so another way to exploit the

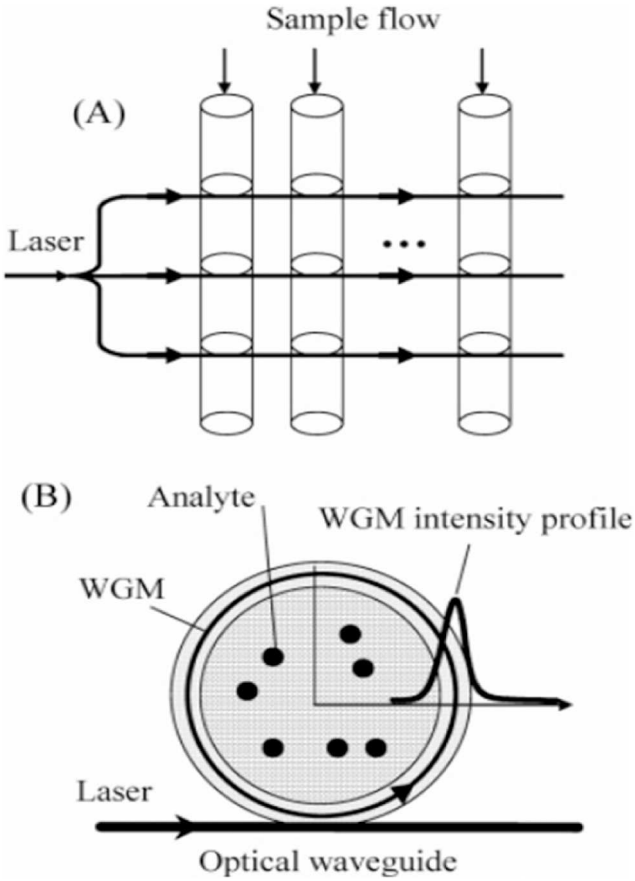

Fig. 14. (A) A conceptual illustration of multiplexed on-capillary detection using a 2-dimensional LCORR array. A waveguide array arranged transversely is in contact with the LCORR and launches the WGM. (B) The cross section of an LCORR. The WGM circulates along the LCORR circumference. Its evanescent field extends beyond the interior surface of the LCORR and interacts with the analytes in the core. Figure reproduced from reference [195].

luminol-oxidant CL for detection involves the measurement of such catalytic agents, e.g., transition metal ions, metal complexes, metalloproteins, metal nanoparticles, enzymes, etc. A recent review [215] explores this in-depth. Some 25 years ago, Harrison and his students demonstrated the injection, separation and luminol CL detection (in a postseparation reaction detector setup) of horseradish peroxidase (HRP) conjugated to various targets of interest, e.g., goat anti-mouse immunoglobulin G (IgG) attached to mouse IgG in a μchip electrophoresis platform. The detection zone was provided with an aluminum mirror to improve LODs, which were 35 nM for a 1-nL sample (35 amol) and a 10 μm deep channel and 7 nM for 8-nL samples (56 amol) and a 40 μm deep channel [216]. Transition metal ions have also long been separated by CE and detected by luminol CL [217].

Peroxyoxalate (PO) CL systems elicit light emission from most fluorescent compounds. The unstable PO compounds are generated in-situ from oxalyl chloride, or more commonly, diaryl oxalate diesters and H_2O_2. Hydrogen peroxide then oxidizes PO to form a peroxyacid intermediate, which undergoes an internal cyclization reaction to form an electronically excited high-energy 1,2-dioxetanedione intermediate that can transfer its energy to a fluorescent compound resulting in fluorescence emission. In the absence of energy transfer, only heat is produced; in either case, the chemical product is CO_2 [218]. With suitable fluorophores, the PO-CL system is one of the most efficient nonbiological CL systems, reaching overall energy transfer efficiencies up to 30%. High luminous efficiency and the ability to tailor CL duration makes this highly suitable for the fabrication of chemical light sources and the detection of various analytes. There are many publications that have used PO-CL in CE or μFSDs. One interesting study demonstrated the separation and nM level detection of hydrophilic rhodamine dyes and hydrophobic polynuclear hydrocarbons in a nonaqueous medium [219].

Acridinium Esters (AEs) are common chemiluminescent tags that behave much like PO, except that one of the aryl groups in the diaryl oxalate is replaced by acridine, a built-in fluorophore moiety, as it were. In basic solution they hydrolyze rapidly so an acidic solution is used until the reaction is initiated with alkaline H_2O_2 that leads ultimately to production of CO_2 and an excited acridine species that emits light. This process is depicted in Fig. 15 [200]. The system was originally proposed for detection in CE three decades ago [220]. It is also possible to transfer the energy to other high quantum efficiency fluors like rhodamine [221]. The process can be accelerated by localized concentration in micellar media to completion in as little as 2 s. Separation of AE-tagged enkephalin-like peptides by CE and subsequent CL detection allowed LODs of 0.88–3.5 nM, which translate to 0.27–0.32 amol [222]. The finite time for CL emission increased peak widths by 10–15%. Comparable sensitivities have been achieved more recently in food analysis and in situ measurement of inorganic species [25,223].

Potassium permanganate-based CL has been known for a long time; it has been used in CE and μfluidic platforms for over a decade. Some recent examples include for example the separation of phenolic acids in botanical pharmaceutical products by CE and CL detection by strongly acidic permanganate [224]. The 75 μm φ CE conduit terminates within a 1 mm φ CL reaction tube placed in front of the light detector, also containing three more liquid I/O ports ($KMnO_4$ and H_2SO_4 in, waste out) and also an inlet for the HV ground wire of the CE separation system. The second example involves a paper microfluidic platform. Deltamethrin is a type-II synthetic pyrethroid that is widely used to safeguard agricultural crops and fish against wide range of parasites, in addition to some human disease vectors. However, prolonged exposure to even trace levels of deltamethrin represents major environmental and health risks. Intense CL is generated by a polyphosphate sensitized $KMnO_4$ – graphene quantum dots reaction system. The detection relies on the highly selective quenching of this CL system by even trace amounts of deltamethrin [225].

Typical LODs in capillary scale CL detection is 10 amol. The notable advantages to CL detection are low LODs and elimination of external light sources; a totally dark background is possible, e.g., in PO-CL systems. Disadvantages include the need for post column processing step (s), additional reagent(s), dilution from the same, band broadening both from dispersion and CL kinetics, limited applicability, and need of tagging. The last two shortcomings mirror those in fluorescence detection.

5. Electrochemical and conductance/admittance detection

Electrochemical detection methods focus on detecting charged or uncharged electroactive species that participate in reduction/oxidation (redox) reactions when exposed to certain potentials. Detection is based on electron transfer between the analyte and the working electrode. Such a definition necessarily implies that electrochemical detection is at least partially consumptive. Although potentiometry, conductometry and admittance detection (more commonly called capacitively coupled contactless conductivity detection or C^4D) will not fall under electrochemical detection with such characterization, these techniques, particularly potentiometry, are generally grouped under the electrochemical detection umbrella; we follow this practice. Conductometry is commonly carried out with an AC excitation voltage, as such, it can also be termed admittance detection. As admittance detection is practiced in C^4D, however, the electrodes are not in contact with the solution. The impedance of the solution and the intervening wall material are in series and what is measured is the reciprocal of the total impedance. To minimize the contribution of the wall impedance, the excitation frequencies typically used are much higher than what is used in conductometry. If such frequencies were used in traditional conductometry, the capacitive reactance of the solution and the solution resistance will be in parallel with each other, and the measured conductance will be higher than the true conductance, especially at low conductance levels. This situation is compounded by the fact that the dielectric constant and hence the capacitance of a solution decreases (hence capacitive reactance increases) with increasing conductance but the exact relationship is electrolyte dependent. True conductance can only be measured by the bipolar pulse method discussed later; this has not generally been used in C^4D.

Several reviews have been written about integration of electrochemical detection methods with microfluidic devices [9,33,226–233]. The most common types of “electrochemical” detection methods for microfluidic devices are amperometry and C^4D. The latter was developed for use in CE and is most often utilized by CE and ion chromatography (IC); it can only be used for charged, i.e., ionic analytes. The origin of C^4D lies in oscillometry [234]; indeed, among the two pioneering papers [235,236] that introduced the technique for CE applications, one [236] called it as such.

5.1. Potentiometry

Some four decades ago, Manz and Simon described potentiometric ion selective electrodes of 1 μm tip size and an estimated 0.5 pL detection volume [237]. Although the same group followed up with some equally impressive papers using such detection methods, the difficulty in actually carrying out such experiments, the logarithmic response behavior, and the lack of robustness, may account for the lack of disciples. There are examples of potentiometric detection in the microscale in less demanding applications, e.g., as a microfabricated sulfide selective sensor on a μfluidic platform [238]. Potentiometric detection is not discussed further.

5.2. Amperometry

Amperometry is perhaps conceptually the simplest detection method. One electrode called the working electrode (WE) is placed in contact with the analyte solution, typically at the end of a flow system/separation device. A controlled voltage is applied between WE and a second electrode (called the auxiliary or counter electrode, AuxE) also in

contact with the solution. Amperometric detectors are designed such that the electrochemical process of interest involving the analyte(s) occur only at the WE. Under the chosen conditions, when analytes reach the WE they are oxidized or reduced, which causes a transfer of electrons either to or from the WE, measurable as a current. Mass transfer of the analyte to the WE is thus important and the detection arrangement needs to facilitate analyte transport to it. The AuxE, however, needs only to be in electrical contact with the solution, as long as the resistance between the two electrodes is not excessive, it can therefore be placed downstream. The dispersion, of crucial importance to capillary systems, in going from the WE to the AuxE is thus not of particular importance. Although such a two-electrode configuration can be and has been used, problems may arise when the background composition changes, or the setup needs to be replicated elsewhere. This is because the absolute potentials at each electrode, which governs if a particular redox process will take place, remains undefined in a two-electrode system. This can be obviated in a three-electrode system when a reference electrode (RE) of fixed known absolute potential (e.g., an Ag/AgCl electrode) is also incorporated, and a potentiostatic circuit maintains the WE at a fixed potential with respect to the RE while the current flowing between the AuxE and the WE is measured. In principle, it is possible to *quantitatively* reduce/oxidize an analyte flowing through the cell. This comprises coulometry, which is an absolute measurement technique and in theory does not require calibration. This is hard to achieve in macroscale HPLC; large electrode areas are required, and the resulting larger cell volume increases dispersion and decreases S/N. Coulometric detection is far easier to achieve in the miniature scale, as sample volumes and the distance required to diffuse to the WE are much smaller. Although there are not many examples of coulometric detection in the miniature scale, it is not apparent whether a system is amperometric or coulometric without examining its coulometric efficiency. Two notable examples include the work of Sassa et al. [239] who demonstrated effective coulometry for determining an analyte in a liquid plug on the nanoliter-scale confined in a flow channel. A constricted flow channel structure with an array of platinum strips as the working electrode(s) was used to improve the sensitivity; the LOD decreased at least 4× over a single working electrode with the same area. More recently, Mizuguchi et al. have demonstrated the utility of radiation track-etched membranes (these contain well defined and highly uniform cylindrical pores), on which a platinum or gold coating has been applied through evaporation, to function as the working electrode (or electrodes, a stack of such membranes has been used as well). The flow cell, with a 100 μm inlet aperture, exhibited a detection volume of 80 pL per membrane electrode (240 pL for a two-membrane stack). A variety of analytes, from ascorbic acid to multiple catecholamines were all quantitatively oxidized below flow rates of 50 μL/min [240]. However, in truly small capillary systems, with an even smaller micro-WE inserted into the mouth of the capillary, diffusion limitations for analyte transport to the WE actually lessen, and quantitative conversion becomes easier to achieve. In the first publication on electrochemical detection in OTLC, a single 9 μm graphite fiber was inserted in a 15 μm φ capillary and the oxidation efficiency for ascorbic acid was observed to be essentially quantitative, and detection limits for this and various catechols were ~1 fmol (or ~100 nM) [241].

Coulometry can be considered as the integrated, exhaustive version of amperometric detection, which has been used far more frequently in miniature systems. The first successful microscale amperometric detectors were reported as early as 1980 [242]. In his prescient review of forthcoming analytical systems. Jorgenson, a pioneer in both CE and OTLC, identified amperometric detection as promising, second only to optical absorption detection approaches (then most prevalent) [243]. He particularly identified carbohydrates and amino acids as attractive analytes amenable to electrochemical detection. Absorption spectroscopy is selective in its wavelength dependence (as it is dependent on light absorption, the same is true for fluorescence), electroactive analytes (susceptible to reduction/oxidation at an electrode) resemble this partially in that analyte A may be oxidized/reduced at a certain potential at which analyte B will not be oxidized/reduced. However, the difference is that light absorption bands have both higher and lower wavelength limits; in our illustrative case if the applied potential is increased/decreased to a value where B will be oxidized/reduced, not only B will undergo this oxidation/reduction, so will A. Measurement of the exact dependence of the current on the applied voltage (voltammetry) can, however, provide more distinguishing details. Again, Jorgenson and his students not only demonstrated the first scanning voltametric detector for OTLC [244], they also subsequently dispelled the myth that such detectors are not compatible with gradient elution

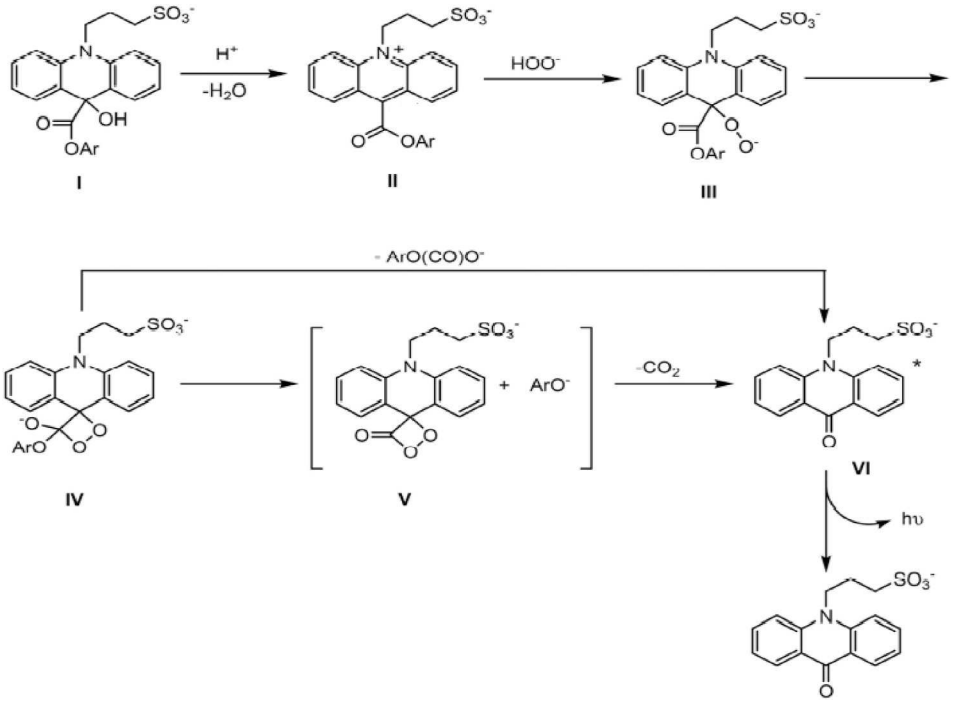

Fig. 15. Chemiluminescence reaction mechanism of an acridinium ester. Figure reproduced from Ref. [200].

[245].

Given how many publications exist on the use of amperometric detection in the capillary scale or on μfluidic platforms and the number of reviews that already exist on the topic, it is neither worthwhile nor feasible to present an account of this field from the early years discussed above to the present. Indeed, even confining our focus to just last five years, there are far too many applications to discuss. We therefore only discuss a few recent μfluidic or CE applications, admittedly our selection is somewhat arbitrary.

The longevity or robustness of electrochemical sensors is not of concern for disposable devices; all of the wearable commercial continuous glucose monitors are microscale amperometric sensors that monitor blood glucose transdermally [246]. Significant complexity can be incorporated into a disposable sensor. Ortega et al. [247] describe a μfluidic amperometric sensor for a colorectal cancer biomarker in circulating extracellular vesicles. An amino functionalized porous nanomaterial was covalently anchored to the flow channel and monoclonal antibodies to the target, immobilized on this substrate, specifically recognized and captured the target present in the samples. The trapped target was then quantified by an HRP-conjugated antibody that binds to the target. An HRP substrate then allowed an amperometric quantitation of the product; the LOD for the biomarker target was 0.1 pg/mL.

One attractive aspect of electrochemical detectors is that they can be constructed rather inexpensively and miniaturization results in little or no loss of performance. The availability of affordable relatively high-resolution 3D printers, inexpensive Programmable Systems On a Chip (PSoC) microcontrollers/microcomputers with onboard capabilities of waveform generation, data acquisition and storage, has had an impact on all types of detectors in the capillary scale but probably most of all in electrochemical detection. A significant number of recent papers reflect this [248]. In a μfluidic thread electroanalytical device (with the endearing acronym of μTED!) 4 cotton threads connected an electrolyte reservoir placed 30 mm above a waste container forming the μfluidic channel (Fig. 16) [249]. The device contained three integrated electrodes printed with conductive carbon black - PLA (polylactic acid) while the body was printed with non-conductive ABS (acrylonitrile butadiene styrene) copolymer. The authors demonstrated the measurement of an electroactive fungicide in real samples and the excellent correspondence of these results with a benchmark GC-MS method.

The need to incorporate and fabricate counter and reference electrodes in the same microfluidic amperometric detector without causing major dispersion can be challenging. In one 3D-printed flow cell, a convenient three-electrode set-up was made possible by providing threaded ports that house commercially available threaded RE's and other electrode(s) fabricated in appropriate available fittings [250]. The authors showed that rather than the traditional thin-layer format, a pillar form WE provides greater sensitivity. The WE and AuxE can be placed directly opposite to each other, reducing iR drop and a more uniform potential is applied across the WE. The authors also incorporated a chemiluminescence detection arrangement downstream on the same chip; a T-port permitted the introduction of luciferin-luciferase to quantify ATP (adenosine 5′-triphosphate). Norepinephrine and ATP were near-simultaneously detected; the first by amperometry, and the second by CL.

A major use of the μchip platform has been conducting electrophoretic separations. One review specifically addresses electrochemical detection, especially amperometric detection for μchip electrophoresis [251]. Even two decades ago, LODs of 0.5–5 fmol were attainable. However, one downside of electrochemical detection where an actual redox reaction takes place at the electrode, is that the reduction/oxidation of the analyte may result in an insoluble or adherent product that slowly coats/fouls the electrode surface, reducing electron transfer efficiency and thence, sensitivity. Frequent periodic cleaning and/or electrode replacement to maintain sensitivity is not only inconvenient, but also often impractical [252]. This is particularly the case with both carbohydrates, polyols, and amino acids, for which amperometric detection is particularly attractive, not only because these compounds are electroactive but also because UV-VIS optical absorption by these analytes are often poor to nonexistent.

Pulsed amperometric detection (PAD) was specifically developed to address electrode fouling. The technique involves the application of a minimally 3-step waveform. For example, for oxidative detection of carbohydrates, a gold WE may be held at 50 mV (vs. an Ag/AgCl RE) for 600 ms. The first 400 ms is simply used for equilibration, the current data is collected for the last 200 ms of the step and integrated (the response is often reported in coulombs). In the next 200 ms, the potential at the WE is stepped to 800 mV, a strongly oxidative potential designed to oxidize any accumulated crud on the electrode. This step may result in oxidizing some of the electrode surface itself, however, and hence a third reducing step at −600 mV is used for 200 ms to reduce any gold oxide formed back to the metal [253]. Another PAD manufacturer recommends a 4-step waveform, the first 400 ms is the measurement step of which only the last half is used to integrate the current. The electrode is then taken through successive −2000 mV (20 ms), ramping up (over 10 ms) to 600 mV, ramping down (over 10 ms) to −100 mV and holding it there for 60 ms and then returning to the working potential after the 500 ms cycle time [254]. The authors find that reductive cleaning as in the 4-step protocol is more effective in maintaining WE response, compared to oxidative cleaning. Some maintain that all fouling cannot be removed completely by such steps, and PAD may only slow the rate of electrode fouling [227,252]. However, without PAD some applications may be altogether untenable. Routine analysis using amperometry always utilizes PAD to reduce time spent in electrode cleaning/replacement and recalibration. In order to maximize the lifespan of the electrode, in the potential step examples given above, only 20–40% of the cycle time is actually used for measurement; however, 200 ms is more than an adequate period to make an accurate measurement of the current with good S/N.

Beyond carbohydrates and amino acids there are many other highly sensitive applications of amperometric detection of practical importance, e.g., detection of acetylcholine release from cancer cells [255]. Widely reported LODs for microfluidic amperometry of complex samples is ~50 fmol. The main advantages of amperometry are its simplicity and selective detection capability. These are often complementary to UV/Vis. Amperometry is very inexpensive to implement [256–258] and is thus seeing wide use in point of care applications, often as disposable sensors [259,260]. The disadvantage as a detector following a separation of unknown analytes is that some of these may not be redox active at all. Even for those that are, operating at some fixed potential optimum for one analyte may result in widely varying responses from the others.

5.3. Conductance and admittance detection

Conductometry specifically detects ionic analytes. Conductivity (or specific conductance) is reported in units of Siemens/meter (S/m), in analytical separation systems more typically as microSiemens/centimeter (μS/cm). This is the inverse of electrical resistivity or specific impedance, and thus measurement of one allows the other to be easily computed. Much like amperometry, the parameter that is actually measured is the current that is induced (across a two-electrode system) by the application of a known voltage, the resistivity or conductivity then can be computed from Ohm's law; the latter being directly proportional to the measured current. The difference from amperometry is that typically AC voltages are applied, and in principle, no chemistry happens at the electrodes.

When possible, DC conductometry is perhaps the simplest electrical measurement but in aqueous solution, current only flows with applied voltages past the electrolytic threshold. As such, it is only useful when the background is of very low conductance [261], e.g., pure water as in suppressed IC (SIC, see next section for an explanation of suppression). There are other prior instances of DC conductometry in flowing systems

with detection volumes as low as 100–120 nL. The exit tubing comprising the cell were 50 μm larger than the 100 or 350 μm electrode wires which exited through the annular gap being bent in a U-shape [262]. The difficulty of gas evolution from an applied DC voltage can be ameliorated by having an arrangement of four serial electrodes; a constant small current is applied between the outermost electrodes and the voltage is measured between the inner electrode pair, where there is no gas evolution. Note that the voltage across these inner electrodes is proportional to the resistivity of the solution, as opposed to conductivity which is proportional to the current observed at a fixed applied voltage. In the specific arrangement used, however, some of the flow, along with any gas, was allowed to escape through each outer electrode [263]. Maintaining a constant flow in the main channel in such an arrangement may be challenging. Another four-electrode DC conductometric system for SIC avoids gas evolution in the interelectrode region through a rather complex arrangement of porous outer electrodes, electrode isolation by ion exchange membranes, and ion exchange connectors to the actual flow channel where the sensing electrodes are placed 200 μm apart. Continuous flow and membrane regeneration is needed in the outer channels [264]. This device was incorporated in a suppressor-detector combination where a fifth electrode helped regenerate a packed column suppressor [265]. To function as a detector only, however, there is no reason why the four-electrode arrangement cannot be used with an applied ac potential to avoid gas evolution, precisely this was done with a microscale chip-based IC system [266]. In this case, of the five serially placed electrodes at the separation channel exit, the first four comprised the ac-excited detection system and the last, fifth electrode was used as a ground (although what performance benefit accrues from its use was not described, nor does any of these publications provide a comparison of real benefits of a 4-electrode detection system vs. that using two electrodes).

DC conductivity detection is not common, however. Typically, the general setup of conductivity detection involves two electrodes connected to an AC voltage source of fixed frequency set at a known amplitude via a current measuring circuit that provides a rectified output. As the impedance of the solution varies, the current flowing through the solution changes proportionally. Most state-of-the art conductance detectors use the more sophisticated bipolar pulse technique [267], however. In this approach, essential when measuring low conductance levels, a square wave excitation is used. The current is measured only during a small portion near the end of the cycle (reminiscent of PAD). By this time, most of the capacitive current has decayed. Further, by measuring the current at the end of the second half of the cycle, the residual capacitive current is largely cancelled because of the opposite directions of the voltage excursion.

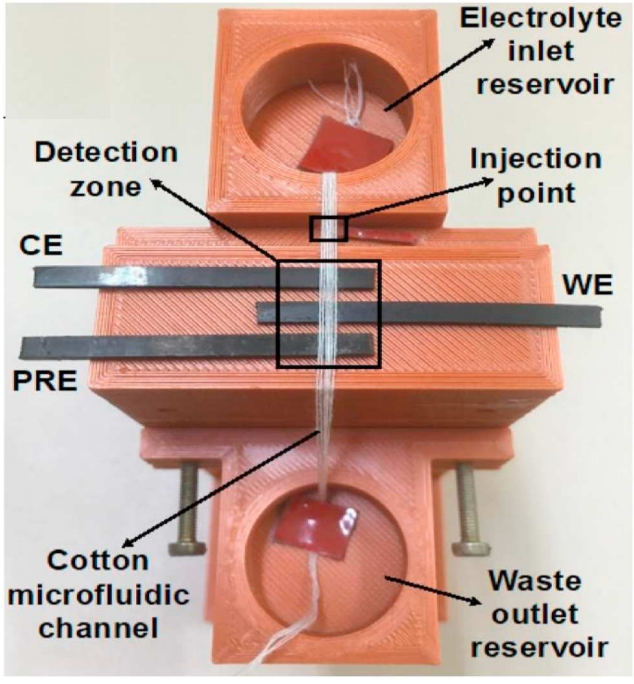

Fig. 16. Top view of the μTED device with 4 cotton threads defining the μfluidic channel and gravity induced (3 cm hydrostatic head) capillary siphon flow. The overall dimensions are 5.4 × 9.5 × 12.2 cm (w x d x h). From Ref. [249].

5.3.1. Conductivity detection in ion exchange chromatography (IEC) and IC

Conductivity detection is most commonly used with ion exchange chromatography (IEC) or CE. In both cases, the analytes are ionic and thus amenable to such detection. In IEC, it is easy to see that ion exchange sites must remain uncharged overall; an analyte ion occupying the site can only be displaced by another ion of the same charge type. In our discussion, we will generally use anion exchange chromatography for illustration, as there are many other alternatives for the determination of cations, especially metal ions. As the practice of ion exchange chromatography differs from most other types of liquid chromatography in a significant way, requiring miniaturization of components beyond the column and the detector, we first provide an overview of the technique itself first.

One may envision IEC as an unusual version of the game of musical chairs where, unlike the actual game, the number of chairs (fixed ion exchange sites), arranged in a linear fashion from the injector to the detector, are invariant in time. All the chairs are always occupied, some by the eluent ions, some by the analyte ions. All occupants move forward, but not at the same speed. Importantly, whenever an analyte ion gets up to move, its place is occupied by an eluent ion. This also happens when an analyte leaves the last chair in the series to enter the detector. Accompanying the appearance of the analyte ion in the detector, there is thus a concomitant and equivalent decrease in the eluent ion concentration. Whatever the conductance from eluent ion background may be, the appearance of an analyte ion will cause an excursion from this background, it can be positive or negative depending on whether the specific conductance of the analyte ion (λ_A) is greater or less than that of the eluent ion (λ_E). Similarly, as the sample is injected and the analyte ions enter the column, they displace an equivalent amount of eluent ions, leading to a positive or negative response, depending on whether the total anion equivalents in the sample exceeds or is less than the anion equivalents present in the same volume of the eluent (modified also by any difference in the specific conductivities of the sample cation(s) vs the eluent cation). One thus has an immediate idea of the total number of ionic equivalents represented in the sample; this is unique to IEC. The constancy of ionic equivalent concentration in the column effluent has also been used for absorbance detection. Using optically absorbing eluent ions, one can readily visualize non-absorbing analyte ions as negative absorbance signals [134]. Although the rationale is not as obvious, local electroneutrality also holds in CE and both conductivity and optical absorbance detection are used in this manner in CE, perhaps far more commonly than in IEC.

Because the detection principle relies on translating the analyte ion into the equivalent difference from the eluent ion in the measured property, such detection is often referred to as indirect detection. When applied to IEC in particular, indirect conductometric detection has both significant advantages and disadvantages. A typical real sample often contains a large concentration of other ions (chloride, sulfate, etc.) and the target analyte ions are present only in much lower concentrations. To prevent overloading and allow the trace analytes to be sufficiently separated from the major constituents, there must be sufficient ion exchange capacity. To elute ions from a high-capacity column, one also typically requires a high concentration of eluent ions, resulting in a high conductivity background. Minor changes in this high background due to the elution of low concentrations of analyte are difficult to discern and

lead to poor LODs. This can only be partly ameliorated by choosing both a relatively low-capacity column, and an eluent ion of high eluting power and low equivalent conductance, typically a large aromatic carboxylate, which can be used in a low enough concentration to have a manageable background conductance. The combination of a low column capacity and the use of a strong eluent ion that effectively reduces the capacity further leads, however, to the undesired situation that the column is easily overloaded. This is further exacerbated by the low eluent concentration: electroneutrality requires that no eluting peak can have a greater concentration (in eq/L) than that of the eluent.

A typical aromatic carboxylate ion also has a low λ_E, so most other analytes show up as positive peaks. However, sensitivity will continually change as λ_A decreases, vanishing to zero as λ_A becomes equal to λ_E and becoming negative with a further decrease. Not only is the loss of response as λ_A approaches λ_E troublesome, coelution of analytes which have opposite signs of λ_A - λ_E, can make quantitation impossible. Gradient elution, common to other types of HPLC, is not possible in this approach as well. To be fair, there are also two advantages to this mode of detection. First, physically this detection arrangement can be the same as all other detection arrangements in standard HPLC, namely that the detector immediately follows the separation column, nothing special is needed. And second, other than the loss of sensitivity as λ_A approaches λ_E, as long as the analyte is ionized at the operating eluent pH, the anion of an acid of *any* pK_a is detectable. From this standpoint, hydroxide can be an attractive eluent, as exploited very early by Okada and Kuwamoto [268,269].

5.3.1.1. Suppressed ion chromatography. Almost 50 years ago Small et al. provided an ingenious solution to the conductometric detection problem in IEC. They proposed using an alkaline eluent and then installing a H^+-form cation exchange (CEX) column (called at first the "stripper" – it strips the eluent of its cation, and later the "suppressor", as it suppresses the eluent conductance) after the separation column and before the detector. The suppressor now exchanges all influent cations for H^+ prior to the detector and eluents like Na-hydroxide/carbonate/borate etc. are converted to very poorly conducting water/carbonic acid boric acid, etc. Analyte ions like chloride, nitrate, sulfate, etc., now enter the detector as the fully ionized highly conducting acids and can be detected with exquisite sensitivity on a poorly conducting background. The suppressor reduces the background by substituting the eluent cation with H^+. The hydrogen ion is by far the most conductive of all cations (λ_{H+} is 480% of λ_{K+} to >1000% of λ_{Li+}), this makes the analyte signal also get a large boost. This suppressed conductometric mode of IEC has more popularly come to be known as ion chromatography (IC). The indirect conductometric detection mode chronologically came *after* the invention of the SIC. Considering the newcomer was more "direct" in terms of the physical arrangement (no suppressor device, column directly connects to detector), its originators chose a different explicit nomenclature for it, single column IC (SCIC). As originally invented, SIC had issues that needed to be addressed. The use of a packed H^+-form CEX column that gradually got converted to the eluent cation form and then stopped working was one such issue – this was compounded by the conflicting demands of making the suppressor column physically large (a larger capacity allows more working time) vs. the behavior of a larger volume device that does not contribute to any separation, only dispersion. Second, while it is easy to see that an alkali hydroxide will be the preferred eluent in anion SIC as it is suppressed to water (and unlike any other eluent, even a gradient run will still produce an invariant detector background, water), it has been a long journey getting there. Truly pure hydroxide is nearly impossible to obtain and even if somehow made, we live in an ocean of carbon dioxide, it is nearly impossible to prevent gradual contamination of that eluent with carbonate. As divalent carbonate is a much more powerful eluent ion compared to hydroxide, accumulation of carbonate continuously decreases the retention of analyte ions and the background increases as greater concentrations of carbonic acid comprise the detector background. In early years there was a further problem: the lack of stationary phases that exhibited high selectivity for hydroxide, thus requiring large hydroxide concentrations for time-efficient separations. This also taxed the suppressor capacity. These problems have been gradually solved; packed column suppressors were replaced with continuously regenerated membrane-based suppressors, where H^+ was initially chemically provided [270] and later electrolytically generated [271], the latter providing very high dynamic suppression capacities. For the eluent, methods were devised to generate highly pure hydroxide electrodialytically on-line, the concentration of which was controlled electrically, not by dilution via mechanical proportioning [272]. Finally, the development of highly hydroxide-selective anion exchanger stationary phases represented overcoming the last major hurdle [273]. Miniaturization of IC began early. Rokushika et al. used 190 μm i.d. packed fused silica columns and thermally stretched available tubular CEX membranes to 0.2 mm i.d.; a 10 mm length sufficed as the suppressor, with dodecylbenzenesulfonic acid (a large anion prevents "leakage" of the acid molecule as a whole through the thin membrane) as the chemical regenerant [274]. The conductivity cell was composed of flow through tubular stainless-steel electrodes, 0.15/0.36 mm id/od, ~0.8 mm apart, one of which terminated at the suppressor exit [275].

This early attempt used a carbonate-bicarbonate eluent. It took more than a decade for SIC in this scale to graduate to hydroxide gradient IC with an electrodialytic hydroxide eluent generator on the high-pressure side of the pump [276]. In the simplest form of an electrodialytic eluent generator (EEG), the pumped influent to the cathode compartment is pure water and the effluent is the electrodialytically produced eluent. A CEX membrane isolates it from the anode compartment (containing a flowing or stationary feed solution containing the desired cation, often in hydroxide form, typically NaOH or KOH). The anode chamber is composed of a nonconductive inert polymer, and a 100 μm Pt-wire functions as the electrode. The electric field brings over the alkali cation to the stainless-steel cathode compartment and water electrolysis provides the hydroxide counterion and generates H_2 gas as well. The gas is subsequently removed by permeative escape through the walls of a PTFE capillary. One difficulty in constructing such EEGs is that the membrane must withstand the entire column backpressure. This was ameliorated by limiting the exposed area of the membrane to a diameter of 2.5 mm and the device could withstand pressures of ~1000 psi (6.9 MPa), with the swept volume of the EEG being 3.8 μL. The wall thickness of the suppressor, comprising 10 mm length of an 80 μm id perfluorosulfonate Nafion® CEX membrane (Nafion) was too small and regenerant leakage was too high – the wall thickness therefore had to be increased by repeated coatings with colloidal Nafion®solutions. The suppressor exit was connected by a 50/360 μm i.d./o.d. fused silica tubing to the conductivity cell comprising two custom 50/360 μm i.d./o.d. metal rings separated by a 125 μm thick PEEK spacer ring, this entire assembly being sandwiched on the other side by a 75/360 μm i.d./o.d. exit tube. As shown in Fig. 17, impressive performance could be obtained. A very similar arrangement permitted a portable SIC [277], the main differences were as follows: A 10 cm long polystyrene capillary, 80/325 μm i.d./o.d. was used to remove the H_2 gas. It was more robust than the PTFE tube and easily withstood pressures of 900 psi and removed H_2 efficiently at least up to 40 nmol/min. The suppressor comprised a 50/200 μm i.d./o.d. radiation grafted and sulfonated PTFE tubing, 1.9 cm long, capable of fully suppressing 40 mM NaOH @ 1.5 μL/min. The conductivity cell was similar in geometry to wall jet cells as used in amperometric detectors (Fig. 18). A 3.1 cm stainless steel tube (150/304 μm i.d./o.d. was the suppressor exit capillary and served as one electrode and a 1–72 threaded screw (terminus 1.85 mm φ) was the other electrode, all but touching the first one.

Electrodialytic eluent generators that can withstand much higher pressures were introduced later based on ion exchange resin beads. A combination of a CEX and an anion exchange resin bead can provide for a gas-free eluent generator [278,279] but a simpler single CEX

bead-based generator provides better eluent purity, the generated gas can be removed subsequently by a polymeric capillary, as previously described [280].

5.3.1.2. Conductivity detection: isotachophoresis to capillary electrophoresis to suppressed open tubular ion chromatography. A review of conductivity detection in capillary to chip-scale electrophoretic separations is available [281]. Isotachophoresis (ITP) is one of the oldest ion separation techniques that uses electrical mobility-based separation in a tubular format and often utilizes conductometric detection, the capillary format (CITP) is common today. In CITP, the sample is sandwiched between a leading electrolyte (LE, in which the ion charged similar to the analyte ions, often referred to as the co-ion, has higher mobility than any sample ion) and a terminating electrolyte (TE, in which the co-ion has lower mobility than any sample ion). Understanding of the process is simplified where all the counterions and concentrations (in eq/L) are the same (although separation will occur without these conditions being met, being accommodated by concentrations of ions changing in the separated bands) – in this case when a potential is applied, it is easy to see that the LE and the TE zones will have the lowest and highest resistance (and therefore lowest and highest electric field strength that appears across the zone), respectively. As ions of different mobility in the sample zone move, a steady state is eventually established where the concentration of the ions in each zone is such that the resistance (and hence the electric field strength) in each zone is proportional reciprocally to the mobility of the ion. This results in all the ions moving at the same speed (tach derives from greek *takhos,* meaning speed, hence isotachophoresis). Conductometry to detect the zone interfaces is an obvious choice. While the tube diameters used for CITP in the early years will not qualify today as capillaries, the strategies used with 0.45–0.7 mm i.d. PTFE/glass tubes [282] can in principle work with much smaller tubes. The detector used with the PTFE tubes uses a cleverly machined union where essentially conductive metal rings/washers of the same i.d. are imbedded in each half and a polymer spacer of the same i.d. separates them. Indeed, the detector design used in the SIC system described in the previous section [276] is very similar. In the case of the glass tube, platinum wires were put on either side of a glass spacer (a small section of the same tube) and the I/O tubes; the assembly is held together by shellac. In a subsequent paper, 50 μm Pt-wires were put in, 100 μm apart, through small purpose-drilled holes and sealed in place [283].

In the wake of CZE, Zare's group published multiple papers on conductometric detection on fused silica capillaries. The first of these [284] was very much the same geometry as that just described. Holes, 40 μm in dia. were drilled with a CO_2 laser radially across 50−75 μm i.d. fused-silica capillaries and 25 μm Pt wire electrodes were cemented therein. This is difficult to construct, and subsequently a simpler end-column design was reported requiring only one hole. In this case, the end of the column terminated in a wire electrode, sealed in place. A single hole was then drilled on the side wall just above the sealed end containing the first electrode. This aperture allowed both for the placement of the second wire electrode and liquid exit [285]. A decade after their first publication, a 25−50 μm diameter insulated wire was simply placed across the face of a 75 μm i.d. capillary and affixed by epoxy adhesive on each side. The wire was then cut where it passed across the capillary bore. While it would appear relatively simple (no laser drilling across a silica capillary wall is involved), a comparison with previous designs would indicate significantly poorer performance. Considering the small mass of the protruding portion of the wire and the velocity of the fluid exiting the capillary, the positional stability of the electrodes is likely compromised, leading to noise.

Interestingly, some of the earliest efforts in devising a capillary or chip scale conductivity detector were in situations where conductivity served merely as a surrogate for absorptance (fraction of incident light absorbed) measurement. Whereas photothermal absorbance measurement typically uses RI as the surrogate measurand (or some effect caused by the thermally induced change in the RI), an increase in temperature decreases viscosity which increases conductivity, the relative change is greater than that for RI as a measurand. McLaren and Dovici [70] used a pair of 200 μm wires, 240 μm apart. With a 4 mW He–Ne laser beam waist on an estimated volume of 10 nL between the wires, the authors were able to achieve an LOD of 300 nM methylene blue using the simplest of conductivity detection electronics. More than two decades later, Dennis et al. attempted a similar experiment in the chip scale in a much more sophisticated arrangement. On a quartz chip with 70 × 30 μm channels and interdigitated platinum electrodes 50 μm wide and 25–100 μm apart (50 μm was optimal) and 48 mW of 488 nm incident laser power, an LOD of 5 nM (actual concentration in the detection zone, injected concentration was much higher) dabsyl-glucosamine was established [286].

In CE and in most capillary formats, end-column conductivity detection presents a lesser challenge than accomplishing it on-column. In contrast, with reasonable microfabrication facilities, it is not a great challenge to locate electrodes for conductivity measurement within a flow channel. There are far too many publications that describe such arrangements. We will merely cite one outstanding example where circulating tumor cells were concentrated more than 5000× from whole blood directly using a series of 51 narrow and deep (35 × 150 μm W x D) antibody coated microchannels and the number of cells captured was counted using an integrated conductivity sensor following release from the capture surface [287].

Suppressed conductometric detection in CE precedes capillary scale SIC [288]. Fused silica separation capillaries (75 × 375 μm φ i.d. x o.d.) were connected to a radiation grafted, sulfonated PTFE membrane tube (dry dimensions 50 × 200 μm i.d.x o.d., using 250 μm φ elastomeric PVC tubing); the dry membrane is easily inserted into the PVC tube and swells upon wetting to form a leak proof seal. An exit capillary is installed the same way (Fig. 19). An active length of 6 mm was found sufficient to completely suppress the 2 mM $Na_2B_4O_7$ background electrolyte (electroosmotic flowrate 3.2 μL/min @ 333 V/cm), the CEX membrane was installed in a vial containing water or dilute H_2SO_4 where the high voltage grounding electrode was placed. This arrangement permits electrodialytic suppression as well as termination of the HV field to facilitate conductometric detection downstream. The design used a 100 μm Pt wire as one electrode deployed across the mouth of the capillary, inserted into a PVC sleeve tube and the second electrode was placed as close to it as possible in parallel configuration, without contacting the first electrode. A different conductance cell design that provides far more reproducible cell constants, using bifilar wire end-column electrodes was introduced soon after [289]. Miniature multiconductor ribbon wires with very thin insulation are made for electronic assembly and termed bifilar, quadrifilar, etc., depending on the number of conductors. They are available with wire diameters as low as 20 μm. Outer insulation can be removed by abrasion or other techniques, but the insulation between the conductors remains, and they remain electrically isolated. In the above work, a pair of 80 μm dia. Ni wires separated by 45 μm of insulation was placed at the capillary exit with the wires perpendicular to the flow direction. The bifilar wire was inserted radially via a hypodermic needle through the walls of the sleeve tubing (e.g., P3 in Fig. 19); one remarkable observation was that the efficiencies (this effectively means the detection volume) are not particularly affected by the bore of this tube, rather, the critical parameter is how centrally the wire is placed so that the capillary effluent immediately flows past the sensing wires. For a 75 μm i.d. capillary, assuming the flow stream passing across the electrodes remained constrained to the capillary exit diameter, the authors computed the detection volume to be ~185 pL! The detector was used with PC-controlled bipolar pulse conductometry electronics; very good peak shapes were observed; efficiencies were often 2× that of the previous detector.

While the simplest conductometry setup may simply apply an AC voltage, amplify and rectify the resulting current and generate a

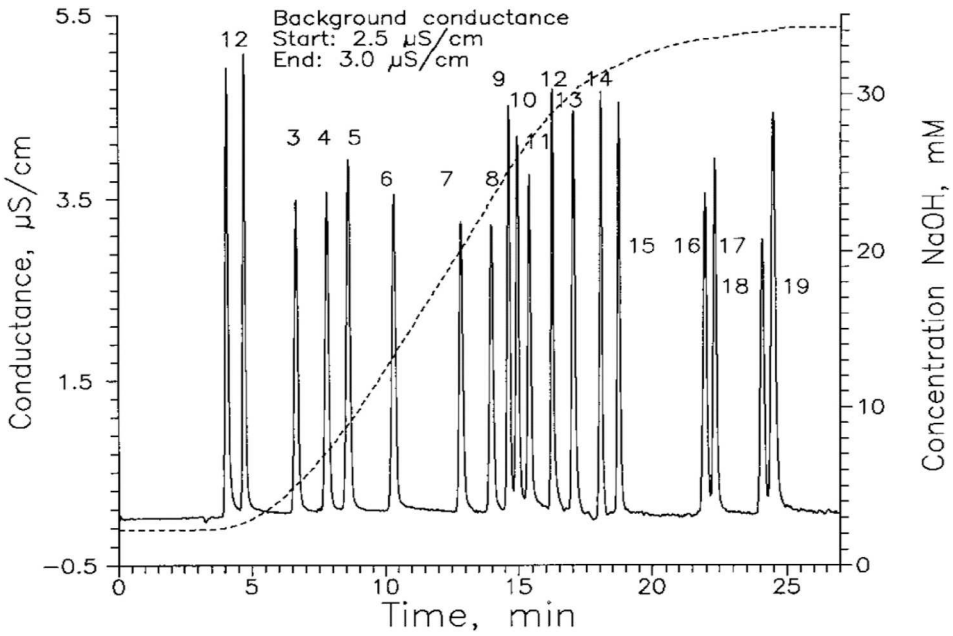

Fig. 17. Gradient chromatogram: The right ordinate shows the gradient (dashed trace) in millimolar NaOH. Peak identities: 1, fluoride; 2, formate; 3, monochloroacetate; 4, bromate; 5, chloride; 6, nitrite; 7, trifluoroacetate, 8, dichloroacetate; 9, bromide; 10, nitrate; 11, chlorate; 12, selenite; 13, tartrate; 14, sulfate; 15, selenate; 16, phthalate; 17, phosphate; 18, arsenate; 19, citrate. All concentrations 50 µM except selenate and sulfate, which were 25 µM. Injection volume 100 nL. Reprinted from Ref. [276] by permission from the American Chemical Society.

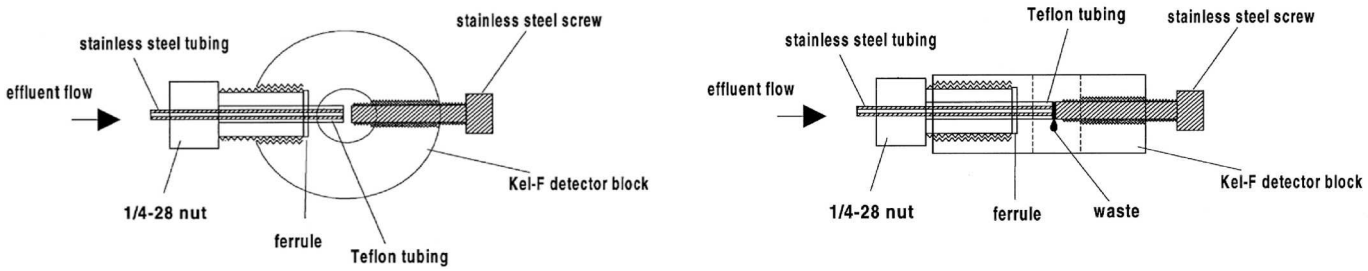

Fig. 18. Conductivity cell design for portable SIC. A Kel-F block was machined with ports to have a 1/4–28 NF threaded fitting at the inlet that accommodated the inlet SS capillary inside a PTFE sleeve tube and a No. 1–72 screw at the outlet. A hole was machined vertically to provide an outlet. The screw is turned until the cell is shorted and then just backed off. Reprinted from Ref. [277].

proportional voltage signal, the measured current is affected by the double layer capacitance at the electrode-solution interface and can cause significant errors at low conductance levels. Bipolar pulse conductance detection [289] avoids these problems.

The only commercially introduced conductometric CE instrument utilized electrodes in a ring disk geometry deployed in a wall-jet configuration: the center electrode (150 µm Pt wire) was separated from a stainless-steel ring electrode by epoxy insulation, see Fig. 20 [290]. To obtain reproducible results from one capillary to another, as would be essential in a commercial instrument, the separation capillaries came equipped with a connector for secure mating with the electrode arrangement; this ensured both concentricity and reproducible separation.

More recently, several end-column conductivity detector designs (Fig. 21) were examined with a view for potential applications in Suppressed Open Tubular Ion Chromatography (SOTIC) [291]. Design (a) mimics the on-column radially opposed electrode design except that the holes are not drilled in the very small i.d. (20–25 µm φ) separation capillary but on a butt-joined 75 µm φ PEEK exit capillary, only 200 µm from the joint to minimize dispersion in the much larger tube. Tungsten wire electrodes (100 µm dia. were used. Design (b) is a version of a ring-disk electrode, where the disk is a tube and allows for fluid exit. It utilized a pair of nested SS capillaries (inner/outer 75/127 µm i.d./o.d., 178/330 µm i.d./o.d.), with epoxy insulation in-between. The tip was honed, lightly coated with epoxy and then only the tip face sanded to expose the tube edges to function as an electrode. Design (c) more closely emulated a ring-disk electrode. A stainless-steel capillary (75/127 µm i.d./o.d.) was affixed within a silica capillary (180/360 µm i.d./o.d.). The tip of the assembly was honed and an insulated microwire (45 µm dia.) was inserted through the steel capillary to function as the central electrode and exited through the wall of a sleeve tubing at the back end, fluid exited through the sleeve tube. Design (d) uses the aforementioned bifilar wire (~20 µm each strand, ~10 µm insulation) that was inserted through the flat end of a one-end prehoned silica capillary (75/360 µm i.d./o.d.). Wire protruding at the tip is cut off with a sharp scalpel and the wire tips act as the electrodes.

In design (e) the liquid of interest flows through a 100 µm hole in two parallel planar electrodes separated by ~175 µm. A 25 µm thick polyimide tape with 75 µm thick silicone adhesive on each side is sandwiched by two 100 µm thick predrilled SS foil electrodes, vertically offset to facilitate electrical contact and a 100 µm hole is drilled through the sandwich. PEEK-sleeved (380/1600 µm i.d./o.d) silica capillary segments (100/360 µm i.d./o.d) are cemented, aligned with the hole, using a 75 µm tungsten wire as a guide.

The authors found that as implemented, dispersion in cells (a) and (b) is much larger than the other designs. Design (a) is essentially the same geometry as some of the earliest detectors used in CITP [283] and is the most common geometry used for conductometry in μfluidic platforms. With very small diameter capillaries (20 μm φ) manually fabricating such a structure would be extremely difficult. Regarding design (b), given availability limitations of the smallest φ conductive tubing, further miniaturization is impractical. Design (c) was thought to be practical if a center wire, less easily corroded than copper, is used; as is, design (d) performed the best among those tested. Limitations of other components did not permit an accurate assessment of the performance of (d) vs. (e) but the latter is much more difficult to fabricate.

5.3.2. *Oscillometry or admittance detection (also called capacitively coupled contactless conductivity detection, C^{4}D)*

One of the difficulties in applying electrical detection methods in CE is the presence of a high electric field. Of course, this difficulty does not arise after the capillary is grounded, typically at the exit end. The possibility of dispersion at or after the exit can be avoided with on-column detection. Monitoring of solution admittance has been known for a long time [234], especially for conductometric titrations, the "conductance" of a solution in a glass container can be readily monitored with the electrodes touching the outsides of a beaker. The once popular Sargent Model V oscillometer used a frequency of 5 MHz, the impedance represented by 1 mm thick glass (dielectric constant ~4) for a 10 cm^2 area will be less than 1 kΩ at this frequency. Several flow-through oscillometric "conductivity" detectors were described in the 80's for flow injection analysis [292] or IC [293], using commercially available oscillometric equipment operating at 42 MHz; the brass electrodes used in the cells were coated with polysiloxane or PTFE. In the 80's, others also described oscillometric detectors operating at 1 MHz for ITP/CITP in PTFE capillaries [294,295]. However, such schemes hardly saw adoption by others until independently and concurrently two groups in two different continents used this principle, albeit at significantly lower frequencies, one at 600 kHz and retaining the *oscillometry* nomenclature [236] and the other at 20–40 kHz, calling it initially Capacitively Coupled Conductivity Detector (CCCD) [235] and later adding the adjective *contactless* to the description; thus the origin of the catchy acronym C^{4}D [296].

In C^{4}D, the electrodes are placed outside the separation channel, in contact with the walls of the channel, not in solution contact. The current measured is no longer a function of only the voltage and the solution impedance; the excitation voltage is attenuated by the capacitive reactance of the wall (although the degree of attenuation is highly dependent on the excitation frequency and cell geometry), then travels through the solution, being attenuated by the solution resistance, and finally exits the cell being coupled capacitively through the wall to the pick-up electrode. When the probe frequency is increased to minimize the wall impedance, across the air transmission between the electrodes become increasingly important. This description generally holds except that it ignores solution capacitance, which becomes important as the solution becomes less conductive. In the latter case, such as with SIC/SOTIC with nearly pure water as the background, the capacitive current through the solution not only becomes important, at higher frequencies it dominates the ohmic current [297].

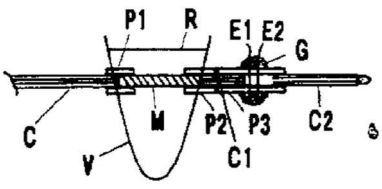

Fig. 19. C: separation capillary, radiation grafted membrane tube M inserted in PVC tubes P1, P2 and butted to capillaries C and C1; E1, E2 Pt-wire electrodes, P3: PVC tube sleeve, G: Epoxy glue, C2: outlet capillary. Reprinted from Ref. [288] with permission from the American Chemical Society.

With CE, however, the specific conductance of the background electrolyte is significantly above where this becomes a problem. With SIC/SOTIC there are conflicting issues that make it difficult to impossible for present C^{4}D approaches to reach LODs that can be achieved with conventional conductometric detection relying on direct solution-electrode contact. The latter strategy has no frequency dependence on the observed cell current (other than electrolysis problems that can still occur with a combination of low frequencies and high excitation amplitude, despite an alternating waveform). With noncontact admittance detection, under many conditions, the largest contributor of the overall cell impedance is the transmission of the excitation energy through the walls of the conduit, once entering the solution from the transmitting electrode and again returning to the pickup electrode. This transfer takes place entirely by capacitive coupling through the wall. Whenever the wall impedance is the limiting factor, the overall current will increase directly with increasing probe frequency and in general, S/N will improve. However, leakage currents and crosstalk (e.g., across the air from one electrode to another) also increases with increasing frequency and most such detectors therefore operate well below 1 MHz. Now consider that much like Fig. 22 implies, the liquid behaves both as a resistor and a capacitor. At specific conductance levels approaching that of pure water (55 nS/cm), as far as the solution admittance is concerned, the capacitive admittance will exceed the resistive (ohmic) admittance at most typical exciting frequencies used in such instruments. For example, specific conductance values of 100–300 nS/cm for a well-operated SIC system detector background is common. Given the dielectric constant of water, at background conductance levels of 100 and 300 nS/cm, the capacitive admittance will exceed the ohmic admittance at all frequencies ≥2.2 kHz and ≥6.7 kHz, respectively. The problem becomes worse when one considers the lowest excitation frequency available in the most widely used commercial admittance detector/C^{4}D is 38 kHz. This situation is compounded by the fact that the dielectric constant of water monotonically decreases as electrolyte is added. Therefore, near the LOD when a small amount of electrolyte appears in a nearly pure water background (when at typical excitation frequencies, the capacitive contribution to the overall current far exceeds the resistive component), the decrease in the capacitive admittance starting from pure water when electrolyte is added, exceeds the increase in the ohmic admittance and a negative "conductance" signal results near the LOD. Indeed, this has been observed both theoretically with more detailed models and experimentally [297].

Again, this is not a problem with CE applications, where solution ohmic admittance is much higher than the capacitive admittance. The wall admittance is invariant and does not change with solution conductance; therefore, as long as the wall admittance is significantly higher than the solution admittance, the overall current or signal will monotonically increase with solution conductivity, it will indeed behave as a "conductivity" detector. The implementation of C^{4}D is substantially simpler than a contact conductivity detector, the detector can be easily placed on-column, obviating dispersion, and the electronics are largely simple and inexpensive; one of the original inventors have created a "openC^{4}D" web resource to facilitate do-it-yourself'ers [298]. As a result, the use of C^{4}D has seen explosive growth since its introduction. It is currently the go-to solution, whenever applicable, for μFSD applications and beyond. Application of C^{4}Ds in capillary format and in μFSDs have been covered in depth through a series of biennial reviews by Hauser and Kubáň [26–29]. The latest installment is a decadal review from one of these authors [39]. There is little that we can add to these comprehensive reviews. C^{4}D has found broad use in μchip CE [299–301] and has demonstrated LODs of 90–250 μg/L for inorganic ions and 200–2000 μg/L for larger organic ions and phosphate [301]. Admittance detection has also become more common for microfluidic IEC as channels continue to decrease in size demonstrating sensitivity for SOTIC similar to CE, achieving LODs from 6.7 to 13 μM (13–26 fmol) [291].

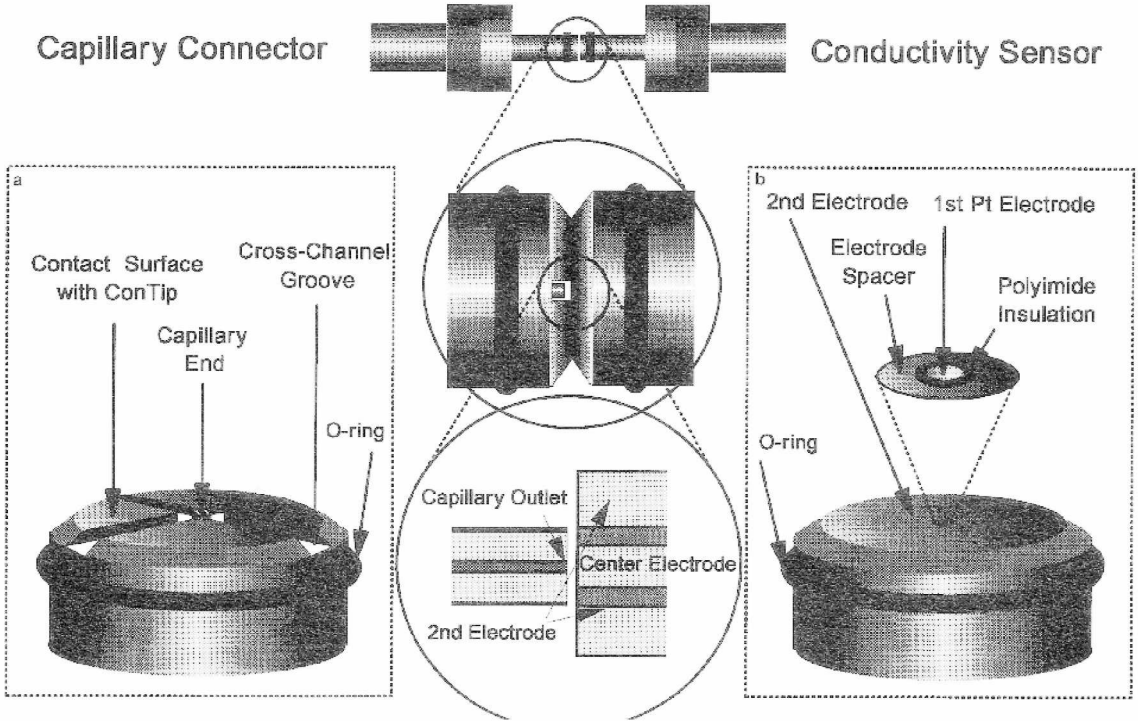

Fig. 20. a) Perspective view of the capillary half of the detector cell (termed ConCap); the grooves allow for facile liquid exit. B) Perspective view of the sensor half of the detector cell (termed Con-Tip). C) Center: Sequential close ups of the detector cell. Reprinted with permission from Ref. [290].

Widely achievable sensitivities for conductivity detection are 10–20 fmol for admittance/contactless methods and 0.5–1 fmol for direct contact methods.

Some limitations of C^4D/admittance detection exist, at least in its original format. At very low background and low analyte concentration end, the linearity and LOD can be improved by operating at a low excitation frequency, e.g., 500 Hz. An example is given in Fig. 23 for SIC – the S/N = 3 LOD was 27 nM bromide injected concentration. Given that chromatographic dilution is ~10×, the actual amount present in the 2.6 nL detection volume at the LOD would be < 10 amol. Such detectors have been demonstrated to work well with capillaries as small as 2–5 μm in diameter [302]. The detector output exhibited excellent linear correspondence with a macroscale SIC system conductance detector output in the 0−6300 nS/cm range for concentrations ≤100 μM but became increasingly nonlinear at higher concentrations ($r^2 \geq 0.9999$, 0.9933, 0.9827,0.9784, and 0.9776 for upper concentration limits of 100, 250, 500, 750, and 1000 μM). The good LOD comes at the expense of limited linearity. Linearity does extend to higher concentrations with a higher excitation frequency, at the expense of an increased LOD. The considerable loss of linearity and loss of detectability when operating at the minimum available frequency of a commercial C^4D instrument is illustrated in Fig. 24.

One of the fundamental limitations in linearity of the observed signal in the simplest C^4D design discussed is that we are discussing three serial impedances, one from the entry wall, then the solution, then the exit wall. Even if the solution admittance changes linearly with concentration, the overall behavior cannot be linear unless the wall impedance is always negligible compared to that of the solution. There have been efforts to accomplish precisely this by putting a carefully chosen inductor in series with the wall such that the wall capacitance and series inductance (real or simulated) forms a resonator leading to negligible impedance [303]. While it has been demonstrated to be effective in large diameter conduits, improvement in μFSD scale performance was limited and the concept was not tested to background conductance values relevant to SIC/SOTIC. An altogether different approach is to make a reference measurement of the system with and without the analyte. This approach, based on the beginning and the end of a μFSD has been reported to increase S/N by a significant factor [304]. Background compensation has also been attempted by making simultaneous measurements in a second "idle" capillary and subtracting this from the output of the "active" capillary [305]. The authors report ~3–7x improvement in S/N (part of which was attributed to lower noise electronics); perhaps of greater interest to the acronym-dazzled reader may be fact that the authors felt they can now add yet another C for "compensated", thus having made a C^5D! A better differential arrangement was reported actually earlier, comprising two sensing cells driven by two ends of a center-tapped transformer and then connected to standard differential amplifier circuitry. Excellent immunity to drift (even in the face of deliberately introduced large temperature changes) was demonstrated [306]. Any improvement in linear dynamic range was not examined in either of the above approaches. Similar approaches using 3 to 5 electrodes continue to be explored; in one recent papert, the authors report extending the linearity to almost 3 orders of magnitude [307], while it is difficult to get linearity in the standard arrangement over two orders of magnitude. Contact conductivity measurement can span 6 orders of magnitude in linearity; to be fair, there are few real situations where this is needed.

Advantages of conductivity detection include excellent sensitivity and robustness, selective detection of ions, and ease of operation. The obvious disadvantage is that it is limited to ionic analytes. In chromatographic separation of ions, the best LODs are only achievable with suppression. This, as well as contact conductance measurements are difficult to implement in a μchip or OT scale. Admittance detection or C^4D is much easier to implement regardless of scale, but present implementations cannot reach both a low LOD and a large dynamic range at the same time.

5.4. OTIC and SOTIC: non-detector essentials

Open tubular IC is a subclass of open tubular LC (OTLC). The first truly impressive work on OTLC was carried out by Jorgenson and Guthrie on 15 μm φ home-drawn glass capillaries 40 years ago [308]

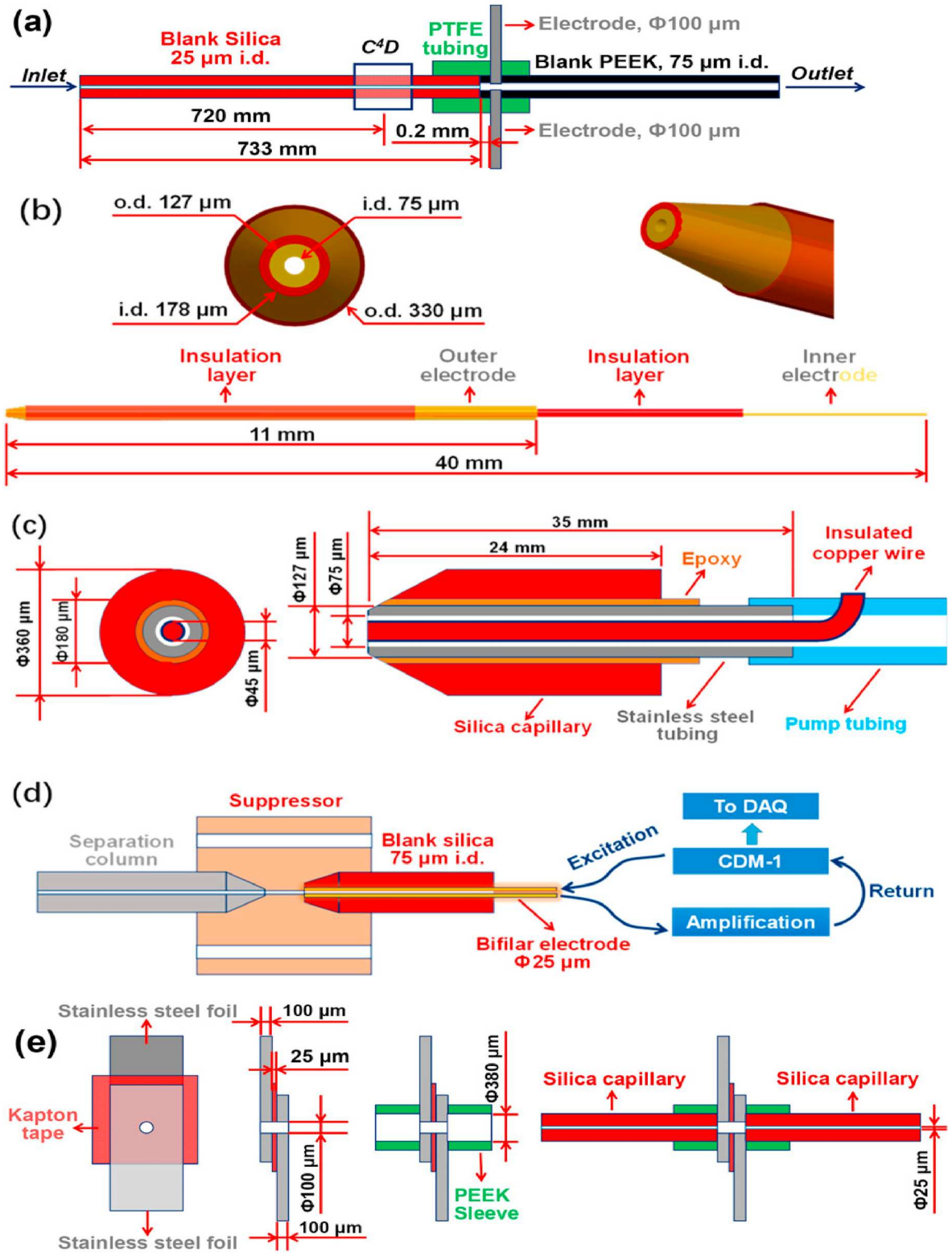

Fig. 21. End-column conductivity probe designs (a) standard radially opposed electrodes, placed end-column rather than on-column for the ease of fabrication and implementation; (b) annular ring electrodes; (c) ring-disk electrodes; (d) bifilar electrodes; (e) planar foil electrodes. From Ref. [291] by permission of the American Chemical Society.

although they credited many earlier studies, mostly from Japan, dating back to 1978. Jorgenson and Guthrie used fluorescence detection with a mercury arc lamp excitation source [309] and examined both the theoretical underpinning and experimental performance. They also demonstrated the applicability of laser-induced fluorescence detection [310] and amperometric [241] and voltammetric [244] detection shortly thereafter. Regardless, Jorgenson said at the time, in his usual prescient fashion: *The most uncertain area is detection. Here we are farthest from our goal of realistic working systems, and any broadly significant developments are probably many years away. It is detection which will*

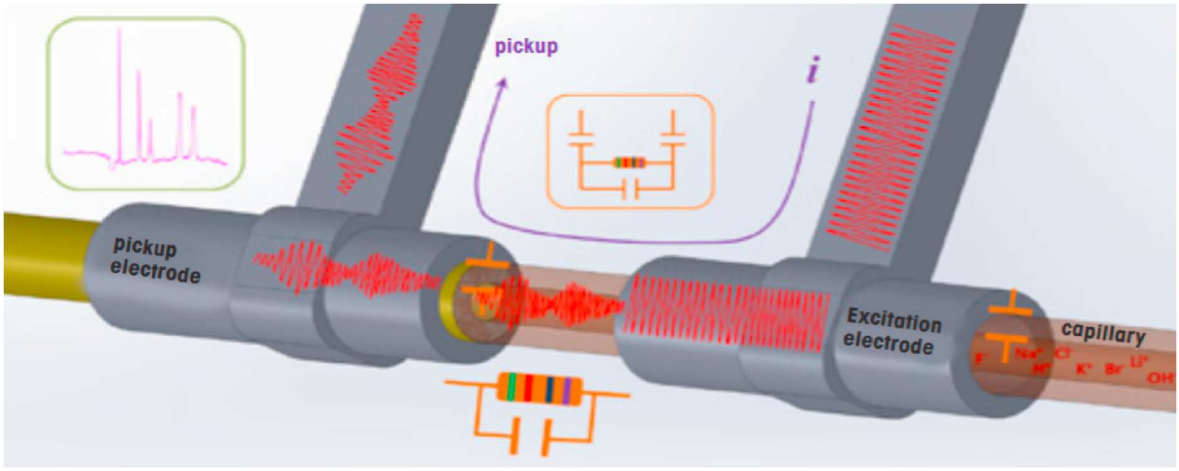

Fig. 22. Illustration of a C^4D detection cell and equivalent circuit. Figure reproduced from Ref. [82].

determine if liquid chromatography in (open) *capillaries is to be a real success.* It is fair to say that despite the demonstrated simplicity and superb separation performance of OTLC, it has not become commonplace. Surely conduit diameters have decreased even further, e.g., to 2 μm, and even more impressive separations have been demonstrated either with LIF [166] or MS [104] detectors. However, beyond the requirement of prior tagging with a fluorescent marker, to be applicable to this size scale, the LIF arrangement requires substantially more refined optics, etc. relative to some of the less expensive LIFs described in section 2.2. Similarly, the MS used was one of the most sophisticated commercially available (to be compatible with sub-nL/min flow rates from the column). Admittedly, amperometric detection is not expensive but at this

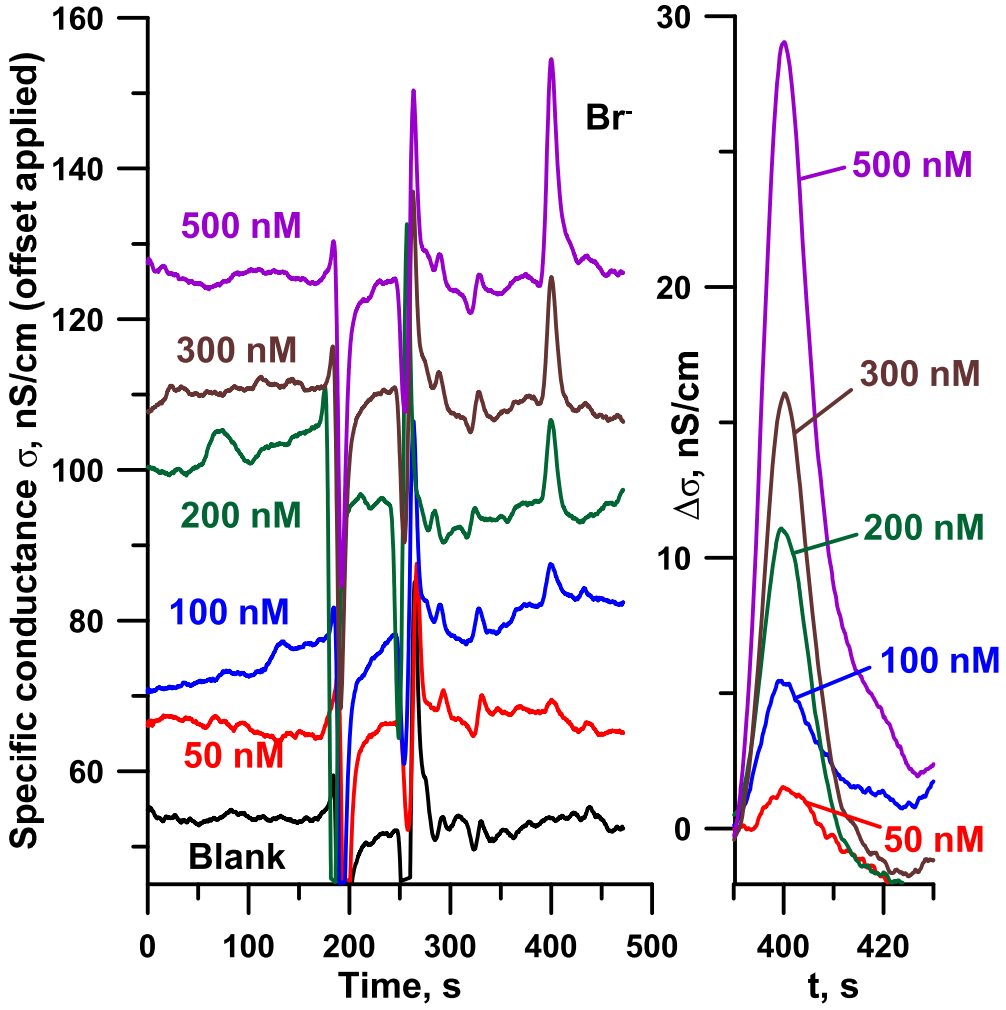

Fig. 23. Suppressed ion chromatogram of bromide standards, Br^- elutes at ~400 s. Right magnified portion shows the blank subtracted view of the standard in the region of interest. V_{app}, p-p = 22 V, f = 500 Hz. Transimpedance gain 1 V/nA Reprinted from Ref. [302] by permission from the American Chemical Society.

scale, not easy to practice, much less in a robust, reproducible manner. OTIC may be an exception among other OTLC techniques regarding detection difficulties, at least in the 15–25 μm diameter scale, especially in the nonsuppressed mode, where admittance detection/C^4D is readily applicable. A recent publication by a group in Thailand with relatively limited resources, for example, has shown a practical application of OTIC, in determining various anions in beverages, after online dialysis [311].

Common requirements to all of these systems are pumping and injection schemes, in SOTIC, eluent generation and suppression are further needed. Common approaches include pneumatic pumping, very simple to use and control, but any changes in downstream restriction affects flow (this can be an issue if membrane devices like suppressors are present, their flow resistance can change over time, especially if allowed to dry out). This can be solved by continuous flow monitoring and feedback based control. Another approach is to use larger flow rate pumps and split off and discard the excess flow, this does not prevent flow variations if flow restrictions change in the capillary column. While the split flow arrangements allow the use of conventional injectors; these set ups cannot take advantage of the ultra-small requirements for eluent volume or solvent volume in OTLC. The options for reliable pumping in the sub-μL/min range are limited. High resolution small volume (e.g., 10 μL) syringe pumps are acceptable unless silica leaching from glass syringes is unacceptable. Continuous multi-barrel syringe pumps like the low flow Milligat (www.Globalfia.com) does provide for adequately low pumping rates and are sufficiently pressure capable, but neither is particularly lightweight or power efficient.

The smallest internal loop injector presently available has a nominal volume of ~2 nL. This may or may not be sufficiently small for some applications. In their original work, Jorgenson and Guthrie [308] introduced the use of a loop injector where the contents of the injection loop pass by the column entrance and only a small amount of the sample is injected by splitting the flow. Such a flow splitting occurs only during the injection. They termed it static splitting to distinguish from the continuous splitting at all times. The same principle has been adopted by others [51], who used a pneumatic pump and showed that the injection volume can be varied over a large range by varying valve timing and pneumatic pressure and further demonstrated that because the sample occupies only a small portion of the column, sample viscosity has very little effect on the injected volume; they, however, chose a different moniker, hydrodynamic injection.

5.4.1. *Electrodialytic eluent generators for SOTIC*

Regarding eluent generation, the single bead generator previously discussed [280] in Sec. 5.3.1.1 was said to have an internal volume of 0.16 μL, this would appear to be adequate for gradient applications with flow rates in the range of 0.1–0.2 μL/min. However, this device generates gas and the internal volume of the degassing tubing referred to in that work would have a volume of 20 μL, unacceptable for gradient applications. Further, when EEGs are used with packed columns, the resulting backpressure on the gas removal device facilitates degassing. The low back pressures of SOTIC does not help degassing. Following an earlier macroscale generator that avoided gas generation by the use of a bipolar membrane [312], a nanovolume generator of 210 nL internal volume was devised. One of the issues with a catex-anex bead-based EEG [278] was that suppressed eluent conductance was not as low as could be produced from single catex membrane/bead based generators; similar observations were made early for CEM/AEM based EEGs [272]

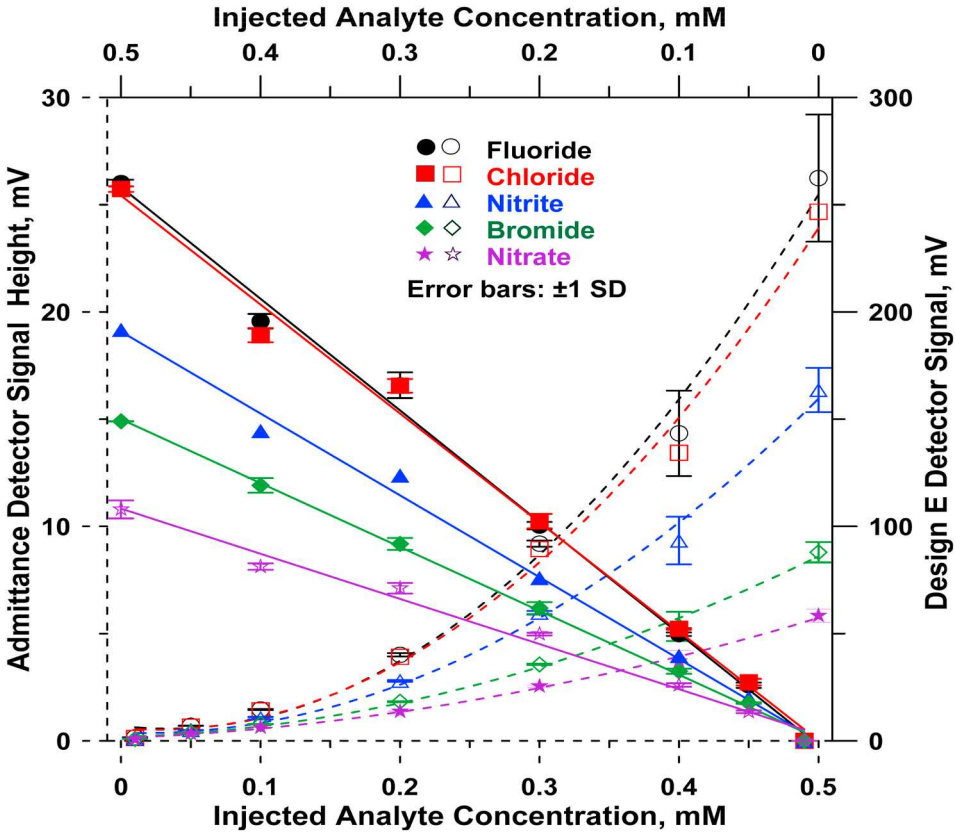

Fig. 24. Calibration plots for five anions under isocratic elution SOTIC conditions with admittance detection at 38 kHz by a commercial detector (left ordinate, bottom abscissa, hollow symbols, quadratic best-fit as dashed line) and contact conductance detection (Design E, Fig. 21, top abscissa - note reversed direction for clarity, right ordinate, filled symbols, linear best-fit as solid line). OT Column: 28 μm i.d., 370 μm o.d., 782 mm in length. Effective length: 782 + 40 mm (Admittance), Suppressor length: 0.80 mm, Suppressor current: 10 μA, Detection frequency: 38 kHz, Eluent: 5 mM KOH, Injection volume: 2.0 nL. Reprinted from Ref. [291] by permission of the American Chemical Society.

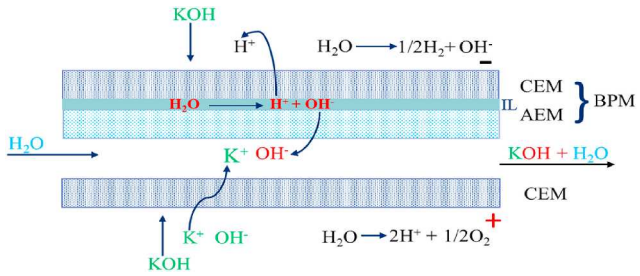

Fig. 25. Ion transport in a reverse-biased BPM, see text for details. Reprinted from Ref. [313] by permission of the American Chemical Society.

and were ascribed to the breakdown of the anex functionalities in a strongly alkaline medium likely affected by direct electrode contact. A bipolar membrane (BPM), consisting of an AEM laminated to a CEM, does not transport hydroxide ion from one side of the membrane to another, as an AEM does, it does not in fact conduct any ion across the whole membrane when reverse biased (CEM-side negative). Imagine some NaCl on the CEM side of the membrane; Na^+ has to move against the electric field, hence does not, and Cl^- is forbidden by the CEM and hence does not. So regardless of what electrolyte is there (or water) on the CEM side of the BPM, with the indicated field direction, the entire electrical field appears across the infinitesimally small CEM-AEM interface within the BPM and this high electric field promotes the dissociation of water.

Now looking from within the interface out, the field direction and the placement of the membranes are both conducive to the transport of H^+ and OH^- as indicated in Fig. 25 for the BPM. The arrangement in Fig. 25, depicting a BPM-based EEG also includes a CEM, the source for the alkali metal ion (typically KOH) flows in the channel outside the CEM where a noble metal positive electrode is located in addition. The eluent production channel is bounded by the CEM on one side and the AEM side of the BPM on the other side. Water or an electrolyte flows on the AEM side of the BPM where the negative electrode is disposed. Unless the latter is in close contact with the BPM, an electrolyte is preferred in this channel to avoid undesirable voltage drop. The effluent from the KOH feed chamber can be directed through here, for simplicity. Water is influent in the central channel and the electrical current drives K^+ and OH- from the CEM and the BPM side, respectively, forming current controlled pure KOH as the product in the central channel. The nanoscale implementation of this concept is centered on a cross-fitting as shown in Fig. 26.

While the successful performance of the device was demonstrated, 10–90% gradient rise time at 3.5 min was longer than desirable. Long term stability and eluent purity of the device has not been characterized.

5.4.2. *Suppressors for SOTIC*

Fig. 27 overleaf shows the first suppressor successfully used in SOTIC [314]. The top panel shows the general arrangement, and the bottom panel shows a perspective drawing with dimensions. The device utilizes a three parallel channel flow configuration, similar to a conventional macroscale suppressor: the central channel is for the eluent. The flanking regenerant channels all contained in a 10 × 5 × 1 mm perfluorosulfonate CEM (Nafion®) block. The central channel is made by piercing the center of the block along its long axis with a 0.3 mm dia. hypodermic needle. No material is removed, it leaves a crack in the elastomeric polymer. The flanking channels are drilled out to 0.35 mm dia. The column end and a silica exit tube end were honed to a 45°–60° taper at the tip. When the column end and the exit capillary are pushed in from opposite ends of the central channel/crack to form a sub-mm gap, the proximity of the capillary ends prevents the channel from closing up. In the regenerant channels inserted PTFE capillaries provide for liquid inlet and tees at the outlet ends provide for liquid exit and insertion of platinum wire electrodes. A 1 mm active suppressor length suppressed up to 100 mM hydroxide at 100 nL/min.

While electrodialytic suppressors are the ones mainly used in macroscale IC; a very strong case can be made for using chemical regeneration in this miniature scale. Arguably chemical regeneration is less complex; it can lead to a lower background without possibilities of added electrical/bubble induced noise. So little regenerant is used that a small amount can almost be indefinitely recycled through a small disposable H^+-form resin packed bed. A chemically regenerated suppressor can be constructed of the device in Fig. 27 with just the central channel, but a crack is not a permanent channel and over a period of unuse tends to close back up, flow must be continuously maintained through it. For 20–25 μm φ columns, suppressors of comparable diameter and requisite length are difficult to impossible to produce by mechanical drilling. Laser drilling is not possible for polymers containing functional groups that are thermally decomposed. A microscale suppressor was made by casting a newly synthesized cation exchange prepolymer between the column end and an exit tube connected by a tiny length of tungsten microwire, curing, thermally annealing, and then removing the wire (Fig. 28) [315].

Such devices have subsequently been tested with a 38/150 μm i.d./o.d. stainless steel exit tube forcibly inserted into the microchannel as one electrode of a conductivity detector, and another similar tube connected by a sleeve tubing, almost touching the first electrode, and poly(styrenesulfonic) acid (the very large counterion, ~70,000 MW, greatly inhibits any leakage of the counterion through the membrane) as the regenerant [316]. Many combinations of suppressor active lengths and eluent flow rates were tested. For a 20 μm bore column, the maximum relevant flow rate is 170 nL/min, a 700 μm active length suppressor was able to suppress at least up to 30 mM KOH, more than adequate for OTIC

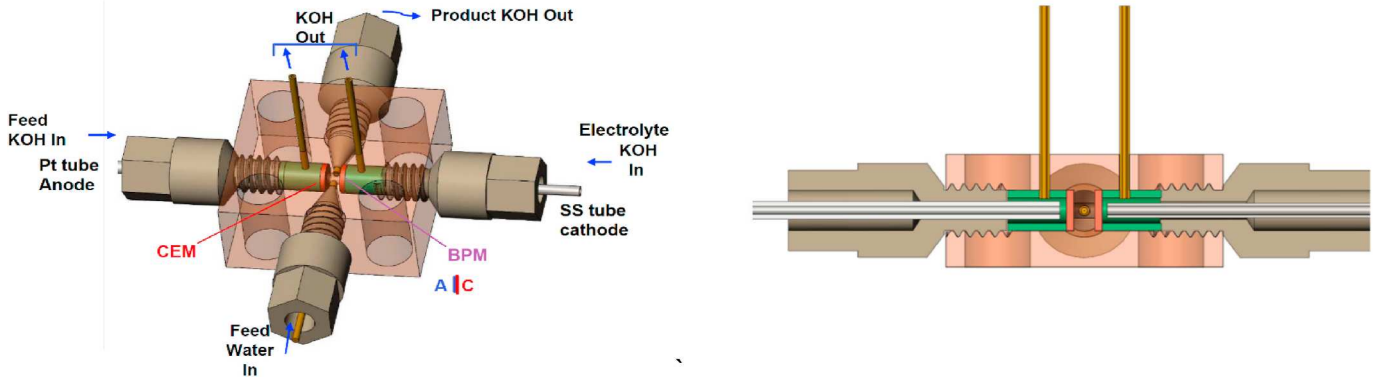

Fig. 26. The nanovolume CEM/BPM EEG (internal swept volume 290 nL) is built on a single 10 × 10 mm cross fitting. The drone view is shown in the left figure where 360/150 μm i.d./o.d. PEEK tubes access the compartments behind the membranes. The right figure shows the cutaway view as seen from the front edge of the left figure. Reprinted from Ref. [313] by permission of the American Chemical Society.

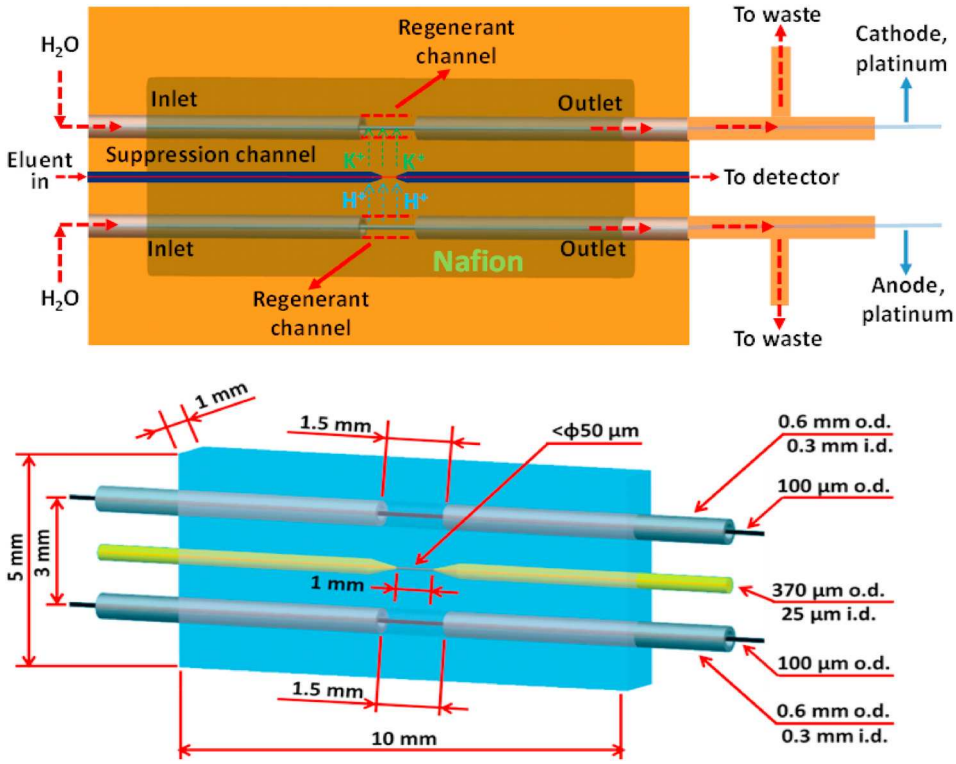

Fig. 27. Electrodialytic suppressor for SOTIC. The top panel shows the general schematic, the bottom panel shows the perspective and dimensions. See text for details. Reprinted from Ref. [314] by permission of the American Chemical Society.

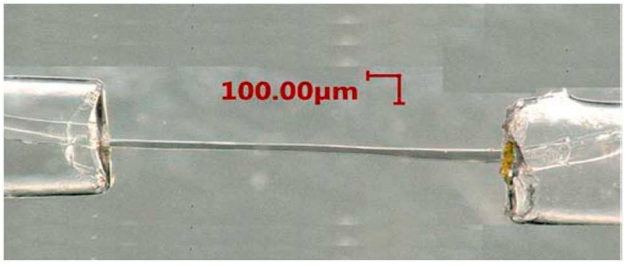

Fig. 28. A ~30 µm i.d. microchannel comprising a poly(vinyl)alcohol-(poly) styrenesufonic acid CEM cast around a 25 µm tungsten wire mandrel, Reprinted from Ref. [315] by permission of the American Chemical Society.

applications. The suppressor effluents were extensively studied for potential leachates from the membranes by ESI-MS and compared with similar studies with commercial macrosuppressors. While it is very difficult to compare such devices directly because of the vast differences in the exposed surface areas and operational flow rates, the micro-suppressor showed virtually no contaminants in the effluent that were not present in the feed water; this was not the case for the commercial device.

6. Mass spectrometry

Mass spectrometry (MS), with or without any separation (miniature or otherwise) system or sample handling system ahead of it is a topic so vast and so varied that it is quite beyond the scope of this review. Mass spectrometry is perhaps unique in its applicability to any analyte type. The combination of different ionization techniques and mass analyzers can be harnessed to detect almost any analyte. The basic principle involves ionizing the analytes introduced into the instrument and then separating them based on their mass to charge ratio (m/z). Specific analytes can be further examined through fragmentation and secondary mass analysis of the fragments through what is called tandem mass spectrometry. While most commonly only one additional mass analysis step is involved (MS/MS), in suitably designed instruments, many sequential fragmentation – mass analysis steps may be carried out. Alternatively, one may rely on high accuracy measurement of the time for target ions to reach the detector (as in time of flight/TOF MS) or the precise frequency utilized to keep the target ion trapped in its orbit (as used in Orbitrap™ mass spectrometers, see below) to produce accurate mass determinations. Mass spectrometers produce a vast amount of raw data, which, with the aid of additional software and accessible libraries, provides a large amount of useful information, including identification of specific analytes, and more. The instruments themselves are typically large, expensive, have sizable vacuum and power needs, and are not as easily miniaturized as optical or electrochemical detectors but the mass sensitivity in some of the more complex units are unequaled by any other instrument, they can be ideal mates to µFSDs [13,317]. In one configuration, commercially available as Orbitrap™ MS, ions of a certain m/z can be selectively trapped in a fixed orbit in an annular cavity and the image current used to detect the ion with exquisite sensitivity [318].

Several miniature mass spectrometers have been developed that can interface with µFSDs [319–323]. However, such miniaturization comes at considerable sacrifice to the attainable sensitivity, the applicable mass range, as well as the mass resolution. Cooks and his students have introduced a series of miniature linear ion trap MS units, with monikers Mini 10, 11, and 12. They range from 5 to 15 kg in weight and 5–15 L in volume [319–321]. Compared to this, an intermediate mass range MS: *Orbitrap Exploris 240* weighs 120 kg (without the needed roughing vacuum pumps or the data system) and has a volume of 286 L [324]. Performance of the miniature units are limited: The Mini 12 has a mass range of 25–900 with a maximum mass resolution of 500 [321]. Miniature quadrupole and triple quadrupole MS systems have also been demonstrated more recently; they offer similar performance to their ion trap counterparts but are somewhat heavier (27–32 kg) [322,323,325].

The distinct sections of a mass spectrometer play unique roles in its operation. The ionization source represents the front end and has a profound effect on the ultimately attainable LODs. This component is responsible for ionizing the analyte(s) and transferring the ions thus generated to the mass analyzer, which then separates the ions based on their *m/z*. The ionization step is typically the least efficient step in the chain, and thus the determinant of the attainable LOD(s). This step can be as much as 3–4 orders of magnitude less efficient than the efficiency of the mass analyzer to transmit the ion(s) of selected *m/z* to the detector [6,13,317,326]. The most utilized ionization sources for μfluidic applications are electrospray ionization (ESI), atmospheric pressure chemical ionization (APCI), and matrix assisted laser desorption/ionization (MALDI) [6]. A recent review goes into more detail about various ionization sources and their integration with μfluidic devices [32].

6.1. Electrospray ionization

Electrospray ionization utilizes an applied high voltage (HV, typ. several kV) to generate a fine spray of droplets from the end of the separation conduit. The solvent comprises the bulk of the droplet; solvent molecules acquire a charge and some of the charge transfers to the analyte molecules as the droplets continue to move onward to the mass analyzer; an analyte molecule may acquire multiple charges [327].

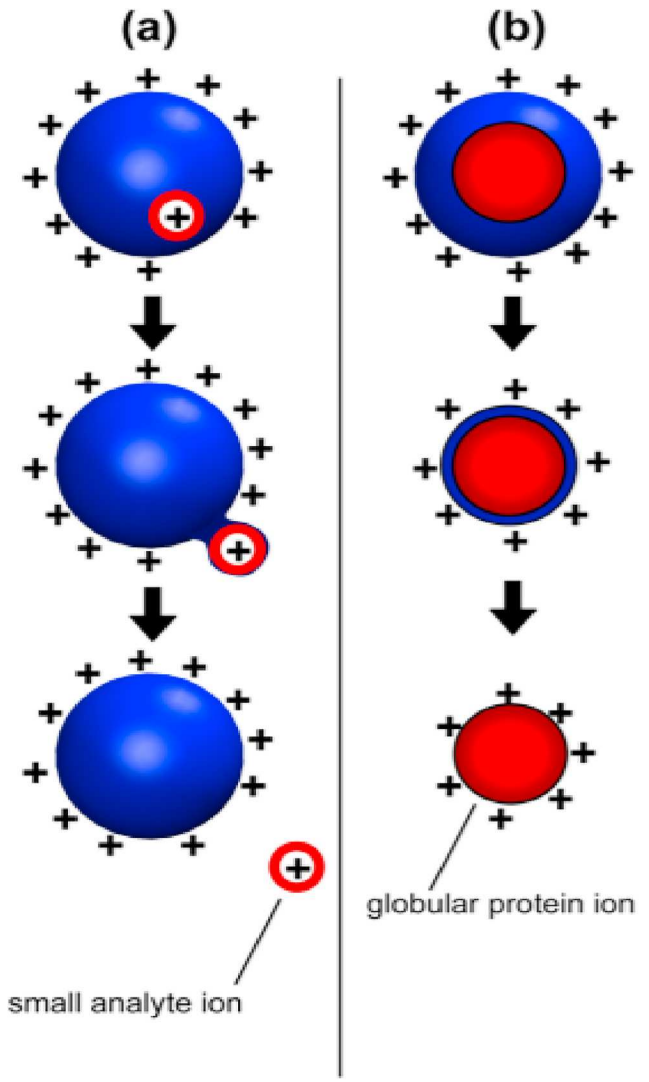

Fig. 29. Illustrations of (a) a sample ion evaporating from a droplet through the ion evaporation model, (b) sample ion accumulating charge as solvent evaporates through the charge residue model. Figure reproduced from Ref. [327].

To create the spray, HV is applied between the end of the separation conduit (typically fashioned into a sharp pointed tip) and a grounded metal plate bearing an aperture that serves as the entry to next section where the applied vacuum reduces the pressure by 100–1000× before entry to the mass analyzer. Either positive or negative HV can be applied to the conduit tip, ultimately generating positive or negative ions. The applied HV causes the formation of a finely pointed cone of solution, called a Taylor cone, that moves towards the ground plate with a high density of charged solvent ions that break up into droplets. As the solvent molecules evaporate, the charge density in the droplets increases to a point that coulombic repulsion literally causes the droplets to blow apart, forming even smaller droplets. As analyte molecules acquire charge left in the droplets, the analytes begin to form ions in the gas or aerosol phase, aided by the electric field, the increasing surface energy of a minute drop, the vacuum, its own vapor pressure and also its lack of affinity to remain in the solvent; this is the scenario envisioned by the *ion evaporation model* [327]. The *charge residue model* invokes that when all the solvent is gone through evaporation leaving only the ionized sample behind, coulombic repulsion alone will be sufficient for disintegration and transfer to the gas/aerosol phase [327]. Fig. 29 illustrates the ion evaporation and charge residue models for ESI. Positive ionization mode, where + HV is applied, is more commonly used although analytes with acid groups that have an intrinsic affinity to form negative ions through deprotonation benefit from application of the -HV mode. Large polar or ionic samples are particularly well suited to ESI; for small mass analytes, multiple charging may cause the ions to drop below the *m/z* range the instrument can handle, as well as complicate the task of separating multiple such analytes. Very non-polar compounds, especially aprotic ones, are not easily amenable to ionization, and are not good candidates for ESI [327].

One unique form of ESI that has been integrated with the miniature mass spectrometers mentioned earlier is Desorption Electrospray Ionization (DESI). DESI operates by directing a pneumatically assisted electrically charged mist/spray to impinge at an acute angle on the sample only a few mm away, adsorbed or immobilized on a surface. Droplets may deposit on the surface and dissolve the sample before being struck by subsequent droplets forming a secondary spray of droplets from the surface containing the sample [16]. The positioning is arranged for the secondary bounce-back spray to be directed toward the MS inlet. Charge transfer to the sample analytes occur from charged solvent molecules via the same mechanisms as standard ESI. In most cases, applying DESI to μFSDs is not straightforward; the sample is already dissolved in a solvent and is thus more amenable to traditional ESI.

ESI-MS is also practiced in the nanoscale (flow rates <1 μL/min), at least in one case, operation at sub-nL/min flow rates has been carried out [104]. The spray tip may consist of a single emitter (the end of the fluidic conduit to which the high ESI voltage is applied, and the Taylor cone is generated), often extremely small in bore (in the sub-μm scale) or may consist of multiple emitters. The emitters may be capillaries drawn out to fine tips, or microfabricated. A variety of emitters have been investigated, from simple glass emitters built directly in the separation devices, as well as custom emitters that are attached the end of separation channels [328–330]. The emitter geometry coupled to the microfluidic channels for ESI analysis is important: the sharpness of the emitter tip influences Taylor cone shape and sensitivity at very low flow rates (<50 nL/min). In these low flow regimes, the electric field and flow rate are not sufficient to maintain the sharpness of the Taylor cone; it will broaden appreciably unless pointed emitter geometries are used. For faster flow rates, the emitter geometry has no effect on the Taylor cone shape and the eventual sensitivity [330]. Generally termed nano-ESI, this adaptation of ESI (which is already typically in the microscale) has many advantages. The two biggest advantages are improved ionization efficiency and much greater immunity to ionization suppression, a phenomenon related to the suppression of analyte

ionization by other ions concurrently present [331]. An excellent recent review discusses many aspects of nano-ESI [36]. Microfluidic devices are frequently interfaced with nano-ESI-MS to achieve higher sensitivity and conserve limited sample and expensive solvents; majority of mass spectrometry done with microfluidic devices are carried out through nano-ESI.

Peptide and proteins analysis have been often performed with Microfluidic LC-nano-ESI and CE-nano-ESI [332,333], achieving LODs as low as 170 zmol (for a 1 nM solution of leucine-enkephalin) [333]. Microfluidic platforms can also offer a large range of sample preparation and post-column processing features, including e.g., protein digestion, further increasing its attractiveness for analysis of biomolecules [331]. Widely achievable LOD for nano-ESI-MS is 500 zmol. Advantages to nano-ESI are its high sensitivity, amenability to a wide range of samples, and relative ease of integration with microfluidic devices. Commercially available nano-ESI sample introduction systems, are, however, expensive.

6.2. Atmospheric pressure chemical ionization (APCI)

APCI works best for the compounds not easily ionized by ESI, e.g., small molecule analytes, regardless of whether they are polar, nonpolar, or ionic [334]. As such, it is often used as a complementary ionization technique to ESI. APCI utilizes high energy ionized gas molecules that in turn ionizes a gas-phase analyte (as opposed to a droplet or aerosol phase analyte in ESI). A positive high voltage is applied to a sharp pointed electrode suspended in a reagent gas (often He, air, N_2, or CH_4). The corona discharge thus generates a plasma comprising positively charged ionized gas molecules and free electrons. The separation conduit effluent is heated to vaporize the analyte, and this is made to pass near the ionized reagent gas [335]. Gases mix rapidly; transit through a short tube is usually enough for sufficient ionization of the analyte, which can then move on to the mass analyzer [335,336]. Atmospheric Pressure Photoionization (APPI) is very similar to APCI, except ionization is not initialized by an ionized plasma, but instead by a stream of high energy (~10 eV) photons [334]. APPI is a softer ionization method than APCI and finds use for particularly unstable samples. Since the same instrument can perform APCI and APPI by swapping the electrode for a UV lamp, the duality helps expand the versatility of these rather niche ionization methods. APCI/APPI ionization efficiency is typically less than that in ESI but unlike ESI, multiple charging is not common.

Most instruments that are able to perform ESI are also able to perform APCI/APPI with minor modifications. While ESI may be more commonly used, APCI may be particularly useful for small analyte molecules; it is also easily integrated with μFSDs. Small biomolecule analyses performed with CE-APCI-MS, LC-APPI-MS, and HPLC-APCI-MS have demonstrated concentration and mass LODs of 1–150 nM or 1–300 fmol [334–337]. Routinely 10–100 fmol LODs are attainable in APCI-MS. Advantages to APCI are its complementary nature to ESI and its ease of integration with microfluidic devices. It does however show poorer ionization efficiencies relative to ESI and it will be challenging to miniaturize the ion source itself further.

6.3. Matrix assisted laser desorption/ionization (MALDI)

In MALDI, the sample is mixed with a matrix compound (e.g., 2,5-dihydroxybenzoic acid, among many others) with a very large matrix: sample ratio (1000:1 or even higher). Sample ionization is initiated by directing a high energy UV laser pulse to the sample/matrix mix. The high energy photon flux vaporizes the sample and ionizes some of the matrix. As the sample and matrix travel to the mass analyzer, charge transfer from the matrix ions to the analyte occurs, ionizing the latter. MALDI is most commonly used for very large biomolecules that are not easily analyzed by other methods and is typically coupled with a time-of-flight mass spectrometer (TOF-MS).

Table 2
Summary of demonstrated and widely achievable limits of detection.[a].

Detection method	Lowest demonstrated LOD	Widely achievable LOD
UV/Vis Absorbance	22 nM, 4 fmol	100 fmol
Fluorescence	150 ymol	1 zmol
Refractive Index	4–400 μM, 0.4–4 pmol	100 pmol
Chemiluminescence	0.88 nM, 0.27 amol	10 amol
Amperometry	100 nM, 1 fmol	50 fmol
Contactless Conductivity	27 nM, 100 amol	10–20 fmol
Suppressed Conductivity	50 nM, 1 fmol	10–20 fmol
Nano-ESI-MS	1 nM, 170 zmol	500 zmol
APCI-MS	1–5 nM,1 fmol	50–100 fmol
MALDI-MS	23 amol	50–100 fmol

[a] We have chosen to specify LODs in units of moles supplemented with concentration LODs when available. Devices used in the various studies not only vary in shape and size but also the injected sample volume. The lowest LODs reported in the literature are often for a specific analyte under optimized conditions and will not be generally applicable to most unknown or complex samples. We therefore also specify 'widely achievable LOD' in this review as an estimate of achievable LOD for real samples using first rate equipment but not a customized one-of-a-kind setup.

MALDI is the only commonly used ionization technique that is typically operated entirely under vacuum. Unlike ESI and APCI, it is difficult to integrate MALDI directly to a separation system because not only the entire ionization process operates in vacuum, MALDI often involves stationary targets that cannot be directly mated with a flowing stream. While there have been many efforts to make the marriage between MALDI and microfluidics seem less discontinuous, this union is still not straightforward [338–342].

Some early attempts to continuously couple a liquid stream to a TOF-MS involved considerable ingenuity. One unique approach from the Murray group involved immobilization in the aerosol phase. Aerosols were continuously generated by pneumatic nebulization of the solution that contained both the MALDI matrix compound and the analyte. A collimated beam of dried particles was formed by passage through a heated tube. Ions were then formed by irradiating the aerosol with pulsed UV radiation as the aerosol stream passed by the source region of a linear TOF-MS [343]. Murray later advocated the use of a rotating ball inlet where both the separation stream and the matrix solution were delivered to the surface of a rotating ball in contact with a polymer gasket that helped maintain a vacuum seal. Liquid adhering to the surface of the ball is dragged past the gasket into the vacuum of the mass spectrometer where it is irradiated by a pulsed UV laser; the resulting ions then enter a TOF-MS [344]. Karger's group similarly proposed a rotating quartz wheel in an evacuated source chamber [345]. Subsequently a moving mylar tape interface was advocated; unlike such interfaces used with IR spectrometers earlier, here the source chamber pressure was kept below the vapor pressure of the solvent – the cooling induced by the rapid evaporation of the solvent caused immediate freezing of the sample and prevented band broadening [346]. When depositing on a continuous surface, another technique to limit broadening is to use a hydrophobic surface so that isolated small drops are formed [347]. Droplet deposition, preceded by droplet based separation or isolation systems is among the most popular techniques today [338, 340]. On-line single droplet deposition for MALDI-MS of droplets as small as 100 pL was demonstrated by Murray's group two decades ago [348]. However, just being droplet-based does not make the process either convenient or attractive. For example, in one study a thin food wrap film was derivatized to form a fluorocarbon surface. This was now sufficiently hydrophobic and could be used as a controllably electrowetted platform. Such a platform comprises a very limited number of pads/spotting areas. A liquid drop on one pad can be moved to another by switching voltages applied to the different pads. The drop can then be transferred to a separate stage where MALDI is performed [342]. It is difficult to speculate how many will adopt such a technique but it does evoke memories of Rube Goldberg.

Robotic fraction collection and spotting of samples on a plate which can hold hundreds of sample spots is very much in current use [339, 349]. The MALDI matrix may be added post-spotting or the plate may already contain the matrix material. Multiple commercial versions for automated transfer of LC effluents to MALDI sample plates have been available for two decades [350].

MALDI has also taken advantage of the versatility of microfluidics and their construction. Entire μchips have been turned into MALDI sample plates and have been used to quantitate small amounts of peptides from rat neuron samples [351]. In this study, a fused silica plate was functionalized with antibodies in specific concentration; these antibodies would bind the target peptides. A polymer mold was then placed over the functionalized glass to make the separation channels, and the sample bearing the target peptides was run through the device. The antibodies were saturated with specific peptides until there was none left in solution, then the polymer layer was removed, and the glass plate was sprayed with MALDI matrix and used as the sample plate. Based on the total area of the plate which contained the peptides, it was possible to calculate the concentration of the bound peptides as the antibody concentration per unit area was known. Depending on the peptide, 400–600 fmol LODs were possible [351]. A more recent droplet μchip MALDI-MS system was able to achieve an LOD of 23 amol for the analysis of γ-aminobutyric acid [352]. Typically, achievable LODs for MALDI-MS are ~50–100 fmol. MALDI is a powerful complementary technique to ESI and APCI and has been the ionization method of choice for large biomolecules for many years, although it is being supplanted due to recent improvements in ESI ionization efficiencies for large biomolecules. The main mode of MALDI use today is still discontinuous, however. Typically used with TOF-MS, overall MALDI-MS systems are more complex and expensive than other MS detection systems. In a critical analysis of MALDI vs. ESI for the identification of peptides, a 2017 study emphasized that the two ionization techniques provide complementary results [353]. However, developments in variants of ESI are increasingly applicable to higher mass ranges and are increasingly favored over the more complex MALDI systems.

7. Conclusions

Reviews are necessarily retrospective. However, it is clear that the future increasingly lies in the small. It also appears that the primary challenge still remains detection, although much progress has surely been made since Jorgenson threw down the gauntlet four decades ago. The best demonstrated and generally achievable LODs for the principal detection methods discussed in this review are listed in Table 2. It has already been demonstrated that state of the art MS or LIF can handle effluents from separation conduits as small as 2 μm in i.d. However, high-end MS still remains bulky, expensive, and requires high operator skill. In the foreseeable future, it is not likely that a high-end MS detector will be used in the field or in a point of care application, both ideally suited for an otherwise microscale analysis system. Inexpensive diode-laser based fluorescence detectors can reach exquisite sensitivities today; while their optical characteristics may not be ideal to use with 2 μm capillaries yet, they can get down comfortably to monitoring fluorescence in conduits that are quite small. To use diode lasers in the wavelengths they are presently available, however, most common analytes will have to be tagged with a high quantum yield fluor. While the detector itself can be built in a small footprint and relatively inexpensively, need for pre-derivatization is also a big hurdle in the field or in point of care use, unless the tagging chemistry will permit its incorporation in the sample handling system. Chemiluminescence detection suffers the same problems, except now it is post-separation and has added issues, it may still however, be attractive in niche applications. Interestingly, electrogenerated CL, which may not require an added reagent, has not been much investigated for detection. Still, fluorescence or CL will typically require pre or post reaction steps in cases where it is applicable, but in most cases, analytes of interest simply cannot be derivatized in this fashion, at least conveniently. A significant amount of defense-related interest exists in UV photonics and highly integrated photonic systems, the lowest available wavelength of diode lasers will continue to go down, making native fluorescence detection possible for many more classes of analytes. We wish for a crystal ball to decide if UV-LIF or a compact, but still adequately capable MS detector will be the first to be the companion of choice for field use of μFSDs.

Our available crystal ball is again too cloudy to judge whether photothermal or cavity-based methods or some other more convoluted approach (e.g., use of ORRs) will make absorbance detection sufficiently sensitive for it to be useful for deployment in very small conduits. However, it is clear that some new paradigm is needed for absorbance measurement to continue to have the impact in microscale, as it has had in macrosystems.

Amperometric sensing can also provide exquisite sensitivity for applicable analytes and is likely to be among the top choices for a single-use measurement system that are more the norm in medical/clinical use. Admittance/C^4D has become a uniquely useful sensitive and inexpensive technique for the measurement of charged species and it is here to stay. What limitations it presently has for very low conductance levels as encountered in SOTIC are not fundamental and are likely to be overcome in near future. On-column suppressor development has already begun [354] but without an on-column detector that can faithfully measure down to the same levels that contact conductivity can, the full potential of the technique cannot be realized.

Finally, simultaneous detection by multiple techniques is likely to be increasingly used. It not only provides for complementarity and opens the application horizon, but the sum of the multidimensional information may be unique and separate from what each approach can provide.

Consent for publication

Written informed consent for publication was obtained from both authors.

CRediT authorship contribution statement

Cable G. Warren: Writing – review & editing, Writing – original draft. **Purnendu K. Dasgupta:** Writing – review & editing, Supervision, Methodology, Conceptualization.

Declaration of competing interest

The authors declare the following financial interests/personal relationships which may be considered as potential competing interests: Purnendu K Dasgupta reports financial support was provided by The University of Texas at Arlington. If there are other authors, they declare that they have no known competing financial interests or personal relationships that could have appeared to influence the work reported in this paper.

Data availability

No data was used for the research described in the article.

Acknowledgements

The authors would like to acknowledge Professor Daniel W. Armstrong, it was because of his encouragement (if not insistence) that this paper was started. We wish we could blame him for the fact that somewhere along the way the paper seemingly developed a will of its own and threatened to run away from the authors. We acknowledge support from the National Science Foundation (CHE-2003324) and the Hamish Small Chair Endowment.

Glossary

μFSD	Microfluidic Separation Device
μPAC	Micropillar Array Column
μTED	Microfluidic Thread Electroanalytical Device
ABS	Acrylonitrile Butadiene Styrene
AE	Acridinium Esters
AEM	Anion Exchange Membrane
AEX	Anion Exchange
APCI	Atmospheric Pressure Chemical Ionization
APD	Avalanche Photodiode
APPI	Atmospheric Pressure Photoionization
ATP	Adenosine 5′-triphosphate
AuxE	Auxillary or Counter Electrode
BGE	Background Electrolyte
BPM	Bipolar Membrane
BSI	Backscatter Interferometry
C^4D	Capacitively Coupled Contactless Conductity Detector
CE	Capillary Electrophoresis/Counter Electrode
CEC	Capillary Electrochromatography
CEM	Cation Exchange Membrane
CEX	Cation Exchange
CGE	Capillary Gel Electrophoresis
CITP	Capillary Isotachophoresis
CL	Chemiluminescence
CZE	Capillary Zone Electrophoresis
DESI	Desorption Electrospray Ionization
EEG	Electrodialytic Eluent Generator
ESI	Electrospray Ionization
FIA	Flow Injection Analysis
GC	Gas Chromatography
HPLC	High Performance Liquid Chromatography
HPZE	High Performance Zone Electrophoresis
HRP	Horseradish Peroxidase
HV	High Voltage
IC	Ion Chromatography
IEC	Ion Exchange Chromatography
IgG	Immunoglobuin G
ITP	Isotachophoresis
LCW	Liquid Core Waveguide
LE	Leading Electrolyte
LED	Light Emitting Diode
LIF	Laser Induced Fluorescence
LOD	Limit of Detection
MALDI	Matrix Assisted Laser Desorption Ionization
MIBD	Microinterferometric Backscatter Detector
MP	Mobile Phase
MS	Mass Spectrometry/Mass Spectrometer
ORR	Optical Ring Resonator
OTIC	Open Tubular Ion Chromatography
OTLC	Open Tubular Liquid Chromatography
PAD	Pulsed Amperometric Detector
PCF	Photonic Crystal Fiber
PDS	Photothermal Deflection Spectroscopy
PLA	Polylactic Acid
PMT	Photomultiplier Tube
PO	Peroxyoxalate
PSD	Position-Sensitive Detector
PSoC	Programmable System on a Chip
PTFE	Polytetrafluoroethylene
RE	Reference Electrode
RI	Refractive Index
RIU	Refrative Index Units
S/N	Signal to Noise Ratio
SERS	Surface Enhanced Raman Spectroscopy
SIC	Suppressed Ion Chromatography
SOTIC	Suppressed Open Tubular Ion Chromatography
SP	Stationary Phase
SPR	Surface Plasmon Resonance
SPW	Surface Plasmon Wave
TE	Terminating Electrolyte
TPE	Two-Photon Excitation
WE	Working Electrode
WGM	Whispering Gallery Mode

References

[1] R.P.W. Scott, Liquid Chromatography Detectors, Elsevier, 1977.
[2] R.P.W. Scott, Liquid Chromatography Detectors, Elsevier, 1986.
[3] S.L. Lin, H.Y. Bai, T.Y. Lin, M.R. Fuh, Microfluidic chip-based liquid chromatography coupled to mass spectrometry for determination of small molecules in bioanalytical applications, Electrophoresis 33 (4) (2012) 635–643.
[4] P.N. Nge, C.I. Rogers, A.T. Woolley, Advances in microfluidic materials, functions, integration, and applications, Chem. Rev. 113 (2013) 2550–2583, https://doi.org/10.1021/cr300337x.
[5] Y. Zhu, Q. Fang, Analytical detection techniques for droplet microfluidics-A review, Anal. Chim. Acta 787 (2013) 24–35, https://doi.org/10.1016/j.aca.2013.04.064.
[6] D. Gao, H. Liu, Y. Jiang, J.M. Lin, Recent advances in microfluidics combined with mass spectrometry: technologies and applications, Lab Chip 13 (2013) 3309–3322, https://doi.org/10.1039/c3lc50449b.
[7] S. de Bruyne, Design and Characterization of Microfabricated On-Chip HPLC Columns, University of Twente, Thesis, 2013. https://ris.utwente.nl/ws/portalfiles/portal/6059502/thesis_S_De_Bruyne.pdf.
[8] S.L. Lin, T.Y. Lin, M.R. Fuh, Microfluidic chip-based liquid chromatography coupled to mass spectrometry for determination of small molecules in bioanalytical applications: an update, Electrophoresis 35 (9) (2014) 1275–1284.
[9] A. Gencoglu, A.R. Minerick, Electrochemical detection techniques in micro- and nanofluidic devices, Microfluid. Nanofluidics 17 (2014) 781–807, https://doi.org/10.1007/s10404-014-1385-z.
[10] S. Hendrickx, W. de Malsche, D. Cabooter, An overview of the use of microchips in electrophoretic separation techniques: fabrication, separation modes, sample preparation opportunities, and on-chip detection, Methods Mol. Biol. 1274 (2015) 3–17, https://doi.org/10.1007/978-1-4939-2353-3_1.
[11] C.E.D. Nazario, M.R. Silva, M.S. Franco, F.M. Lanças, Evolution in miniaturized column liquid chromatography instrumentation and applications: an overview, J. Chromatogr. A. 1421 (2015) 18–37, https://doi.org/10.1016/j.chroma.2015.08.051.
[12] J. Šesták, D. Moravcová, V. Kahle, Instrument platforms for nano liquid chromatography, J. Chromatogr. A 1421 (2015) 2–17.
[13] X. Feng, B.F. Liu, J. Li, X. Liu, Advances in coupling microfluidic chips to mass spectrometry, Mass Spectrom. Rev. 34 (2015) 535–557, https://doi.org/10.1002/mas.21417.
[14] J.A. Huang, Y.L. Zhang, H. Ding, H.B. Sun, SERS-Enabled lab-on-a-chip systems, Adv. Opt. Mater. 3 (5) (2015) 618–633.
[15] X. Wang, L. Yi, N. Mukhitov, A.M. Schrell, R. Dhumpa, M.G. Roper, Microfluidics-to-mass spectrometry: a review of coupling methods and applications, J. Chromatogr. A 1382 (2015) 98–116.
[16] D.T. Snyder, C.J. Pulliam, Z. Ouyang, R.G. Cooks, Miniature and fieldable mass spectrometers: recent advances, Anal. Chem. 88 (2016) 2–29, https://doi.org/10.1021/acs.analchem.5b03070.
[17] A. Kecskemeti, A. Gaspar, Particle-based liquid chromatographic separations in microfluidic devices-A review, Anal. Chimica Acta 1021 (2018) 1–19.
[18] X. Yuan, R.D. Oleschuk, Advances in microchip liquid chromatography, Anal. Chem. 90 (2018) 283–301, https://doi.org/10.1021/acs.analchem.7b04329.
[19] M. Ramos-Payán, J.A. Ocaña-Gonzalez, R.M. Fernández-Torres, A. Llobera, M.Á. Bello-López, Recent trends in capillary electrophoresis for complex samples analysis: a review, Electrophoresis 39 (1) (2018) 111–125.
[20] J. Merrin, Frontiers in microfluidics, a teaching resource review, Bioengineering 6 (2019), https://doi.org/10.3390/bioengineering6040109.
[21] M.A. Ahmed, B.M.B. Felisilda, J.P. Quirino, Recent advancements in open-tubular liquid chromatography and capillary electrochromatography during 2014–2018, Anal. Chim. Acta 1088 (2019) 20–34.
[22] S. Mohith, P.N. Karanth, S.M. Kulkarni, Recent trends in mechanical micropumps and their applications: a review, Mechatronics 60 (2019) 34–55.
[23] L. Li, X. Wang, Q. Pu, S. Liu, Advancement of electroosmotic pump in microflow analysis: a review, Anal. Chim. Acta 1060 (2019) 1–16.
[24] D.A.V. Medina, E.V.S. Maciel, F.M. Lanças, Miniaturization of liquid chromatography coupled to mass spectrometry. 3. Achievements on chip-based LC-MS devices, TrAC Trends Anal. Chem. (2020) 116003.
[25] B. Al Mughairy, H.A.J. Al-Lawati, Recent analytical advancements in microfluidics using chemiluminescence detection systems for food analysis, TrAC Trends Anal. Chem. 124 (2020), https://doi.org/10.1016/j.trac.2019.115802.
[26] P. Kubáň, P.C. Hauser, Contactless conductivity detection for analytical techniques-Developments from 2012 to 2014, Electrophoresis 36 (2015) 195–211, https://doi.org/10.1002/elps.201400336.
[27] P. Kubáň, P.C. Hauser, Contactless conductivity detection for analytical techniques— developments from 2014 to 2016, Electrophoresis 38 (2017) 95–114, https://doi.org/10.1002/elps.201600280.

[28] P. Kubáň, P.C. Hauser, Contactless conductivity detection for analytical techniques: developments from 2016 to 2018, Electrophoresis 40 (2019) 124–139, https://doi.org/10.1002/elps.201800248.

[29] P.C. Hauser, P. Kubáň, Capacitively coupled contactless conductivity detection for analytical techniques – developments from 2018 to 2020, J. Chromatogr. A. 1632 (2020), https://doi.org/10.1016/j.chroma.2020.461616.

[30] B. Pecar, D. Resnik, M. Mozek, D. Vrtacnik, Microfluidics: a review, Inform. MIDEM 51 (2021) 3–23, https://doi.org/10.33180/infmidem2021.101.

[31] B. Bao, Z. Wang, D. Thushara, A. Liyanage, S. Gunawardena, Z. Yang, S. Zhao, Recent advances in microfluidics-based chromatography—a mini review, Separations 8 (1) (2021) 3–19.

[32] N.S. Ha, M. De Raad, L.Z. Han, A. Golini, C.J. Petzold, T.R. Northen, Faster, better, and cheaper: Harnessing microfluidics and mass spectrometry for biotechnology, RSC Chem. Biol. 2 (2021) 1331–1351, https://doi.org/10.1039/d1cb00112d.

[33] T. Li, J.A. Díaz-Real, T. Holm, Design of electrochemical microfluidic detectors: a review, Adv. Mater. Technol. 6 (2021), https://doi.org/10.1002/admt.202100569.

[34] L. Shan, B. Jones, Nano liquid chromatography, an updated review, Biomed. Chromatogr. 36 (5) (2022) e5317.

[35] A. Agha, W. Waheed, N. Alamoodi, B. Mathew, F. Alnaimat, E. Abu-Nada, A. Abderrahmane, A. Alazzam, A review of cyclic olefin copolymer applications in microfluidics and microdevices, Macromol. Mater. Engg. 307 (8) (2022) 2200053.

[36] S. Chen, J. Zeng, Z. Zhang, B. Xu, B. Zhang, Recent advancements in nanoelectrospray ionization interface and coupled devices, J. Chromatogr. Open (2022) 100064.

[37] Y.J. Wei, Y.N. Zhao, X. Zhang, X. Wei, M.L. Chen, X.W. Chen, Biochemical analysis based on optical detection integrated microfluidic chip, TrAC - Trends Anal. Chem. 158 (2023), https://doi.org/10.1016/j.trac.2022.116865.

[38] L. Zhao, J. Xu, L. Xiong, S. Wang, C. Yu, J. Lv, J.M. Lin, Recent development of chemiluminescence for bioanalysis, TrAC - Trends Anal. Chem. (2023) 117213.

[39] P. Kubáň, P. Kubáň, Novel developments in capillary electrophoresis miniaturization, sampling, detection and portability: an overview of the last decade, TrAC - Trends Anal. Chem. 159 (2023) 116941.

[40] M. Hemida, A. Ghiasvand, M. Macka, V. Gupta, P.R. Haddad, B. Paull, Recent advances in miniaturization of portable liquid chromatography with emphasis on detection, J. Separ. Sci. (2023) 2300283.

[41] L. Chen, A. Ghiasvand, B. Paull, Applications of thread-based microfluidics: approaches and options for detection, TrAC - Trends Anal. Chem. (2023) 117001.

[42] S. Hartung, R. Minkner, M. Olabi, H. Wätzig, Performance of capillary electrophoresis instruments–State of the art and outlook, TrAC - Trends Anal. Chem. 163 (2023) 117056.

[43] C. Fanali, L. Dugo, P. Dugo, L. Mondello, Capillary-liquid chromatography (CLC) and nano-LC in food analysis, TrAC - Trends Anal. Chem. 52 (2013) 226–238.

[44] M. Noga, F. Sucharski, P. Suder, J. Silberring, A practical guide to nano-LC troubleshooting, J. Separ. Sci. 30 (14) (2007) 2179–2189.

[45] N. Avdalovic, Y. Liu, Capillary Ion Chromatography. Separation Science and Technology, vol. 13, Academic Press, 2021, pp. 303–322 (Chapter 12).

[46] S. Sharma, A. Plistil, H.E. Barnett, H.D. Tolley, P.B. Farnsworth, S.D. Stearns, M. L. Lee, Hand-portable gradient capillary liquid chromatography pumping system, Anal. Chem. 87 (20) (2015) 10457–10461.

[47] H.D. Ponce-Rodríguez, J. Verdú-Andrés, R. Herráez-Hernández, P. Campíns-Falcó, Exploring hand-portable nano-liquid chromatography for in place water analysis: determination of trimethylxanthines as a use case, Sci. Total Environ. 747 (2020) 140966.

[48] M. Pham, S.W. Foster, S. Kurre, R.A. Hunter, P. Grinias, Use of portable capillary liquid chromatography for common educational demonstrations involving separations, J. Chem. Educ. 98 (7) (2021) 2444–2448.

[49] R. Knob, M. Macka, P.R. Haddad, Capillary electrochromatography, Encyclopedia of Analytical Science (2013) 353–365, https://doi.org/10.1016/B0-12-369397-7/00114-X.

[50] X. Wang, C. Cheng, S. Wang, M. Zhao, P.K. Dasgupta, S. Liu, Nanocapillaries for open tubular chromatographic separations of proteins in femtoliter to picoliter samples, Anal. Chem. 81 (17) (2009) 7428–7435.

[51] B. Yang, M. Zhang, T. Kanyanee, B.N. Stamos, P.K. Dasgupta, An open tubular ion chromatograph, Anal. Chem. 86 (23) (2014) 11554–11561.

[52] Y. Yang, H. Chen, M.A. Beckner, P. Xiang, J.J. Lu, C. Cao, S. Liu, Narrow, open, tubular column for ultrahigh-efficiency liquid-chromatographic separation under elution pressure of less than 50 bar, Anal. Chem. 90 (18) (2018) 10676–10680.

[53] S.C. Lam, L.J. Coates, M. Hemida, V. Gupta, P.R. HaddadP.R, M. Macka, B. Paull, Miniature and fully portable gradient capillary liquid chromatograph, Anal. Chim. Acta 1101 (2020) 199–210.

[54] C. Gu, Z. Jia, Z. Zhu, C. He, W. Wang, A. Morgan, J.J. Lu, S. Liu, Miniaturized electroosmotic pump capable of generating pressures of more than 1200 bar, Anal. Chem. 84 (21) (2012) 9609–9614.

[55] A. Ishida, T. Nishimura, K. Koyama, M. Maeki, H. Tani, M. Tokeshi, A portable liquid chromatography system based on a separation/detection chip module consisting of a replaceable ultraviolet-visible absorbance or contactless conductivity detection unit, J. Chromatogr. A. 1706 (2023), https://doi.org/10.1016/j.chroma.2023.464272.

[56] M.F. Wahab, P.K. Dasgupta, P.K.A.F. Kadjo, D.W. Armstrong, Sampling frequency, response times and embedded signal filtration in fast, high efficiency liquid chromatography: a tutorial, Anal. Chim. Acta 907 (2016) 31–44, https://doi.org/10.1016/j.aca.2015.11.043.

[57] A. Fernández, Y. Zhu, R.J. FitzGerald, F.A. Riera, Membrane fractionation of a β-lactoglobulin tryptic digest: effect of the membrane characteristics, J. Chem. Technol. Biotechnol. 89 (4) (2014) 508–515.

[58] Waters Corporation. nanoACQUITY UPLC system. https://www.waters.com\webassets\cms\library\docs\720001083en.pdf.

[59] Waters Corporation, What light guided flow cells are available. https://support.waters.com/KB_Inst/Chromatography/WKB61002_What_Light_Guided_Flow_Cells_are_available.

[60] S. Liu, Microfabricated injector and capillary array assembly for high-resolution and high throughput separation, US Patent (2003), 6,533,914, March 18.

[61] W. Wang, C. Gu, K.B. Lynch, J.J. Lu, Z. Zhang, Q. Pu, S. Liu, High-pressure open-channel on-chip electroosmotic pump for nanoflow high performance liquid chromatography, Anal. Chem. 86 (4) (2014) 1958–1964.

[62] H.J. Tarigan, P. Neill, C.K. Kenmore, D.J. Bornhop, Capillary-scale refractive index detection by interferometric backscatter, Anal. Chem. 68 (10) (1996) 1762–1770.

[63] K. Swinney, D. Markov, D.J. Bornhop, Chip-scale universal detection based on backscatter interferometry, Anal. Chem. 72 (13) (2000) 2690–2695.

[64] A. Kussrow, C.S. Enders, D.J. Bornhop, Interferometric methods for label-free molecular interaction studies, Anal. Chem. 84 (2) (2012) 779–792.

[65] R.J. Dijkstra, F. Ariese, C. Gooijer, U.Th Brinkman, Raman spectroscopy as a detection method for liquid-separation techniques, TrAC Trends Anal. Chem. 24 (4) (2005) 304–323.

[66] C.B. Adamo, A.S. Junger, L.P. Bressan, J.A.F. da Silva, R.J. Poppi, D.P. de Jesus, Fast and straightforward in-situ synthesis of gold nanoparticles on a thread-based microfluidic device for application in surface-enhanced Raman scattering detection, Microchem. J. 156 (2020) 104985.

[67] S.E. Bialkowski, Photothermal Spectroscopy Methods for Chemical Analysis, Wiley, New York, 1996.

[68] J. Whinnery, in: R.Y. Chiao (Ed.), Amazing Light, Springer, New York, 1996, pp. 643–649.

[69] R.D. Snook, R.D. Lowe, Thermal lens spectrometry. A review, Analyst 120 (1995) 2051–2068.

[70] R. McLaren, N.J. Dovichi, High-sensitivity absorbance determination by laser-induced thermal modulation of electrical conductivity, Anal. Chem. 60 (1988) 730–733.

[71] B. Chouhan, P.K. Dasgupta, Direct photothermal measurement of optical absorption in a flow system, Anal. Chem. 91 (4) (2019) 2923–2931.

[72] A.G. Bell, On the production and reproduction of sound by light, Am. J. Sci. 20 (118) (1880) 305–324.

[73] A. Rosencwaig, Photoacoustics and Photoacoustic Spectroscopy, Krieger, Malabar, FL, 1980.

[74] G.A. West, J.J. Barrett, D.J. Siebert, K.V. Reddy, Photoacoustic spectroscopy, Rev. Sci. Instrum. 54 (1983) 797–817.

[75] M.D. Morris, F.K. Fotiou, in: J.A. Sell (Ed.), Photothermal Investigations of Solids and Fluids, Academic Press, Boston, MA, 1989, pp. 127–154.

[76] Q.X. Yang, H.P. Loock, I. Kozin, D. Pedersen, Fiber Bragg grating photoacoustic detector for liquid chromatography, Analyst 133 (2008) 1567–1572.

[77] J.Z. Li, P.K. Dasgupta, Chemiluminescence detection with a liquid-core waveguide. Determination of ammonium with electrogenerated hypochlorite based on the luminol-hypochlorite reaction, Anal. Chim. Acta 398 (1999) 33–39, https://doi.org/10.1016/S0003-2670(99)00378-5.

[78] J.Z. Li, P.K. Dasgupta, Measurement of gaseous hydrogen peroxide with a liquid core waveguide chemiluminescence detector, Anal. Chim. Acta 442 (2001) 63–70, https://doi.org/10.1016/S0003-2670(01)01102-3.

[79] L. Ganranoo, S.K. Mishra, A.K. Azad, A. Shigihara, P.K. Dasgupta, Z.S. Breitbach, D.W. Armstrong, K. Grudpan, B. Rappenglueck, Measurement of nitrophenols in rain and air by two-dimensional liquid chromatography – chemically active liquid core waveguide spectrometry, Anal. Chem. 82 (2010) 5838–5843, https://doi.org/10.1021/ac101015y.

[80] Z. Dong, H. Cui, H. Zhang, F. Wang, X. Zhan, F. Mayer, B. Nestler, M. Wegener, P. A. Levkin, 3D printing of inherently nanoporous polymers via polymerization-induced phase separation, Nature comm 12 (1) (2021) 247.

[81] X.B. Yin, E. Wang, Capillary electrophoresis coupling with electrochemiluminescence detection: a review, Anal. Chim. Acta 533 (2) (2005) 113–120.

[82] M. Zhang, P.K. Dasgupta, Conductance or admittance? Q&More. Issue 215. http://q-more.chemeurope.com/q-more-articles/215/conductance-or-admittance.html, 2015.

[83] W.M. Gilliland Jr., J.M. Ramsey, Development of a μchip CE-HPMS platform for cell growth monitoring, Anal. Chem. 90 (21) (2018) 13000–13006.

[84] G. Hulthe, M.A. Petersson, E. Fogelqvist, Coupling of open tubular liquid chromatography to electrospray mass spectrometry with a nanospray interface, Anal. Chem. 71 (14) (1999) 2915–2921.

[85] S.Y. Teh, R. Lin, L.H. Hung, A.P. Lee, Droplet microfluidics, Lab Chip 8 (2) (2008) 198–220.

[86] D.T.T. Nguyen, D. Guillarme, S. Rudaz, J.L. Veuthey, Chromatographic behaviour and comparison of column packed with sub-2 μm stationary phases in liquid chromatography, J. Chromatogr. A 1128 (1–2) (2006) 105–113, https://doi.org/10.1016/j.chroma.2006.06.069.

[87] R. Hayes, A. Ahmed, T. Edge, H. Zhang, Core–shell particles: preparation, fundamentals and applications in high performance liquid chromatography, J. Chromatogr. A 1357 (2014) 36–52, https://doi.org/10.1016/j.chroma.2014.05.010.

[88] R.T. Kennedy, J.W. Jorgenson, Preparation and evaluation of packed capillary liquid chromatography columns with inner diameters from 20 to 50 micrometers, Anal. Chem. 61 (10) (1989) 1128–1135.

[89] M.A. Moseley, L.J. Deterding, K.B. Tomer, J.W. Jorgenson, Nanoscale packed-capillary liquid chromatography coupled with mass spectrometry using a coaxial continuous-flow fast atom bombardment interface, Anal. Chem. 63 (14) (1991) 1467–1473.

[90] S. Bruns, E.G. Franklin, J.P. Grinias, J.M. Godinho, J.W. Jorgenson, U. Tallarek, Slurry concentration effects on the bed morphology and separation efficiency of capillaries packed with sub-2 μm particles, J. Chromatogr. A 1318 (2013) 189–197.

[91] K.D. Patel, A.D. Jerkovich, J.C. Link, J.W. Jorgenson, In-depth characterization of slurry packed capillary columns with 1.0-μm nonporous particles using reversed-phase isocratic ultrahigh-pressure liquid chromatography. Anal. Chem., 76(19), pp.5777-5786..

[92] K. Killeen, H. Yin, D. Sobek, R. Brennen, T. Van de Goor, Chip-LC/MS: HPLC-MS using polymer microfluidics, Proc. MICROTAS 2003 (2003) 481–484.

[93] H. Yin, K. Killeen, R. Brennen, D. Sobek, M. Werlich, T. van de Goor, μchip for peptide analysis with an integrated hplc column, sample enrichment column, and nanoelectrospray tip, Anal. Chem. 77 (2005) 527–533.

[94] S. Ehlert, K. Kraiczek, J.A. Mora, M. Dittmann, G.P. Rozing, U. Tallarek, Separation efficiency of particle-packed HPLC μchips, Anal. Chem. 80 (15) (2008) 5945–5950.

[95] Agilent Technologies, Agilent HPLC-chip: g4240-65001 ZORBAX 80SB-C18. http://www.prep-hplc.com/Uploads/ueditor/file/20190816/5d5656ebb2995.pdf. (Accessed 6 January 2022).

[96] P.A. Levkin, S. Eeltink, T.R. Stratton, R. Brennen, K. Robotti, H. Yin, K. Killeen, F. Svec, J.M. Fréchet, Monolithic porous polymer stationary phases in polyimide chips for the fast high-performance liquid chromatography separation of proteins and peptides, J. Chromatogr. A 1200 (1) (2008) 55–61.

[97] H. Yin, K. Killeen, The fundamental aspects and applications of Agilent HPLC-Chip, J. Separ. Sci. 30 (10) (2007) 1427–1434.

[98] J.S. Johnson, P.D. Rainville, J.M. Murphy, Taking advantage of significant reductions in ion suppression using ionKey/MS compared to standard flow LC/MS, White Paper (2013). http://www.gimitec.com/file/720004966en.pdf.

[99] P.D. Rainville, C. Doneanu, Robustness of ionKey/MS system in the analysis of pharmaceutical compounds in biological fluids, Waters Application Note, APNT134783313 (2014) 1–4.

[100] A.J. Kleinnijenhuis, M. Ingola, J.H. Toersche, F.L. van Holthoon, W.D. van Dongen, Quantitative bottom up analysis of infliximab in serum using protein A purification and integrated μLC-electrospray chip IonKey MS/MS technology, Bioanalysis 8 (9) (2016) 891–904.

[101] S. Jung, U. Effelsberg, U. Tallarek, μchip electrospray: improvements in spray and signal stability during gradient elution by an inverted postcolumn makeup flow, Anal. Chem. 83 (2011) 9167–9173.

[102] J.H. Knox, M.T. Gilbert, Kinetic optimization of straight open-tubular liquid chromatography, J. Chromatogr. 106 (1979) 405–418.

[103] T.J. Kaiser, J.W. Thompson, J.S. Mellors, J.W. Jorgenson, Capillary-based instrument for the simultaneous measurement of solution viscosity and solute diffusion coefficient at pressures up to 2000 bar and implications for ultrahigh pressure liquid chromatography, Anal. Chem. 81 (8) (2009) 2860–2868.

[104] P. Xiang, Y. Zhu, Y. Yang, Z. Zhao, S.M. Williams, R.J. Moore, R.T. Kelly, R. D. Smith, S. Liu, Picoflow liquid chromatography–mass spectrometry for ultrasensitive bottom-up proteomics using 2-μm-id open tubular columns, Anal. Chem. 92 (7) (2020) 4711–4715.

[105] M.J.E. Golay, Opening address, Chromatographia 8 (1975) 421, https://doi.org/10.1007/BF02267576.

[106] R.F. Meyer, P.B. Champlin, R.A. Hartwick, Theory of multicapillary columns for HPLC, J. Chromatogr. Sci. 21 (10) (1983) 433–438.

[107] P. Russell, Photonic crystal fibers, Science 299 (2003) 358–362.

[108] S. Currivan, N. Upadhyay, B. Paull, Multi-channel capillaries and photonic crystal fibres for separation sciences, TrAC Trend. Anal. Chem. 102 (2018) 322–331.

[109] M.R.O.K. Brandtzaeg, T. Vehus, F.M. Lanças, S.R. Wilson, E. Lundanes, An automated and self-cleaning nano liquid chromatography mass spectrometry platform featuring an open tubular multi-hole crystal fiber solid phase extraction column and an open tubular separation column, J.Chromatogr. A 1518 (2017) 104–110.

[110] A.A. Kazarian, E.S. Rodriguez, J.A. Deverell, J. McCord, D.C. Muddiman, B. Paull, Wall modified photonic crystal fibre capillaries as porous layer open tubular columns for in-capillary micro-extraction and capillary chromatography, Anal. Chim. Acta 905 (2016) 1–7.

[111] T. Hara, S. Futagami, S. Eeltink, W. De Malsche, G.V. Baron, G. Desmet, Very high efficiency porous silica layer open-tubular capillary columns produced via in-column sol–gel processing, Anal. Chem. 88 (20) (2016) 10158–10166.

[112] B. He, N. Tait, F. Regnier, Fabrication of nanocolumns for liquid chromatography, Anal. Chem. 70 (18) (1998) 3790–3797.

[113] N.V. Lavrik, L.T. Taylor, M.J. Sepaniak, Nanotechnology and chip level systems for pressure driven liquid chromatography and emerging analytical separation techniques: a review, Anal. Chim. Acta 694 (1–2) (2011) 6–20.

[114] G. Rozing, Micropillar array columns for advancing nanoflow HPLC, Microchem. J. 170 (2021) 106629.

[115] P. Gzil, N. Vervoort, G.V. Baron, G. Desmet, Advantages of perfectly ordered 2-D porous pillar arrays over packed bed columns for LC separations: a theoretical analysis, Anal. Chem. 75 (22) (2003) 6244–6250.

[116] W. De Malsche, H. Eghbali, D. Clicq, J. Vangelooven, H. Gardeniers, G. Desmet, Pressure-driven reverse-phase liquid chromatography separations in ordered nonporous pillar array columns, Anal. Chem. 79 (15) (2007) 5915–5926.

[117] W. De Malsche, J. Op De Beeck, S. De Bruyne, H. Gardeniers, G. Desmet, Realization of 1 × 106 theoretical plates in liquid chromatography using very long pillar array columns, Anal. Chem. 84 (3) (2012) 1214–1219.

[118] G. Desmet, M. Callewaert, H. Ottevaere, W. De Malsche, Merging open-tubular and packed bed liquid chromatography, Anal. Chem. 87 (14) (2015) 7382–7388.

[119] G. Desmet, J.O. de Beeck, G. Van Raemdonck, K. Van Mol, B. Claerebout, N. Van Landuyt, P. Jacobs, Separation efficiency kinetics of capillary flow micro-pillar array columns for liquid chromatography, J. Chromatogr. A 1626 (2020) 461279.

[120] J.O. De Beeck, W. De Malsche, D.S. Tezcan, P. De Moor, G. Desmet, Impact of the limitations of state-of-the-art micro-fabrication processes on the performance of pillar array columns for liquid chromatography, J. Chromatogr. A 1239 (2012) 35–48.

[121] J.W. Jorgenson, K.D. Lukacs, Zone electrophoresis in open-tubular glass capillaries, Anal. Chem. 53 (8) (1981) 1298–1302.

[122] F.E. Mikkers, F.M. Everaerts, T.P. Verheggen, High-performance zone electrophoresis, J. Chromatogr. A 169 (1979) 11–20.

[123] D.J. Harrison, A. Manz, Z. Fan, H. Luedi, H.M. Widmer, Capillary electrophoresis and sample injection systems integrated on a planar glass chip, Anal. Chem. 64 (17) (1992) 1926–1932.

[124] G.D. Chistian, P.K. Dasgupta, K.A. Schug, Analytical Chemistry, seventh ed., Wiley, 2013, p. 678.

[125] K.K.C. Yeung, C.A. Lucy, Ultrahigh-resolution capillary electrophoretic separation with indirect ultraviolet detection: isotopic separation of [14N]- and [15N] ammonium, Electrophoresis 20 (12) (1999) 2554–2559.

[126] H. Swerdlow, R. Gesteland, Capillary gel electrophoresis for rapid, high resolution DNA sequencing, Nucleic Acids Res. 18 (6) (1990) 1415–1419.

[127] N.E. Good, G.D. Winget, W. Winter, T.N. Connolly, S. Izawa, R.M. Singh, Hydrogen ion buffers for biological research, Biochemistry 5 (2) (1966) 467–477.

[128] H. Gai, Y. Li, E.S. Yeung, Optical detection systems on μchips, in: Microfluidics: Technologies and Applications Topics Curr. Chem, vol. 304, Springer, 2011, pp. 171–201.

[129] B. Kuswandi, J.H. Nuriman, H.W. Verboom, Optical sensing systems for microfluidic devices: a review, Anal. Chim. Acta 601 (2007) 141–155, https://doi.org/10.1016/j.aca.2007.08.046.

[130] A.G. Campaña, W.R.G. Baeyens, N.A. Guzman, Trends towards sensitive detection in capillary electrophoresis: an overview of some recent developments, Biomed. Chromatogr. 12 (3) (1998) 172–176.

[131] K. Swinney, D. Bornhop, A review of CE detection methodologies, Crit. Rev. Anal. Chem. 30 (2000) 1–30, https://doi.org/10.1080/10408340091164162.

[132] American Meteorological Society. Glossary of Meteorology. http://glossary.ametsoc.org/wiki/Bouguer's_law Last accessed February 9, 2022.

[133] T.G. Mayerhöfer, S. Pahlow, J. Popp, The bouguer-beer-lambert law: shining light on the obscure, ChemPhysChem 21 (18) (2020) 2029–2046.

[134] H. Small, T.E. Miller, Indirect photometric chromatography, Anal. Chem. 54 (3) (1982) 462–469.

[135] C. Johns, M. Macka, P.R. Haddad, Enhancement of detection sensitivity for indirect photometric detection of anions and cations in capillary electrophoresis, Electrophoresis 24 (12-13) (2003) 2150–2167.

[136] K.G. Kraiczek, J. Mannion, S. Post, A. Tsupryk, V. Raghunathan, R. Brennen, R. Zengerle, Micromachined fused silica liquid core waveguide capillary flow cell, Anal. Chem. 88 (2016) 1100–1105.

[137] K.G. Kraiczek, G.P. Rozing, R. Zengerle, Relation between chromatographic resolution and signal-to-noise ratio in spectrophotometric HPLC detection, Anal. Chem. 85 (10) (2013) 4829–4835.

[138] A.F. Kadjo, P.K. Dasgupta, C.P. Shelor, Optimum cell pathlength or volume for absorbance detection in liquid chromatography: transforming longer cell results to virtual shorter cells, Anal. Chem. 92 (9) (2020) 6391–6400.

[139] V. Kahle, Fiber optic Z-cell for CZE, Biomed. Chromatogr. 13 (1) (1999) 93–94.

[140] Y. Xue, E.S. Yeung, Characterization of band broadening in capillary electrophoresis due to nonuniform capillary geometries, Anal. Chem. 66 (21) (1994) 3575–3580.

[141] J.P. Chervet, M. Ursem, J.P. Salzmann, Instrumental requirements for nanoscale liquid chromatography, Anal. Chem. 68 (1996) 1507–1512, https://doi.org/10.1021/ac9508964.

[142] J. Šesták, J. Planeta, V. Kahle, Nanolitre-scale cell based on L-shaped silica capillary and optical fibre for absorption photometric detection in capillary liquid chromatography, Anal. Chim. Acta 1073 (2019) 99–108.

[143] P.K. Dasgupta, Z. Genfa, J.Z. Li, C.B. Boring, S. Jambunathan, R. Al-Horr, Luminescence detection with a liquid core waveguide, Anal. Chem. 71 (1999) 1400–1407, https://doi.org/10.1021/ac981260q.

[144] J. Šesták, J. Planeta, V. Kahle, Compact optical detector utilizing light emitting diodes, 50 nL L-shaped silica capillary cell and CCD spectrometer for simultaneous multi-wavelength monitoring of absorbance and fluorescence in microcolumn liquid chromatography, Anal. Chim. Acta 1112 (2020) 80–91.

[145] Z. Gogaľová, V. Kahle, J. Šesták, An improved design of the fused silica capillary flow cell for absorbance detection in microcolumn liquid chromatography, Anal. Chim. Acta 1238 (2023) 340637.

[146] A.K. Malik, W. Faubel, Photothermal and light emitting diodes as detectors for trace detection in capillary electrophoresis, Chem. Soc. Rev. 29 (4) (2000) 275–282.

[147] M. Hemida, L.J. Coates, S. Lam, V. Gupta, M. Macka, H.J. Wirth, A.A. Gooley, P. R. Haddad, B. Paull, Miniature multiwavelength deep UV-LED-based absorption detection system for capillary LC, Anal. Chem. 92 (20) (2020) 13688–13693.

[148] I.E. Mikhail, M. Hemida, L. Lebanov, S. Astrakhantseva, V. Gupta, P. Hortin, J. S. Parry, M. Macka, B. Paull, Multi-wavelength deep-ultraviolet absorbance detector based upon program-controlled pulsing light-emitting diodes, J. Chromatogr. A 1709 (2023) 464382.
[149] X. Xi, E.S. Yeung, Axial-beam on-column absorption detection for open tubular capillary liquid chromatography, Anal. Chem. 62 (15) (1990) 1580–1585.
[150] X. Xi, E.S. Yeung, Axial-beam absorption detection for capillary electrophoresis with a conventional light source, Appl. Spectrosc. 45 (7) (1991) 1199–1203.
[151] J.A. Taylor, E.S. Yeung, Axial-beam absorbance detection for capillary electrophoresis, J. Chromatogr. A 550 (1991) 831–837.
[152] T. Dallas, P.K. Dasgupta, Light at the end of the tunnel: recent analytical applications of liquid-core waveguides, TrAC Trends. Anal. Chem. 23 (5) (2004) 385–392.
[153] T. Wang, J.H. Aiken, C.W. Huie, R.A. Hartwick, Nanoliter-scale multireflection cell for absorption detection in capillary electrophoresis, Anal. Chem. 63 (14) (1991) 1372–1376.
[154] T. Wang, Capillary multireflective cell, US Patent (1993), 5,273,635, December 28.
[155] H. Salimi-Moosavi, Y. Jiang, L. Lester, G. McKinnon, D.J. Harrison, A multireflection cell for enhanced absorbance detection in μchip-based capillary electrophoresis devices, Electrophoresis 21 (7) (2000) 1291–1299.
[156] P.S. Ellis, A.J. Lyddy-Meaney, P.J. Worsfold, I.D. McKelvie, Multi-reflection photometric flow cell for use in flow injection analysis of estuarine waters, Anal. Chim. Acta 499 (1–2) (2003) 81–89.
[157] S.K. Mishra, P.K. Dasgupta, Capillary scale light emitting diode based multi-reflection absorbance detector, Anal. Chim. Acta 605 (2007) 166–174, https://doi.org/10.1016/j.aca.2007.10.030.
[158] N. Yanagisawa, S. Mahmud, D. Dutta, Absorbance detection in multireflection microfluidic channels using a commercial microplate reader system, Anal. Chem. 92 (2020) 13050–13057, https://doi.org/10.1021/acs.analchem.0c01961.
[159] S. Sharma, H.D. Tolley, P.B. Farnsworth, M.L. Lee, LED-based UV absorption detector with low detection limits for capillary liquid chromatography, Anal. Chem. 87 (2015) 1381–1386, https://doi.org/10.1021/ac504275m.
[160] G.L. Nelson, A.M. Lines, J.M. Bello, S.A. Bryan, Online monitoring of solutions within μchips: simultaneous Raman and uv-vis absorption spectroscopies, ACS Sens. 4 (2019) 2288–2295, https://doi.org/10.1021/acssensors.9b00736.
[161] M.E. Johnson, J.P. Landers, Fundamentals and practice for ultrasensitive laser-induced fluorescence detection in microanalytical systems, Electrophoresis 25 (2004) 3513–3527, https://doi.org/10.1002/elps.200406086.
[162] A.M.G. Campaña, W.R.G. Baeyens, N.A. Guzman, Trends towards sensitive detection in capillary electrophoresis: an overview of some recent developments, Biomed. Chromatogr. 12 (1998) 172–176.
[163] R.L. Nouwairi, K.C. O'Connell, L.M. Gunnoe, J.P. Landers, μchip electrophoresis for fluorescence-based measurement of polynucleic acids: recent developments, Anal. Chem. 93 (1) (2020) 367–387.
[164] M.T. Veledo, C. Pelaez-Lorenzo, R. Gonzalez, M. de Frutos, J.C. Diez-Masa, Protein fingerprinting of Staphylococcus species by capillary electrophoresis with on-capillary derivatization and laser-induced fluorescence detection, Anal. Chim. Acta 658 (2010) 81–86, https://doi.org/10.1016/j.aca.2009.10.053.
[165] A. Chen, S. Liu, Open tubular liquid chromatographic system for using columns with inner diameter of 2 μm. A tutorial, J. Chromatogr. A 1673 (2022) 463202.
[166] M.T. Weaver, K.B. Lynch, Z. Zhu, H. Chen, J.J. Lu, Q. Pu, S. Liu, Fluorescence detector for narrow capillary system with yoctomole limit of detection, Talanta 165 (2017) 240–244.
[167] Y.M. Peng, J.Z. Pan, Q. Fang, Handheld laser-induced fluorescence detection systems with different optical configurations, Talanta 230 (2021) 122329.
[168] J.L. Felhofer, L. Blanes, C.D. Garcia, Recent developments in instrumentation for capillary electrophoresis and μchip-capillary electrophoresis, Electrophoresis 31 (2010) 2469–2486, https://doi.org/10.1002/elps.201000203.
[169] J.P. Devadhasan, S. Kim, J. An, Fish-on-a-chip: a sensitive detection microfluidic system for alzheimer's disease, J. Biomed. Sci. 18 (2011), https://doi.org/10.1186/1423-0127-18-33.
[170] C.D. Whitmore, D. Essaka, N.J. Dovichi, Six orders of magnitude dynamic range in capillary electrophoresis with ultrasensitive laser-induced fluorescence detection, Talanta 80 (2009) 744–748, https://doi.org/10.1016/j.talanta.2009.07.060.
[171] S. Nie, D.T. Chiu, R.N. Zare, Probing Individual molecules with confocal fluorescence microscopy, Science 266 (1994) 1018–1021.
[172] Y. Wang, J. Wu, P. Sun, J. Yu, Q. Pu, A fully functional palmtop μchip electrophoresis analyzer with laser-induced fluorescence detection, Sens. Actuators B Chem. 372 (2022) 132645.
[173] J. Prikryl, F. Foret, Fluorescence detector for capillary separations fabricated by 3D printing, Anal. Chem. 86 (2014) 11951–11956, https://doi.org/10.1021/ac503678n.
[174] B. Yang, H. Tian, J. Xu, Y. Guan, An integrated light emitting diode-induced fluorescence detector for capillary electrophoresis, Talanta 69 (2006) 996–1000, https://doi.org/10.1016/j.talanta.2005.12.005.
[175] M.F. Mora, F. Kehl, E. Tavares da Costa, N. Bramall, P.A. Willis, Fully automated μchip electrophoresis analyzer for potential life detection missions, Anal. Chem. 92 (19) (2020) 12959–12966.
[176] D.B. Craig, N.J. Dovichi, K.A. Cobb, V. Dolnik, M. Novotny, Multiple labeling of proteins, Anal. Chem. 70 (1998) 2493–2494, https://doi.org/10.1021/ac970856v.
[177] C. Hackl, R. Beyreiss, D. Geissler, S. Jezierski, D. Belder, Rapid prototyping of electrochromatography chips for improved two-photon excited fluorescence detection, Anal. Chem. 86 (2014) 3773–3779, https://doi.org/10.1021/ac500793e.
[178] D. Geissler, D. Belder, Two-photon excitation in chip electrophoresis enabling label-free fluorescence detection in non-UV transparent full-body polymer chips, Electrophoresis 36 (2015) 2976–2982, https://doi.org/10.1002/elps.201500192.
[179] D.O. Hancock, R.E. Synovec, Microbore liquid chromatography and refractive index gradient detection of low-nanogram and low-ppm quantities of carbohydrates, J. Chromatogr. A. 464 (1991) 83–91, https://doi.org/10.1016/S0021-9673(00)94225-0.
[180] C.K. Kenmore, S.R. Erskine, D.J. Bornhop, Refractive-index detection by interferometric backscatter in packed-capillary high-performance liquid chromatography, J. Chromatogr. A 762 (1997) 219–225, https://doi.org/10.1016/S0021-9673(96)00852-7.
[181] D.J. Bornhop, Microvolume index of refraction determinations by interferometric backscatter, Appl. Opt. 34 (1995) 3234–3239, https://doi.org/10.1364/AO.34.003234.
[182] K. Swinney, D. Markov, D.J. Bornhop, Ultrasmall volume refractive index detection using microinterferometry, Rev. Sci. Instrum. 71 (2000) 2684–2692, https://doi.org/10.1063/1.1150675.
[183] H.S. Sørensen, H. Pranov, N.B. Larsen, D.J. Bornhop, P.E. Andersen, Absolute refractive index determination by microinterferometric backscatter detection, Anal. Chem. 75 (2003) 1946–1953, https://doi.org/10.1021/ac0206162.
[184] Z. Wang, D.J. Bornhop, Dual-capillary backscatter interferometry for high-sensitivity nanoliter-volume refractive index detection with density gradient compensation, Anal. Chem. 77 (2005) 7872–7877, https://doi.org/10.1021/ac050752h.
[185] R.C. Dunn, Wavelength modulated back-scatter interferometry for universal, on-column refractive index detection in picoliter volumes, Anal. Chem. 90 (11) (2018) 6789–6795.
[186] R.C. Dunn, Compact, inexpensive refractive index detection in femtoliter volumes using commercial optical pickup technology, Anal. Methods 11 (17) (2019) 2303–2310.
[187] R.C. Dunn, High-speed capillary electrophoresis using a thin-wall fused-silica capillary combined with backscatter interferometry, Anal. Chem. 92 (11) (2020) 7540–7546.
[188] M. De Silva, P.M. Opallage, R.C. Dunn, Direct detection of inorganic ions and underivatized amino acids in seconds using high-speed capillary electrophoresis coupled with back-scatter interferometry, Anal. Methods 13 (11) (2021) 1340–1348.
[189] P.M. Opallage, M. De Silva, R.C. Dunn, Dual detection high-speed capillary electrophoresis for simultaneous serum protein analysis and immunoassays, Sci. Rep. 12 (1) (2022) 1951.
[190] M. De Silva, R.C. Dunn, Sample plug induced peak splitting in capillary electrophoresis studied using dual backscattered interferometry and fluorescence detection, Electrophoresis 44 (5–6) (2023) 549–557.
[191] I.M. White, X. Fan, On the performance quantification of resonant refractive index sensors, Opt Express 16 (2008) 1020–1028, https://doi.org/10.1007/s10404-007.
[192] S.S. Yee, G. Gauglitz, Surface plasmon resonance sensors: review, Sens. Actuators B Chem. 54 (1999) 3–15, https://doi.org/10.1016/S0925-4005(98)00321-9.
[193] D. Brennan, P. Lambkin, P. Galvin, Refractive index measurements in a shallow multichannel microfluidic system, Meas. Sci. Technol. 19 (2008), https://doi.org/10.1088/0957-0233/19/8/085403.
[194] Z. Yang, L. Xia, S. Li, R. Qi, X. Chen, W. Li, Highly sensitive refractive index detection based on compact HSC-SPR structure in a μchip, Sens. Actuators A Phys. 297 (2019), https://doi.org/10.1016/j.sna.2019.111558.
[195] H. Zhu, I.M. White, J.D. Suter, M. Zourob, X. Fan, Integrated refractive index optical ring resonator detector for capillary electrophoresis, Anal. Chem. 79 (2007) 930–937, https://doi.org/10.1021/ac061279q.
[196] S.K. Chamoli, S.C. Singh, C. Guo, Design of extremely sensitive refractive index sensors in infrared for blood glucose detection, IEEE Sens J 20 (2020) 4628–4634, https://doi.org/10.1109/JSEN.2020.2964715.
[197] T. Chen, H. Zhang, W. Lin, H. Liu, B. Liu, Highly sensitive refractive index sensor based on vernier effect in coupled micro-ring resonators, J. Light. Technol. 40 (2022) 1216–1223, https://doi.org/10.1109/JLT.2021.3126307.
[198] I. Jalaludin, J. Kim, Comparison of ultraviolet and refractive index detections in the HPLC analysis of sugars, Food Chem. 365 (2021), https://doi.org/10.1016/j.foodchem.2021.130514.
[199] R. Mhatre, I.S. Krull, Determination of on-line differential refractive index and molecular weight via gradient HPLC interfaced with low-angle laser light scattering, ultraviolet, and refractive index detection, Anal. Chem. 65 (3) (1993) 283–286.
[200] A. Natrajan, D. Wen, D. Sharpe, Synthesis and properties of chemiluminescent acridinium ester labels with fluorous tags, Org. Biomol. Chem. 12 (2014) 3887–3901, https://doi.org/10.1039/c4ob00456f.
[201] M. Yamaguchi, H. Yoshida, H. Nohta, Luminol-type chemiluminescence derivatization reagents for liquid chromatography and capillary electrophoresis, J. Chromatogr. A 950 (1–2) (2002) 1–19.
[202] P.S. Francis, N.W. Barnett, S.W. Lewis, K.F. Lim, Hypohalites and related oxidants as chemiluminescence reagents: a review, Luminescence 19 (2004) 94–115, https://doi.org/10.1002/bio.756.
[203] J.F. Huertas-Pérez, D. Moreno-González, D. Airado-Rodríguez, F.J. Lara, A. M. García-Campaña, Advances in the application of chemiluminescence detection in liquid chromatography, TrAC – Trends. Org. Biomol. Chem. 75 (2016) 35–48, https://doi.org/10.1016/j.trac.2015.07.004.
[204] J.L. Adcock, P.S. Francis, N.W. Barnett, Acidic potassium permanganate as a chemiluminescence reagent-A review, Anal. Chim. Acta 601 (2007) 36–67, https://doi.org/10.1016/j.aca.2007.08.027.

[205] J.L. Adcock, N.W. Barnett, C.J. Barrow, P.S. Francis, Advances in the use of acidic potassium permanganate as a chemiluminescence reagent: a review, Anal. Chim. Acta 807 (2014) 9–28, https://doi.org/10.1016/j.aca.2013.11.016.
[206] A.J. Brown, P.S. Francis, J.L. Adcock, K.F. Lim, N.W. Barnett, Manganese(III) and manganese(IV) as chemiluminescence reagents: a review, Anal. Chim. Acta 624 (2008) 175–183, https://doi.org/10.1016/j.aca.2008.06.041.
[207] H.A. Al Lawati, Flow-based analysis using microfluidics–chemiluminescence systems, Luminescence 28 (5) (2013) 618–627.
[208] X. Huang, J. Ren, Chemiluminescence detection for capillary electrophoresis and μchip capillary electrophoresis, TrAC, Trends Anal. Chem. 25 (2) (2006) 155–166.
[209] B.U. Moon, M.G. De Vries, B.H.C. Westerink, E. Verpoorte, Development and characterization of a microfluidic glucose sensing system based on an enzymatic microreactor and chemiluminescence detection, Sci. China Chem. 55 (2012) 515–523.
[210] H. Li, C. Liu, D. Wang, C. Zhang, Chemiluminescence cloth-based glucose test sensors (CCGTSs): a new class of chemiluminescence glucose sensors, Biosens. Bioelectron. 91 (2017) 268–275.
[211] T. Richter, L.L. Shultz-Lockyear, R.D. Oleschuk, U. Bilitewski, D.J. Harrison, Bi-enzymatic and capillary electrophoretic analysis of non-fluorescent compounds in microfluidic devices: determination of xanthine, Sens. Actuators, B: Chem. 81 (2–3) (2002) 369–376.
[212] P. Khan, D. Idrees, M.A. Moxley, J.A. Corbett, F. Ahmad, G. von Figura, W.S. Sly, A. Waheed, M.I. Hassan, Luminol-based chemiluminescent signals: clinical and non-clinical application and future uses, Appl. Biochem. Biotechnol. 173 (2014) 333–355.
[213] Z.X. Gao, H.F. Li, J. Liu, J.M. Lin, A simple microfluidic chlorine gas sensor based on gas–liquid chemiluminescence of luminol-chlorine system, Anal. Chim. Acta 622 (1–2) (2008) 143–149.
[214] W. Som-Aum, H. Li, J. Liu, J.M. Lin, Determination of arsenate by sorption pre-concentration on polystyrene beads packed in a microfluidic device with chemiluminescence detection, Analyst 133 (9) (2008) 1169–1175.
[215] S. Deepa, R. Venkatesan, S. Jayalakshmi, M. Priya, S.C. Kim, Recent advances in catalyst-enhanced luminol chemiluminescence system and its environmental and chemical applications, J. Environ. Chem. Eng. (2023) 109853.
[216] S.D. Mangru, D.J. Harrison, Chemiluminescence detection in integrated post-separation reactors for μchip-based capillary electrophoresis and affinity lectrophoresis, Electrophoresis 19 (13) (1998) 2301–2307.
[217] K. Tsukagoshi, M. Hashimoto, R. Nakajima, A. Arai, Application of μchip capillary electrophoresis with chemiluminescence detection to an analysis for transition-metal ions, Anal. Sci. 16 (11) (2000) 1111–1112.
[218] L. Delafresnaye, F.R. Bloesser, K.B. Kockler, C.W. Schmitt, I.M. Irshadeen, C. Barner-Kowollik, All eyes on visible-light peroxyoxalate chemiluminescence read-out systems, Chem. Eur J. 26 (1) (2020) 114–127.
[219] H.M. Hu, X.F. Yin, X.Z. Wang, H. Shen, A study on the system of nonaqueous μchip electrophoresis with on-line peroxyoxalate chemiluminescence detection, J. Separ. Sci. 36 (4) (2013) 713–720.
[220] M.A. Ruberto, M.L. Grayeski, Acridinium chemiluminescence detection with capillary electrophoresis, Anal. Chem. 64 (22) (1992) 2758–2762.
[221] M.J. Chaichi, Z. Va'ezi, M. Hosseini, S. Hosseinkhani, M. Shamsipur, The study of chemiluminescence of acridinium ester in presence of rhodamin B as a fluorescer, Iran. J. Chem. Chem.Eng. 30 (2011) 89–96.
[222] L. Guo, B. Qiu, Y. Jiang, Z. You, J.M. Lin, G. Chen, Capillary electrophoresis chemiluminescent detection system equipped with a two-step postcolumn flow interface for detection of some enkephalin-related peptides labeled with acridinium ester, Electrophoresis 29 (2008) 2348–2355, https://doi.org/10.1002/elps.200700713.
[223] P. Inpota, D. Nacapricha, P. Sunintaboon, W. Sripumkhai, W. Jeamsaksiri, P. Wilairat, R. Chantiwas, Chemiluminescence detection with microfluidics for innovative in situ measurement of unbound cobalt ions in dynamic equilibrium with bound ions in binding study with polyethyleneimine and its functionalized nanoparticles, Talanta 188 (2018) 606–613, https://doi.org/10.1016/j.talanta.2018.06.017.
[224] X. Chen, J. Mao, F. Wen, X. Xu, Determination of phenolic acids in botanical pharmaceutical products by capillary electrophoresis with chemiluminescence detection, Anal. Lett. 54 (5) (2021) 817–829.
[225] I. Al Yahyai, J. Hassanzadeh, H.A. Al-Lawati, A novel and selective multi-emission chemiluminescence system for the quantification of deltamethrin in food samples, Sens. Actuators B: Chem. 327 (2021) 128927.
[226] C.M. Kang, S. Joo, J.H. Bae, Y.R. Kim, Y. Kim, T.D. Chung, In-channel electrochemical detection in the middle of microchannel under high electric field, Anal. Chem. 84 (2012) 901–907, https://doi.org/10.1021/ac2016322.
[227] C. Zhu, G. Yang, H. Li, D. Du, Y. Lin, Electrochemical sensors and biosensors based on nanomaterials and nanostructures, Anal. Chem. 87 (2015) 230–249, https://doi.org/10.1021/ac5039863.
[228] M. Trojanowicz, Recent developments in electrochemical flow detections-A review. Part I. Flow analysis and capillary electrophoresis, Anal. Chim. Acta 653 (2009) 36–58, https://doi.org/10.1016/j.aca.2009.08.040.
[229] X. Xu, S. Zhang, H. Chen, J. Kong, Integration of electrochemistry in micro-total analysis systems for biochemical assays: recent developments, Talanta 80 (2009) 8–18, https://doi.org/10.1016/j.talanta.2009.06.039.
[230] H.L. Lee, S.C. Chen, μchip capillary electrophoresis with electrochemical detector for precolumn enzymatic analysis of glucose, creatinine, uric acid and ascorbic acid in urine and serum, Talanta 64 (2004) 750–757, https://doi.org/10.1016/j.talanta.2004.03.046.
[231] L.A. Holland, S.M. Lunte, Highlight. capillary electrophoresis coupled to electrochemical detection: a review of recent advances, Anal. Commun. 35 (2) (1998) 1H–4H.
[232] Y. Ding, A. Ayon, C.D. García, Electrochemical detection of phenolic compounds using cylindrical carbon-ink electrodes and μchip capillary electrophoresis, Anal. Chim. Acta 584 (2007) 244–251, https://doi.org/10.1016/j.aca.2006.11.064.
[233] G. Chen, Y. Lin, J. Wang, Monitoring environmental pollutants by μchip capillary electrophoresis with electrochemical detection, Talanta 68 (2006) 497–503, https://doi.org/10.1016/j.talanta.2005.07.004.
[234] E. Pungor, Oscillometry and Conductometry: International Series of Monographs on Analytical Chemistry, Elsevier, Amsterdam, Netherlands, 2016.
[235] A.J. Zemann, E. Schnell, D. Volgger, G.K. Bonn, Contactless conductivity detection for capillary electrophoresis, Anal. Chem. 70 (3) (1998) 563–567.
[236] J.A. Fracassi da Silva, C.L. do Lago, An oscillometric detector for capillary electrophoresis, Anal. Chem. 70 (20) (1998) 4339–4343.
[237] A. Manz, W. Simon, Picoliter cell volume potentiometric detector for open-tubular column LC, J. Chromatogr. Sci. 21 (7) (1983) 326–330.
[238] R. Pol, F. Céspedes, D. Gabriel, M. Baeza, Fully integrated screen-printed sulfide-selective sensor on a 3D-printed potentiometric microfluidic platform, Sens. Actuators B: Chem. 290 (2019) 364–370, b.
[239] F. Sassa, H. Laghzali, J. Fukuda, H. Suzuki, Coulometric detection of components in liquid plugs by microfabricated flow channel and electrode structures, Anal. Chem. 82 (20) (2010) 8725–8732.
[240] H. Mizuguchi, D. Nishimori, T. Kuwabara, M. Takeuchi, M. Iiyama, T. Takayanagi, Track-etched membrane-based dual-electrode coulometric detector for microbore/capillary high-performance liquid chromatography, Anal. Chim. Acta 1102 (2020) 46–52.
[241] L.A. Knecht, E.J. Guthrie, J.W. Jorgenson, On-column electrochemical detector with a single graphite fiber electrode for open-tubular liquid chromatography, Anal. Chem. 56 (3) (1984) 479–482.
[242] Y. Hirata, P.T. Lin, M. Novotný, R.M. Wightman, Small-volume electrochemical detector for microcolumn liquid chromatography, J. Chromatogr. B Biomed. Appl. 181 (3–4) (1980) 287–294.
[243] J.W. Jorgenson, Trends in analytical scale separations, Science 226 (4672) (1984) 254–261.
[244] J.G. White, R.L. St Claire, J.W. Jorgenson, Scanning on-column voltammetric detector for open-tubular liquid chromatography, Anal. Chem. 58 (2) (1986) 293–298.
[245] M.D. Oates, J.W. Jorgenson, Voltammetric detection with gradient elution for open tubular liquid chromatography, Anal. Chem. 61 (17) (1989) 1977–1980.
[246] Y. Liu, L. Yang, Y. Cui, Transdermal amperometric biosensors for continuous glucose monitoring in diabetes, Talanta 253 (2023) 124033.
[247] F.G. Ortega, G.E. Gomez, C. Boni, I.C. García, C.G. Navas, R.F. D'vries, M.P. M. Vallejos, M.J. Serrano, G.A. Messina, J.E. Hernández, M.A. Fernández-Baldo, Microfluidic amperometric immunosensor based on porous nanomaterial towards claudin7 determination for colorectal cancer diagnosis, Talanta 251 (2023) 123766.
[248] D. Agustini, L. Fedalto, D. Agustini, L.G.D.M. dos Santos, C.E. Banks, M. F. Bergamini, L.H. Marcolino-Junior, A low cost, versatile and chromatographic device for microfluidic amperometric analyses, Sens. Actuators B: Chem. 304 (2020) 127117.
[249] R.A. Yamashita, R.M. Carvalho, J.M. Petroni, E.R. Pedão, F.M.R. Guerbas, M. P. Tronchini, V.S. Ferreira, E.I. de Melo, R.A.B. da Silva, B.G. Lucca, 3D-printed microfluidic thread device with integrated detector: a green and portable tool for amperometric detection of fungicide benzovindiflupyr in forensic samples, Microchem. J. 182 (2022) 107853.
[250] E.A. Hayter, A.D. Castiaux, R.S. Martin, 3D-printed microfluidic device with in-line amperometric detection that also enables multi-modal detection, Anal. Methods 12 (15) (2020) 2046–2051.
[251] J.J. Xu, A.J. Wang, H.Y. Chen, Electrochemical detection modes for μchip capillary electrophoresis, TrAC, Trends Anal. Chem. 26 (2007) 125–132, https://doi.org/10.1016/j.trac.2006.08.006.
[252] J.A. Vickers, C.S. Henry, Simplified current decoupler for μchip capillary electrophoresis with electrochemical and pulsed amperometric detection, Electrophoresis (2005) 4641–4647, https://doi.org/10.1002/elps.200500508.
[253] BASi, Pulsed amperometric detection. https://www.basinc.com/manuals/LC_epsilon/Operation/PAD/pad. (Accessed 28 October 2023).
[254] J. Rohrer. https://assets.thermofisher.com/TFS-Assets/CMD/Application-Notes/TN-21-Optimal-Settings-Pulsed-Amperometric-Detection-Carbohydrates-ED40-TN70670-EN.pdf. (Accessed 28 October 2023).
[255] M.H. Akhtar, K.K. Hussain, N.G. Gurudatt, Y.B. Shim, Detection of Ca2+-induced acetylcholine released from leukemic T-cells using an amperometric microfluidic sensor, Biosens. Bioelectron. 98 (2017) 364–370, https://doi.org/10.1016/j.bios.2017.07.003.
[256] E.A. Carneiro, D. Agustini, L.C.S. Figueiredo-Filho, C.E. Banks, L.H. Marcolino-Junior, M.F. Bergamini, 3D-printed microfluidic device based on cotton threads for amperometric estimation of antioxidants in wine samples, Electroanalysis 30 (2018) 101–108, https://doi.org/10.1002/elan.201700579.
[257] E.N.T. da Silva, V.S. Ferreira, B.G. Lucca, Rapid and inexpensive method for the simple fabrication of PDMS-based electrochemical sensors for detection in microfluidic devices, Electrophoresis 40 (2019) 1322–1330, https://doi.org/10.1002/elps.201800478.
[258] D. Agustini, L. Fedalto, D. Agustini, L.G. de Matos dos Santos, C.E. Banks, M. F. Bergamini, L.H. Marcolino-Junior, A low cost, versatile and chromatographic device for microfluidic amperometric analyses, Sens. Actuators B: Chem. 304 (2020), https://doi.org/10.1016/j.snb.2019.127117.

[259] D. Evans, K.I. Papadimitriou, N. Vasilakis, P. Pantelidis, P. Kelleher, H. Morgan, T. Prodromakis, A novel microfluidic point-of-care biosensor system on printed circuit board for cytokine detection, Sensors 18 (2018), https://doi.org/10.3390/s18114011.
[260] G. Kaur, M. Tomar, V. Gupta, Development of a microfluidic electrochemical biosensor: prospect for point-of-care cholesterol monitoring, Sens. Actuators B: Chem. 261 (2018) 460–466, https://doi.org/10.1016/j.snb.2018.01.144.
[261] D. Qi, T. Okada, P.K. Dasgupta, Direct current conductivity detection in ion chromatography, Anal. Chem. 61 (1989) 1383–1387, https://doi.org/10.1021/ac00188a015.
[262] D. Kouřilová, K. Šlais, M. Krejčí, A conductivity detector for liquid chromatography with a cell volume of 0.1 µl, Collect. Czechoslov. Chem. Commun. 48 (4) (1983) 1129–1136.
[263] D. Qi, T. Okada, P.K. Dasgupta, Direct current conductivity detection in ion chromatography, Anal. Chem. 61 (1989) 1383–1387, https://doi.org/10.1021/ac00188a015.
[264] W. Huang, H. Chen, Y. Su, R. Hu, A four-electrode microconstant direct current resistance detector for ion chromatography applying ion-exchange membrane and porous electrode, Talanta 82 (4) (2010) 1364–1370.
[265] W. Huang, R. Hu, H. Chen, Y. Su, Five-electrode direct current suppressor–detector combiner for ion chromatography: an integration of eluent suppression and resistance detection, Analyst 136 (5) (2011) 901–903.
[266] X. Li, H. Chang, Chip-based ion chromatography (chip-IC) with a sensitive five-electrode conductivity detector for the simultaneous detection of multiple ions in drinking water, Microsyst. Nanoeng. 6 (1) (2020) 66, https://doi.org/10.1038/s41378-020-0175-x.
[267] D.E. Johnson, C.G. Enke, Bipolar pulse technique for fast conductance measurements, Anal. Chem. 42 (3) (1970) 329–335.
[268] T. Okada, T. Kuwamoto, Nonsuppressor ion chromatography of inorganic and organic anions with potassium hydroxide as eluent, Anal. Chem. 55 (7) (1983) 1001–1004.
[269] T. Okada, T. Kuwamoto, Potassium hydroxide eluent for nonsuppressed anion chromatography of cyanide, sulfide, arsenite, and other weak acids, Anal. Chem. 57 (4) (1985) 829–833.
[270] T.S. Stevens, J.C. Davis, H. Small, Hollow fiber ion-exchange suppressor for ion chromatography, Anal. Chem. 53 (9) (1981) 1488–1492.
[271] D.L. Strong, P.K. Dasgupta, Electrodialytic membrane suppressor for ion chromatography, Anal. Chem. 61 (9) (1989) 939–945.
[272] D.L. Strong, P.K. Dasgupta, K. Friedman, J.R. Stillian, Electrodialytic eluent production and gradient generation in ion chromatography, Anal. Chem. 63 (5) (1991) 480–486.
[273] P.E. Jackson, C. Weigert, C.A. Pohl, C.A. Saini, Determination of inorganic anions in environmental waters with a hydroxide-selective column, J. Chromatogr. A 884 (1–2) (2000) 175–184.
[274] S. Rokushika, Z.Y. Qiu, H. Hatano, Micro column ion chromatography with a hollow fibre suppressor, J. Chromatogr. A 260 (1983) 81–87.
[275] S. Rokushika, H. Hatano, Miniaturized Ion Chromatography, vol. 30, J. of Chromatogr. Library Elsevier., 1985, p. p284.
[276] A. Sjögren, C.B. Boring, P.K. Dasgupta, J.N. Alexander, Capillary ion chromatography with on-line high-pressure electrodialytic NaOH eluent production and gradient generation, Anal. Chem. 69 (7) (1997) 1385–1391.
[277] C.B. Boring, P.K. Dasgupta, A. Sjögren, Compact, field-portable capillary ion chromatograph, J. Chromatogr. A 804 (1–2) (1998) 45–54.
[278] B. Yang, M. Takeuchi, P.K. Dasgupta, On-line gas-free electrodialytic eluent generator for capillary ion chromatography, Anal. Chem. 80 (1) (2008) 40–47.
[279] B. Yang, F. Zhang, X. Liang, P.K. Dasgupta, A multifunctional dual membrane electrodialytic eluent generator for capillary ion chromatography, J. Chromatogr. A 1216 (12) (2009) 2412–2416.
[280] B. Yang, F. Zhang, X. Liang, A simplified ion exchange based KOH electrodialytic generator for capillary ion chromatography, Talanta 79 (1) (2009) 68–71.
[281] V. Šolínová, V. Kašička, Recent applications of conductivity detection in capillary and chip electrophoresis, J. Separ. Sci. 29 (12) (2006) 1743–1762.
[282] T.P. Verheggen, E.C. Van Ballegooijen, C.H. Massen, F.M. Everaerts, Detection electrodes for electrophoresis, J. Chromatogr. 64 (1) (1972) 185–189.
[283] J. Vacík, J. Zuska, F.M. Everaerts, T.P. Verheggen, Capillary isotachophoresis. III. high-voltage sources with adjustable constant current, Chem. Listy 66 (6) (1972) 647–652.
[284] X. Huang, T.K.J. Pang, M.J. Gordon, R.N. Zare, On-column conductivity detector for capillary zone electrophoresis, Anal. Chem. 59 (23) (1987) 2747–2749.
[285] X. Huang, R.N. Zare, Improved end-column conductivity detector for capillary zone electrophoresis, Anal. Chem. 63 (19) (1991) 2193–2196.
[286] P.J. Dennis, E.F. Welch, J.P. Alarie, J.M. Ramsey, J.W. Jorgenson, Development of a photothermal absorbance detector for use with microfluidic devices, Anal. Chem. 82 (10) (2010) 4063–4071.
[287] A.A. Adams, P.I. Okagbare, J. Feng, M.L. Hupert, D. Patterson, J. Göttert, R. L. McCarley, R.L. Nikitopoulos, M.C. Murphy, S.A. Soper, Highly efficient circulating tumor cell isolation from whole blood and label-free enumeration using polymer-based microfluidics with an integrated conductivity sensor, J. Am. Chem. Soc. 130 (27) (2008) 8633–8641.
[288] P.K. Dasgupta, L. Bao, Suppressed conductometric capillary electrophoresis separation systems, Anal. Chem. 65 (8) (1993) 1003–1011.
[289] S. Kar, P.K. Dasgupta, H. Liu, H. Hwang, Computer-interfaced bipolar pulse conductivity detector for capillary systems, Anal. Chem. 66 (15) (1994) 2537–2543.
[290] C. Haber, W.R. Jones, J. Soglia, M.A. Surve, M. McGlynn, A. Caplan, J.R. Reineck, C. Krstanovic, Conductivity detection in capillary electrophoresis-a powerful tool in ion analysis, J. Capill. Electrophor. 3 (1996) 1–12.
[291] W. Huang, B. Chouhan, P.K. Dasgupta, Capillary scale admittance and conductance detection, Anal. Chem. 90 (2018) 14561–14568, https://doi.org/10.1021/acs.analchem.8b04561.
[292] E. Pungor, F. Pal, K. Toth, Oscillometric flow cell for measurement of conductivity and permittivity, Anal. Chem. 55 (11) (1983) 1728–1731.
[293] F. Pal, E. Pungor, E.S. Kovats, Oscillometric detector for ion chromatography. A note on detection limit and detector sensitivity, Anal. Chem. 60 (20) (1988) 2254–2258.
[294] B. Gaš, M. Demjaněnko, J. Vacik, High-frequency contactless conductivity detection in isotachophoresis, J. Chromatogr. A 192 (2) (1980) 253–257.
[295] J. Vacík, J. Zuska, I. Muselasová, Improvement of the performance of a high-frequency contactless conductivity detector for isotachophoresis, J. Chromatogr. A 320 (1) (1985) 233–240.
[296] J.G. Alves Brito-Neto, J.A. Fracassi Da Silva, L. Blanes, C.L. do Lago, Understanding capacitively coupled contactless conductivity detection in capillary and µchip electrophoresis. part 1. fundamentals, Electroanalysis 17 (2005) 1198–1206, https://doi.org/10.1002/elan.200503237.
[297] M. Zhang, B.N. Stamos, N. Amornthammarong, P.K. Dasgupta, Capillary scale admittance detection, Anal. Chem. 86 (23) (2014) 11538–11546.
[298] C. Lago, OpenC4D. https://github.com/claudimir-lago/openC4D. (Accessed 5 January 2024).
[299] E.M. Abad-Villar, P. Kubáň, P.C. Hauser, Determination of biochemical species on electrophoresis chips with an external contactless conductivity detector, Electrophoresis 26 (2005) 3609–3614, https://doi.org/10.1002/elps.200500149.
[300] Z. guang Chen, O. lian Li, C. Liu, X. juan Yang, Electromagnetic induction detector with a vertical coil for capillary electrophoresis and µchip, Sens. Actuators B: Chem. 141 (2009) 130–133, https://doi.org/10.1016/j.snb.2009.05.042.
[301] P. Kubáň, P.C. Hauser, Application of an external contactless conductivity detector for the analysis of beverages by µchip capillary electrophoresis, Electrophoresis 26 (2005) 3169–3178, https://doi.org/10.1002/elps.200500178.
[302] M. Zhang, B.N. Stamos, P.K. Dasgupta, Admittance detector for high impedance systems: design and applications, Anal. Chem. 86 (23) (2014) 11547–11553.
[303] Y. Lyu, H. Ji, S. Yang, Z. Huang, B. Wang, H. Li, New C4D sensor with a simulated inductor, Sensors 16 (2) (2016) 165.
[304] G. Fercher, A. Haller, W. Smetana, M.J. Vellekoop, End-to-end differential contactless conductivity sensor for µchip capillary electrophoresis, Anal. Chem. 82 (8) (2010) 3270–3275.
[305] M. Jaanus, A. Udal, V. Kukk, K. Umbleja, J. Gorbatsova, L. Molder, Improved C5D electronic realization of conductivity detector for capillary electrophoresis, Elektron Elektrotech 22 (3) (2016) 29–32.
[306] M. Stojkovic, B. Schlensky, P.C. Hauser, Referenced capacitively coupled conductivity detector for capillary electrophoresis, Electroanalysis 25 (12) (2013) 2645–2650.
[307] H. Nie, Z. Li, X. Wang, R. Gu, H. Yuan, Y. Guo, D. Xiao, An improved dual-channel capacitively coupled contactless conductivity detector with high detection performance, Analyst 147 (10) (2022) 2106–2114.
[308] J.W. Jorgenson, E.J. Guthrie, Liquid chromatography in open-tubular columns: theory of column optimization with limited pressure and analysis time, and fabrication of chemically bonded reversed-phase columns on etched borosilicate glass capillaries, J. Chromatogr. A 255 (1983) 335–348.
[309] E.J. Guthrie, J.W. Jorgenson, On-column fluorescence detector for open-tubular capillary liquid chromatography, Anal. Chem. 56 (3) (1984) 483–486.
[310] E.J. Guthrie, J.W. Jorgenson, P.R. Dluzneski, On-column helium cadmium laser fluorescence detector for open-tubular capillary liquid chromatography, J. Chromatogr. Sci. 22 (4) (1984) 171–176.
[311] T. Kanyanee, K. Tianrungarun, W. Somboot, C. Puangpila, J. Jakmunee, Open tubular capillary ion chromatography with online dilution for small ions determination in drinks, Food Chem. 382 (2022) 132055.
[312] Y. Lu, L. Zhou, B. Yang, S. Huang, F. Zhang, Online gas-free electrodialytic KOH eluent generator for ion chromatography, Anal. Chem. 90 (21) (2018) 12840–12845.
[313] B. Chouhan, C.P. Shelor, W. Huang, Y. Chen, P.K. Dasgupta, Nanovolume gas-free hydroxide eluent generator for open tubular ion chromatography, Anal. Chem. 92 (7) (2020) 5561–5568.
[314] W. Huang, P.K. Dasgupta, Electrodialytic capillary suppressor for open tubular ion chromatography, Anal. Chem. 88 (24) (2016) 12021–12027.
[315] F. Maleki, P.K. Dasgupta, Moldable strong cation exchange polymer and microchannel fabrication, Anal. Chem. 92 (19) (2020) 13378–13386.
[316] F. Maleki, B. Chouhan, C.P. Shelor, P.K. Dasgupta, Moldable capillary suppressor for open tubular ion chromatography based on a polymeric ion exchanger, Talanta Open 4 (2021) 100062.
[317] X. Wang, L. Yi, N. Mukhitov, A.M. Schrell, R. Dhumpa, M.G. Roper, Microfluidics-to-mass spectrometry: a review of coupling methods and applications, J. Chromatogr. A 1382 (2015) 98–116, https://doi.org/10.1016/j.chroma.2014.10.039.
[318] A. Makarov, Electrostatic axially harmonic orbital trapping: a high-performance technique of mass analysis, Anal. Chem. 72 (2000) 1156–1162, https://doi.org/10.1021/ac991131p.
[319] L. Gao, Q. Song, G.E. Patterson, R.G. Cooks, Z. Ouyang, Handheld rectilinear ion trap mass spectrometer, Anal. Chem. 78 (2006) 5994–6002, https://doi.org/10.1021/ac061144k.
[320] E. Sokol, R.J. Noll, R.G. Cooks, L.W. Beegle, H.I. Kim, I. Kanik, Miniature mass spectrometer equipped with electrospray and desorption electrospray ionization

for direct analysis of organics from solids and solutions, Int. J. Mass Spectrom. 306 (2011) 187–195, https://doi.org/10.1016/j.ijms.2010.10.019.
[321] L. Li, T.-C. Chen, Y. Ren, P.I. Hendricks, R.G. Cooks, Z. Ouyang, Mini 12, miniature mass spectrometer for clinical and other applications-Introduction and characterization, Anal. Chem. 86 (2014) 2909–2916, https://doi.org/10.1021/ac403766c.
[322] S. Wright, A. Malcolm, C. Wright, S. O'Prey, E. Crichton, N. Dash, R.W. Moseley, W. Zaczek, P. Edwards, R.J. Fussell, R.R.A. Syms, A microelectromechanical systems-enabled, miniature triple quadrupole mass spectrometer, Anal. Chem. 87 (2015) 3115–3122.
[323] A. Malcolm, S. Wright, R.R.A. Syms, R.W. Moseley, S. O'Prey, N. Dash, A. Pegus, E. Crichton, G. Hong, A.S. Holmes, A. Finlay, P. Edwards, S.E. Hamilton, C. J. Welch, A miniature mass spectrometer for liquid chromatography applications, Rapid Commun. Mass Spectrom. 25 (2011) 3281–3288, https://doi.org/10.1002/rcm.5230.
[324] https://www.thermofisher.com/order/catalog/product/BRE725535. https://assets.thermofisher.com/TFS-Assets/CMD/Specification-Sheets/ps-73409-ms-orbitrap-exploris-240-ps73409-en.pdf.
[325] http://www.microsaic.com/products/the-mid-platform/.
[326] R.D. Oleschuk, D.J. Harrison, Analytical microdevices for mass spectrometry, TrAC, Trends Anal. Chem. 19 (6) (2000) 379–388.
[327] L. Konermann, E. Ahadi, A.D. Rodriguez, S. Vahidi, Unraveling the mechanism of electrospray ionization, Anal. Chem. 85 (2013) 2–9, https://doi.org/10.1021/ac302789c.
[328] X. Sun, R.T. Kelly, K. Tang, R.D. Smith, Membrane-based emitter for coupling microfluidics with ultrasensitive nanoelectrospray ionization-mass spectrometry, Anal. Chem. 83 (2011) 5797–5803, https://doi.org/10.1021/ac200960h.
[329] L. Sainiemi, T. Sikanen, R. Kostiainen, Integration of fully microfabricated, three-dimensionally sharp electrospray ionization tips with microfluidic glass chips, Anal. Chem. 84 (2012) 8973–8979, https://doi.org/10.1021/ac301602b.
[330] C. Lotter, J.J. Heiland, S. Thurmann, L. Mauritz, D. Belder, HPLC-MS with glass chips featuring monolithically integrated electrospray emitters of different geometries, Anal. Chem. 88 (2016) 2856–2863, https://doi.org/10.1021/acs.analchem.5b04583.
[331] S. Koster, E. Verpoorte, A decade of microfluidic analysis coupled with electrospray mass spectrometry: an overview, Lab Chip 7 (2007) 1394–1412, https://doi.org/10.1039/b709706a.
[332] T. Rob, P.K. Gill, D. Golemi-Kotra, D.J. Wilson, An electrospray MS-coupled microfluidic device for sub-second hydrogen/deuterium exchange pulse-labelling reveals allosteric effects in enzyme inhibition, Lab Chip 13 (2013) 2528–2532, https://doi.org/10.1039/c3lc00007a.
[333] X. Sun, R.T. Kelly, K. Tang, R.D. Smith, Ultrasensitive nanoelectrospray ionization-mass spectrometry using poly(dimethylsiloxane) μchips with monolithically integrated emitters, Analyst 135 (2010) 2296–2302, https://doi.org/10.1039/c0an00253d.
[334] M. Haapala, L. Luosujärvi, V. Saarela, T. Kotiaho, R.A. Ketola, S. Franssila, R. Kostiainen, μchip for combining gas chromatography or capillary liquid chromatography with atmospheric pressure photoionization-mass spectrometry, Anal. Chem. 79 (2007) 4994–4999, https://doi.org/10.1021/ac070157a.
[335] P. Östman, S.J. Marttila, T. Kotiaho, S. Franssila, R. Kostiainen, μchip atmospheric pressure chemical ionization source for mass spectrometry, Anal. Chem. 76 (2004) 6659–6664, https://doi.org/10.1021/ac049345g.
[336] P. Östman, S. Jäntti, K. Grigoras, V. Saarela, R.A. Ketola, S. Franssila, T. Kotiaho, R. Kostiainen, Capillary liquid chromatography-μchip atmospheric pressure chemical ionization-mass spectrometry, Lab Chip 6 (2006) 948–953, https://doi.org/10.1039/b601290f.
[337] V. Vrkoslav, B. Rumlová, T. Strmeň, P. Nekvasilová, M. Šulc, J. Cvačka, Applicability of low-flow atmospheric pressure chemical ionization and photoionization mass spectrometry with a microfabricated nebulizer for neutral lipids, Rapid Commun. Mass Spectrom. 32 (2018) 639–648, https://doi.org/10.1002/rcm.8086.
[338] S.K. Küster, S.R. Fagerer, P.E. Verboket, K. Eyer, K. Jefimovs, R. Zenobi, P. S. Dittrich, Interfacing droplet microfluidics with matrix-assisted laser desorption/ionization mass spectrometry: label-free content analysis of single droplets, Anal. Chem. 85 (2013) 1285–1289, https://doi.org/10.1021/ac3033189.
[339] C.W. Tsao, S. Tao, C.F. Chen, J. Liu, D.L. Devoe, Interfacing microfluidics to LDI-MS by automatic robotic spotting, Microfluid. Nanofluidics 8 (2010) 777–787, https://doi.org/10.1007/s10404-009-0510-x.
[340] S.K. Küster, M. Pabst, K. Jefimovs, R. Zenobi, P.S. Dittrich, High-resolution droplet-based fractionation of nano-LC separations onto microarrays for MALDI-MS analysis, Anal. Chem. 86 (2014) 4848–4855, https://doi.org/10.1021/ac4041982.
[341] J. Liu, K. Tseng, B. Garcia, C.B. Lebrilla, E. Mukerjee, S. Collins, R. Smith, Electrophoresis separation in open microchannels. A method for coupling electrophoresis with MALDI-MS, Anal. Chem. 73 (2001) 2147–2151, https://doi.org/10.1021/ac001326t.
[342] J. Gorbatsova, M. Borissova, M. Kaljurand, Electrowetting on dielectric actuation of droplets with capillary electrophoretic zones for MALDI mass spectrometric analysis, Electrophoresis 33 (2012) 2682–2688, https://doi.org/10.1002/elps.201200096.
[343] K.K. Murray, D.H. Russell, Liquid sample introduction for matrix-assisted laser desorption ionization, Anal. Chem. 65 (18) (1993) 2534–2537.
[344] H. Ørsnes, T. Graf, H. Degn, K.K. Murray, A rotating ball inlet for on-line MALDI mass spectrometry, Anal. Chem. 72 (1) (2000) 251–254.
[345] J. Preisler, F. Foret, B.L. Karger, On-line MALDI-TOF MS using a continuous vacuum deposition interface, Anal. Chem. 70 (24) (1998) 5278–5287.
[346] J. Preisler, P. Hu, T. Rejtar, B.L. Karger, Capillary Electrophoresis– matrix-assisted laser desorption/ionization time-of-flight mass spectrometry using a vacuum deposition interface, Anal. Chem. 72 (20) (2000) 4785–4795.
[347] M. Schürenberg, C. Luebbert, H. Eickhoff, M. Kalkum, H. Lehrach, E. Nordhoff, Prestructured MALDI-MS sample supports, Anal. Chem. 72 (2000) 3436–3442.
[348] X. Zhang, D.A. Narcisse, K.K. Murray, On-line single droplet deposition for MALDI mass spectrometry, J. Am. Soc. Mass Spectrom. 15 (2004) 1471–1477.
[349] S.B. Ficarro, W.M. Alexander, I. Tavares, J.A. Marto, Open source fraction collector/MALDI spotter for proteomics, HardwareX 11 (2022) e00305.
[350] R. Mukhopadhyay, The automated union of LC and MALDI MS, Anal. Chem. 77 (2005) 150A–152A.
[351] M. Zhong, C.Y. Lee, C.A. Croushore, J.V. Sweedler, Label-free quantitation of peptide release from neurons in a microfluidic device with mass spectrometry imaging, Lab on a Chip, Royal Society of Chemistry 12 (2012) 2037–2045.
[352] S.E. Bell, I. Park, S.S. Rubakhin, R. Bashir, Y. Vlasov, J.V. Sweedler, Droplet microfluidics with MALDI-MS detection: the effects of oil phases in GABA analysis, ACS Meas. Sci. Au 1 (2021) 147–156, https://doi.org/10.1021/acsmeasuresciau.1c00017.
[353] N.W. Maria, W. Dietmar, K. Alexander, H. Sabrina, B. Regina, T. Andreas, R. Christoph, MALDI versus ESI: the impact of the ion source on peptide identification, J. Proteome Res. 16 (3) (2017) 1207–1215, 2017.
[354] W. Huang, G. He, On-column capillary suppressor for open tubular ion chromatography, Anal. Chim. Acta p342372 (2024).

Cable Warren obtained his Bachelor of Science in Chemistry at the University of Washington in 2021. He is currently a Ph.D. student in Analytical Chemistry at the University of Texas at Arlington. His current research interests include micro/capillary-scale separation techniques for liquid and ion chromatography as well as development of portable instrumentation for environmental analyses. His previous research includes development of novel instrumentation and data processing techniques for multidimensional gas chromatography.

Purnendu K. (Sandy) Dasgupta, native of India, received his PhD in Analytical Chemistry with a minor in Electrical Engineering from Louisiana State University (LSU), in 1977, simultaneously earning a home-study diploma as a TV mechanic. He has spent essentially all his professional life in Texas; 25 years at Texas Tech and since 2007 at UT Arlington where he is now the Hamish Small Chair of ion analysis. He has authored 450+ papers in peer-reviewed journals, co-authored an undergraduate text on Analytical Chemistry, and has 40+ US patents to his name. He thinks of himself not a specialist but as a problem solver. Above all, he likes building things: His website proclaims: *We foster builders, not users.* He says that his original ambition was to be a poet. In his native language, Bengali, he has a published a collection of poetry, a novel, and many little pieces here and there.